Source Attribution, Physicochemical Properties and Spatial Distribution of Wet Deposited Mercury to the Ohio River Valley

by

Emily Mae White

A dissertation submitted in partial fulfillment
of the requirements for the degree of
Doctor of Philosophy
(Atmospheric and Space Sciences)
in The University of Michigan
2009

Doctoral Committee:

Professor Gerald J. Keeler, Chair
Professor Perry J. Samson
Assistant Professor Anna M. Michalak
Assistant Research Scientist Frank J. Marsik
Matthew S. Landis, United States Environmental Protection Agency

To

Grandma White, the essence of vitality

and

Grandma Holmgren, the epitome of class

Acknowledgments

This work has been funded wholly or in part by the U.S. Environmental Protection Agency Office of Research and Development through cooperative agreement R-82971601-0, and Student Services Contract EP07D000572.

Every member of my committee has had a distinct impact on my academic and personal growth. Perry probably doesn't remember, but I took AOSS 202 in 1999 (!), and on the first day of class he said that some of us might get interested enough in meteorology that we would end up in the field. Here I am. I owe Frank my deepest thanks for keeping the secret safe: I can't forecast to save my life. But in all seriousness, he is one of the most fair, genuine and upstanding teachers I have come across. Anna serves as the quintessential role model for women in science; I was so lucky to be in her course and am honored to have been one of her students. Matt has afforded me every opportunity, and might be one of the most intelligent people I have ever met, thank you Matt, for taking me on and continuing to support me.

Thank you to Dr. Slater and his students. None of this would have been possible without your support. Thank you also for your kindness, the extensive use of your labs (I know we had a 'lot of stuff') and your wife's wonderful strawberry shortcake.

Professor Kuhn, thank you for teaching in such a way that yours was the first course I 'cared' about, and Dr. Barker, thank you for the academic challenges, I don't know if I would be here without them.

Jim, you amaze me. You are the most patient person I have ever met. I always tell people, if there is ANYTHING you want to know, ask Jim. From astronomy to cats, music to SAS, power tools to the appropriate cold weather gear, you always had the right answer or knew where to look. Your humbleness is only rivaled by your knowledge and ability to teach. They make posters that say 'Everything I need to know in life I learned in kindergarten.' I want a shirt that ends the phrase with '…I learned from Jim.'

Brie, thank you for living with nuns in the name of science and bringing such life to Steubenville. David Reed, I enjoyed our rides and appreciate your continued

friendship. Matt, thanks for all the special drinks, for listening to my endless stories, and all the fun-nels washed. Torrone, I'm glad you're okay with being my friend, thanks for coming down and visiting my cubicle every day. If the bottle washing seemed endless, please know that every time I went to set-up or analyze a sample, I would recognize the hand writing on the blue tape and thank you in my head. Thank you now. Lil' Emily, you are fantastic and brilliant, I can't imagine the places you'll go.

Lynnie, we have been through a lot together. Honestly, I have no idea how I am going to meet deadlines or show up to meetings on time without your reminders. What in the world will I do without you? But we will still take a vacation to a big city every year together, right? I mean, attend the same conferences.

Naima, the purple princess, I will never forget setting up tents, to camp 200 yards from our dorm room, 3 feet from our samples, so that I wouldn't miss a drop and you wouldn't get a drop. I am so sorry for failing on your birthday, every year. I will never forget February 10 again.

Ali, as you once wrote in one of my birthday cards, you are the best ambient air sampling traveling buddy anyone could ask for. Thank you for being the never-tired lab supervisor, not blinking when I said we needed 1,000 bottles, driving tirelessly through the night so as to not miss a single event, and almost dying in a junk yard for the sake of a high concentration sample. Thank you for being a fellow student, and friend, talking with me and helping me chill out when I was on the verge of tears over another cell that I couldn't forecast, and lending your SAS, Excel, and printing skills at the last hour.

Ed, Nazia, Nur, Ahmed, Ayesha and Mary, thank you for being my second family. You kept my heart and body nourished at a time in life when things were so hard. You brought me more joy and meaning than words can express. I promise, someday, I will be strong and return the kindness. Nazia, I have never felt so loved as when you told me to 'peel the carrots!' on Thanksgiving morning.

SJ, Abby, Gina, Tiff, Gaby and Jayme. You are the best friends a girl could ask for. Looking forward to MLK weekend sustains me all year long, and knowing we will have each other for a lifetime means the world. I think about every one of you every day.

Jerry, thank you for this opportunity. I know I was bratty, difficult and very stubborn to deal with at times, but thank you for seeing through this part of my growing

up. I also want to thank you for picking such wonderful students and employees, I feel honored to have worked with such exceptional people, you are an excellent judge of character and have filled the lab with extensions of you. Thank you for keeping us a priority when you were certainly under no obligation to do so. I have learned so much from this situation, it has given me a different perspective, the kind people give lip service to, but don't live. I have witnessed your dedication to family and hope to be able to emulate that some day with my own. I don't know the appropriate way to express it, but I am so incredibly thankful you are here today, and that I was able to be with you in the past year.

Thank you to my aunts and uncles and cousins. Aunt Barb and Uncle George, for having an open, inviting and loving home and hearts, Aunt Nan and Pam I love your facebook and email messages, they truly keep me going. My sisters and brother and Angelina and Max, I am privileged to have such a great family. I love you.

Mom and Loren, you raised me to love nature and appreciate science. Thank you for a childhood that encouraged reading, learning and never allowed a single academic self doubting thought to enter the equation. I love you.

Dad and Teri, thank you for your continuing support. Even when I made decisions that didn't fit what you thought I should do next, you were still there. Even when I didn't call for weeks on end, you were still happy to hear from me when I did. I love you.

And finally, thank you to Jane, my best friend and sister. I feel lucky that we are both. You calmed me down, made me laugh (really hard) and gave me perspective when I needed it most. I have learned so much from you, and love that we are so different as to see every bit of life from a different angle. Thank you for being exactly who you are and choosing to share it with me. I love you.

Statements of Co-authorship: This dissertation is written in the manuscript form. All chapters were written, as presented here, solely by me, with the exception of Chapter II. Chapters III - V will, however, be submitted and published with additional authors listed. Chapter II: Sources of Mercury Wet Deposition in Eastern Ohio, USA, was authored by Gerald J. Keeler, Matthew S. Landis, Gary A. Norris, Emily M. Christianson (self), and J. Timothy Dvonch and was published in Environmental Science and Technology in 2006, Volume 40, 5874-5881. Chapter III: Spatial Variability of Mercury Wet Deposition in Eastern Ohio: Summertime Meteorological Case Study Analysis of Local Source Influences was submitted to Environmental Science and Technology in December of 2008, accepted April 2009, with Emily M. White, Gerald J. Keeler and Matthew S. Landis as authors. Chapter IV: Source Type and Attribution for Wet Deposited Hg in Eastern Ohio, USA will be submitted with Emily M. White, Gerald J. Keeler, Matthew S. Landis and James Slater as authors. Chapter V: Determination of Wet Deposited Hg Physicochemistry in the Ohio River Valley Through Sub-event Sampling Using the Automated Sequential Precipitation System will be submitted with Emily M. White, Gerald J. Keeler and James A. Barres as authors.

Table of Contents

List of Tables

List of Figures

List of Appendices

ABSTRACT

Mercury (Hg) is a bioaccumulative neurotoxin that is emitted from anthropogenic sources through fossil fuel combustion. The spatial scale of atmospheric transport prior to deposition is dependent on the chemical and physical form of Hg emissions, and has yet to be quantitatively defined. A five-year comprehensive Hg monitoring and source apportionment study was conducted in Steubenville, Ohio to investigate atmospheric Hg deposition to the highly industrialized Ohio River Valley region. Long-term event-precipitation measurements revealed a significant 30% to three-fold enrichment of Hg concentrations and total Hg deposition flux to the Steubenville site over other Great Lakes regional sites. Multivariate receptor models attributed ~70% of Hg wet deposition to local coal combustion sources. While local stagnant atmospheric conditions led to moderately high volume-weighted mean Hg concentrations and the majority of Hg wet deposition flux, regional transport from the Chicago/Gary and Detroit/Windsor urban areas also led to elevated precipitation Hg concentrations, but did not contribute significantly to the overall Hg deposition. The degree of local source influence was established during a summertime field intensive study in which a local scale network of concurrently collected rain samples revealed that 42% of Hg wet deposition measured less than one km from the base of coal fired utilities could be attributed to the adjacent source, corresponding to 170% Hg concentration enhancement over regionally representative precipitation collected concurrently. In addition, 69±37% of the Hg collected in rain was in a soluble form, entering the precipitation as reactive gas phase or fine particle associated Hg. The Hg scavenging coefficient (rate of concentration reduction throughout a single precipitation event) was particularly low when compared to other trace elements. Furthermore, when compared to an upwind but non-locally source impacted site, the scavenging coefficient for Hg in the locally source influenced

precipitation was significantly lower. These results indicate that a continuous source of soluble gaseous Hg may be the reason for the low scavenging coefficient. Therefore, this work revealed through measurements that the chemical forms of Hg in coal combustion emissions, and the physicochemical properties therein, explain the locally elevated Hg wet deposition observed.

CHAPTER I

Introduction

Mercury (Hg) is a highly toxic, persistent heavy metal that bioaccumulates in the food chain. While the major concern to the general public is of Hg concentrations in fish and the subsequent consumption of such species, it is essential to understand the means by which the contaminant entered the food chain. Atmospheric transport is widely recognized as the primary distribution vehicle of Hg. Hg is emitted naturally into the atmosphere in relatively small amounts from volcanoes, plant transpiration, forest fires, sea salt spray, airborne soil particles and general geologic out gassing. Anthropogenic emissions may account for between 50 and 75% of total global emissions, however (1). Mercury is emitted in three forms (Elemental Mercury - Hg^0, Divalent Reactive Gaseous Mercury (RGM) - Hg^{2+} and Particulate Bound Mercury - Hg(p)) from cement plants, crematoriums, fluorescent light factories, metallurgical coke ovens, ferrous and non-ferrous production facilities, oil combustion, landfills, municipal and medical waste incinerators and most notably, coal-burning power plants. Source sampling has found emissions from municipal and medical waste incinerators to be between 60 and 98 % (7, 8), cement kilns 25% and coal fired power plants 67% ± 27% (7) in the divalent state.

RGM and Hg(p) are relatively soluble and have a high affinity for surface reactions, resulting in much shorter atmospheric residence times than Hg^0, which is recognized as a global pollutant. Hg^0 is eventually removed from the atmosphere through dry deposition or via aqueous oxidation (e.g. O_3, Cl_2) and subsequent wet deposition (2). This fact has been reinforced by observations of significant mercury deposition gradients near highly industrial and urbanized areas (3,4). Gradients in mercury concentration and deposition have also been found on larger spatial scales in the Great Lakes (5, 6). Of the various deposition pathways in the Great Lakes Area, precipitation has been shown to be the most significant (3). The effective spatial range of Hg deposition is location specific

and quantifying the relative contributions of global, regional and local sources is essential to understanding mercury cycling within a given ecosystem.

Established by the US Environmental Protection Agency in March of 2005, The Clean Air Mercury Rule (CAMR) was the first Federal rule to require Hg emission reductions from coal-fired power plants. The market based cap-and-trade approach of CAMR was similar to EPA's SO_2 and NO_x reductions as part of the successful the Acid Rain Program, and was based on model predictions that attributed the majority of US continental Hg deposition to long range transport. CAMR was overturned by the U.S. Court of Appeals on February 8, 2008 for failure to comply with aspects of the original treatment of Hazardous Air Pollutants under the Clean Air Act Section 112. The removal of coal- and oil-fired power plants from the sources regulated under this section, as well as the new performance-based standards placed on power plants that emit mercury, was "effectively invalidating CAMR's regulatory approach" according to the Appeal's Court decision. Most recently, requests for appeals have been revoked, the current administration citing plans for a more stringent rule, and negotiations are under way for an international Hg emissions treaty. Politics and controversy surrounding the appropriate approach to regulate Hg emissions make the characterization and clear explanation and understanding of Hg deposition physiochemistry of utmost importance.

Current nationally recognized mercury wet deposition sampling is under the National Atmospheric Deposition Program's (NADP) Mercury Deposition Network (MDN) (See Figure I.1). Recent work has elucidated a direct link between Hg wet deposition and methylmercury concentrations in fish, using MDN's deposition data (9). While there was a high correlation between the two factors, it was most interesting to note the cases that did not fit the regression. Three of the 28 cases studied found methylmercury concentrations in small mouth bass greatly exceeding the representative Hg deposition amounts. The study was conducted using state-wide averages, and it was hypothesized that the 'mismatch' could probably be attributed to wet deposition collection in exceptionally rural, 'regionally representative' areas of the state, and therefore not necessarily representative of the local areas in which the fish were caught.

My work with the University of Michigan Air Quality Lab (UMAQL) originated in investigations of long-term Hg wet deposition data-sets from the Great Lakes area:

Dexter, Pellston, Grand Rapids, Flint, Detroit and Eagle Harbor Michigan. A recurring theme presented itself: not only did I see a distinct North South gradient in Hg concentration and deposition, but it could be directly linked to proximity to urban and industrial airsheds. Repeated references and reliance on the MDN interpolated Hg deposition maps seemed to leave a significant void, not only in the Great Lakes region, but also in a spatial scale representation. Through geostatistical analysis methods, I created my own Great Lakes Region interpolation map – using a decades worth of data from the University of Michigan Air Quality Laboratory (UMAQL), MDN and various other studies. See Figure I.2 for a Great Lakes region surface definition compared to MDN's current deposition map (Figure I.1). It was clear that Hg to the Great Lakes region was being underestimated, and that the gradients where possibly steeper than could be predicted by the regionally representative siting criteria of MDN.

While 'background' measurements taken in the Upper Peninsula of Michigan (Eagle Harbor, approximately 7-9 $\mu g\ m^{-2}yr^{-1}$) were fairly close to those estimated by the MDN interpolation, the collection of wet deposition in the heart of the urban and industrial locales of Chicago and Detroit were vastly underestimated, measured depositions (>16 $\mu g\ m^{-2}yr^{-}1$) were twice those predicted by MDN (8-10 $\mu g\ m^{-2}yr^{-1}$). We have hypothesized that spatial deposition gradients are much more local in scale. Samples collected a decade apart in 1996 and 2007 in southern Michigan showed between 25 and 35% Hg concentration enhancement between urban sites in Detroit and a rural site (Dexter, MI), approximately 60 km upwind (11,12). This indicates that MDN may correctly estimate fluxes to regionally representative background type airsheds, but that deposition to locally influenced urban and industrial regions are underrepresented.

At the southern reaches of the Great Lakes region, the Ohio River Valley remains one of the most industrialized areas of the United States. Iron and Steel manufacturing is incredibly important to the area's economy, and the accessibility of the Ohio River allows for regionally mined coal to be easily transported and used for energy production fairly cheaply. The Ohio Mercury Monitoring and Modeling Study was established to determine the impact of these point sources on Hg deposition in the immediate vicinity. Situated atop a cliff overlooking the Ohio River Valley, the enhanced Hg monitoring site in Steubenville, Ohio afforded a unique opportunity to combine several measurement

methods to conduct experiments over both long term collection of ambient and precipitation measurements, as well as to conduct in-depth short term field intensives. A quick premonition of the conclusions to come can be immediately observed in the comparison of Figures I.1 and I.2: while MDN estimates Hg wet deposition to be between 8 and 10 $\mu g\ m^{-2}$ for the Ohio River Valley for the 2007 calendar year, we measured 13.1 $\mu g\ m^{-2}$.

The following dissertation spans both spatial and temporal scales to elucidate trends, sources, causation of variability, and inclusion processes of Hg wet deposition in the immediate vicinity of coal fired utility boilers and numerous other Hg emission sources for Stuebenville Ohio. Chapter II, published in Environmental Science and Technology October, 2006 explores the first two years of event precipitation data, using multivariate statistical analysis methods and a brief climatological and synoptic meteorological discussion for source attribution. Chapter III, submitted to ES&T December 2008, accepted April 2009, is an event case study analysis of Hg concentration in locally distributed precipitation samples and the meteorological parameters that produce near field enhancement during summertime events. Chapter IV revisits source attribution, with a more robust 5 ½ year event data set. The increase in number of samples allowed for a much more in-depth synoptic meteorological and trajectory analysis, a key to understanding source regions. Local ambient data is coupled with event and sub-event precipitation data for physiochemical removal process insight in Chapter V. Also included in Chapter V is a methods section describing the Automated Sequential Precipitation Sampler, developed at the University of Michigan Air Quality Laboratory. Chapters IV and V will be submitted for publication after confirmation of this dissertation. Chapter VI pulls together time scales, from the 5 ½ year source attribution to the sub-event and hourly process analysis, as well as spatial scales, from continental transport and regional interpolation to near-field deposition, in a study conclusion.

Figure I.1: Mercury Deposition Network continental scale Hg deposition interpolation map, 2007 (10). Inset box represents boundary of map in Figure I.2.

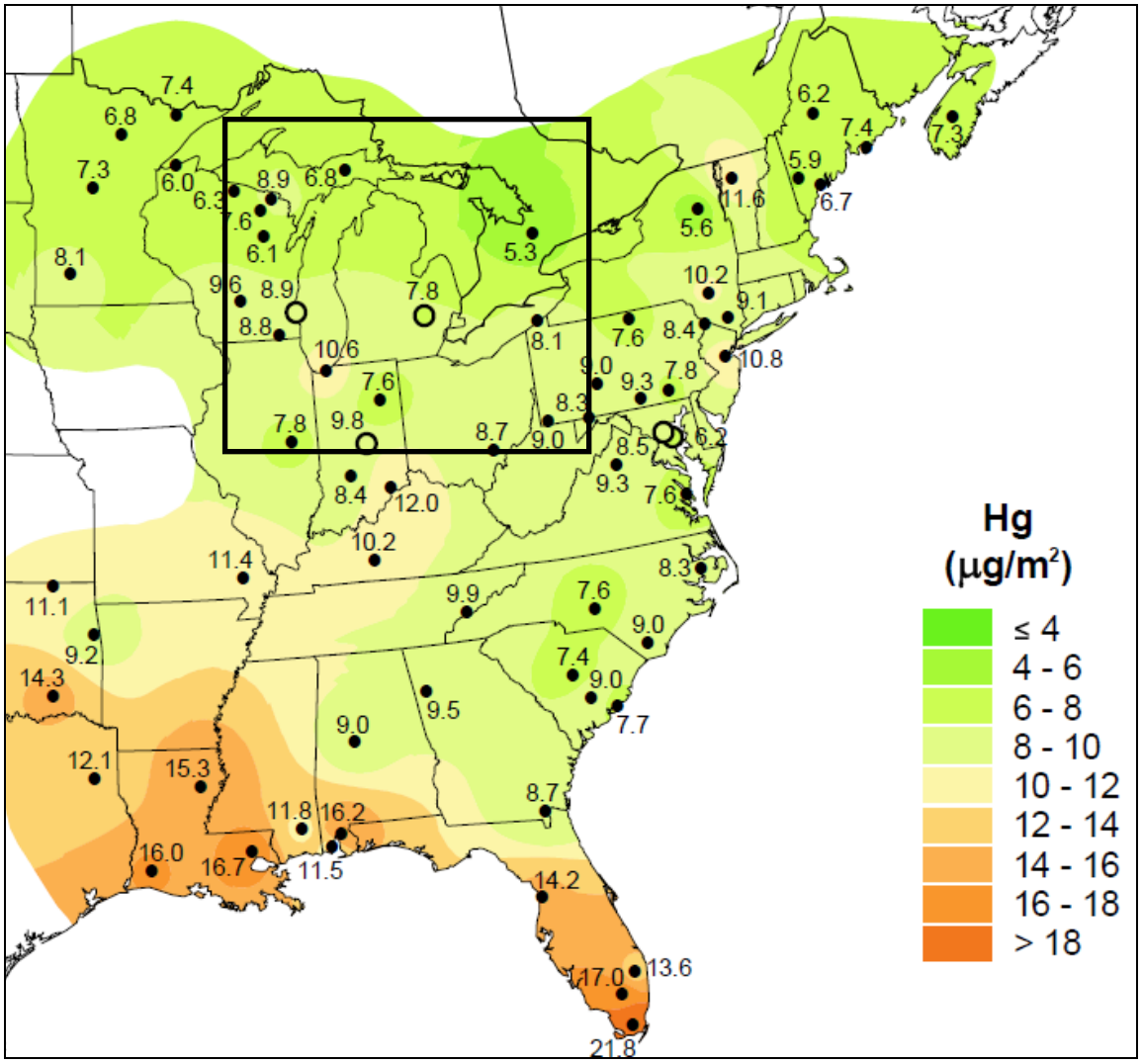

Figure I.2: Great Lakes Regional Hg wet deposition (μg m^{-2}) interpolation surface using ordinary kriging.

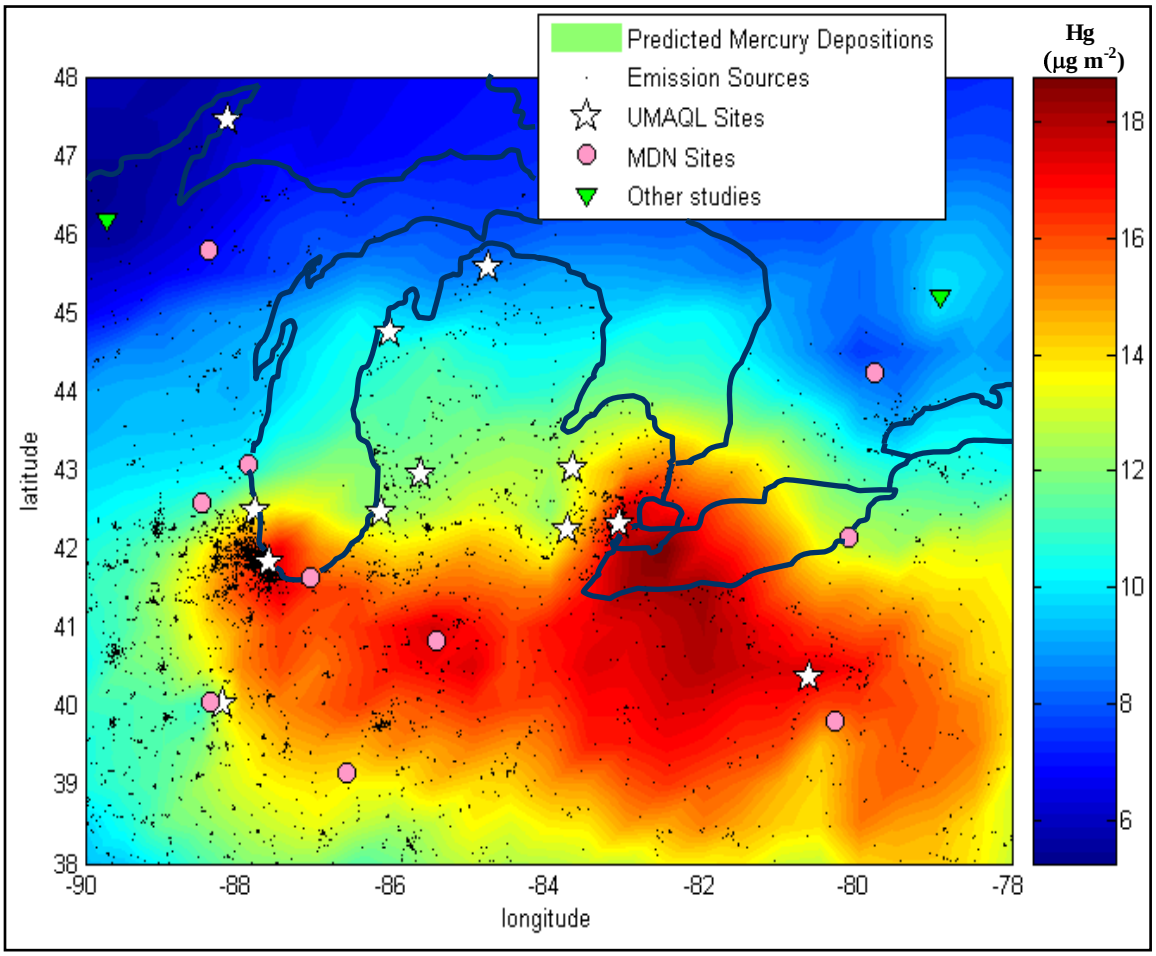

CHAPTER I: References

(1) Expert Panel on Mercury Atmospheric Processes. *Technical Report EPRI/TR-104214;* **1994**.

(2) Lin, C.; Pehkonen, S.O.The chemistry of atmospheric mercury: a review *Atmos. Environ.* **1998**, 33, 2067-2079.

(3) Landis, M. S.; Keeler, G. J. Atmospheric mercury deposition to Lake Michigan during the Lake Michigan Mass Balance Study *Environ. Sci. Technol.* **2002**, 36, 4518-4524.;

(4) U.S. Environmental Protection Agency. *Mercury Study Report to Congress,* EPA-452/R-97-005; Office of Air Quality Planning and Standards, Office of Research and Development: Washington, DC **1997.**

(5) Hoyer, M. PhD thesis, Wet Deposition of mercury in Michigan: Meteorological associations and spatial variability. University of Michigan, Ann Arbor, MI, **1995.**;

(6) Keeler, G.J.; Dvonch, J.T. In *Dynamics of Mercury Pollution on Regional and Global Scales,* Pirrone, N. and Mahaffey, K.R. Eds.; Kluwer Academic Publishers, New York, NY. **2005.**

(7) Dvonch, J.T.; Graney, J.R.; Marsik, F.J.; Keeler, G.J.; Stevens, R.K. Use of elemental tracers to source apportion mercury in south Florida precipitation. *Environ. Sci. Technol.* **1999**, 33, 4522-4527.

(8) Stevens, R.K.; Zweidenger, R.; Edgerton, E.; Mayhew, W.; Kellog, R.; Keeler G.J.; Source Characterization in Support of Modeling the Transport of Mercury Emissions in South Florida. Presented at *Measurement of Toxic and Related Air Pollutants Symposium*, May 7-9, Research Triangle Park, NC, **1996.**

(9) Hammerschmidt, C. R.; Fitzgerald, W. F. Methylmercury in freshwater fish linked to atmospheric mercury deposition *Environ. Sci. Technol.* **2006**, 40, 7764-7770.

(10) National Atmospheric Deposition Program, Mercury Deposition Network. **2007**. available at http://nadp.sws.uiuc.edu/.
(11) Gildemiester, A. E. PhD thesis, Urban Atmospheric Mercury, University of Michigan, Ann Arbor, MI, **2001**.
(12) Hall, N. L.; Keeler, G. J.; Landis, M. S. Personal communication.

CHAPTER II

Sources of Mercury Wet Deposition in Eastern Ohio, USA

Abstract

In the fall of 2002, an enhanced air monitoring site was established in Steubenville, Ohio as part of a multi-year comprehensive mercury monitoring and source apportionment study to investigate the impact of local and regional coal combustion sources on atmospheric mercury deposition in the Ohio River Valley. This study deployed advanced monitoring instrumentation, utilized innovative analytical techniques, and applied state-of-the-art statistical receptor models. This paper will present wet deposition data and source apportionment modeling results from daily event precipitation samples collected during the calendar years 2003-2004. The volume-weighted mean mercury concentrations for 2003 and 2004 were 14.0 and 13.5 ng L^{-1}, and total annual mercury wet deposition was 13.5 and 19.7 μg m^{-2}, respectively. Two new EPA implemented multivariate statistical models, Positive Matrix Factorization (PMF) and Unmix, were applied to the data set and six sources were identified. The dominant contributor to the mercury wet deposition was found by both models to be coal combustion (~70%). Meteorological analysis also indicates that a majority of the mercury deposition found at the Steubenville site was due to local and regional sources.

Keywords: Precipitation chemistry, trace elements, receptor modeling, meteorology

Introduction

Mercury (Hg) is a persistent, bioaccumulative toxic pollutant. Once Hg is released into the environment it can be converted to the organic form, methylmercury (MeHg) and then bioaccumulate in organisms within the food chain, such as fish, posing a consumption risk to wildlife and humans. In the Great Lakes Region, atmospheric deposition is widely considered to be the primary pathway for Hg into aquatic and terrestrial ecosystems (1,2). Mercury is emitted into the atmosphere through both natural and anthropogenic processes with 50-75% of global emissions attributed to anthropogenic sources (3,4). Major anthropogenic sources of mercury to the atmosphere include: fossil fuel combustion, waste incineration, iron-steel production, coke and lime production, hazardous waste recycling, non-ferrous metal smelting, petroleum refining, and mercury cell chlor-alkali plants (5,6).

While natural emissions of Hg are primarily in the gaseous elemental form (Hg^0), combustion processes release Hg in three major forms: Hg^0, divalent reactive gaseous Hg (RGM) and particulate Hg (Hg(p)). RGM and Hg(p) are more efficiently deposited on a local and regional scales near major sources because of their solubility and affinity for surface reactions which results in much shorter atmospheric lifetimes (4). Researchers in both the US and Europe have observed significant mercury deposition gradients with maximums found near urban and industrial areas (6,7,8,9,) highlighting the importance of near field deposition enhancement in proximity to large anthropogenic sources. Deposition of atmospheric Hg at any particular location is therefore a complex combination of local, regional, and global emissions as well as transport, transformation, and deposition processes (4).

In a 1998 Report to Congress, the U.S. Environmental Protection Agency (EPA) identified coal-fired utility boilers as the largest source of domestic anthropogenic mercury emissions to the atmosphere and provided evidence of a causal link between such releases and the presence of methylmercury in fish tissue (9). At that time, EPA recognized that the Ohio River Valley contained a high density of coal-fired utility boilers and that monitoring of atmospheric mercury deposition was not being conducted in this area. In 1999, EPA initiated planning for a mercury monitoring and source

apportionment study to investigate the impact of local and regional coal combustion sources on atmospheric mercury deposition in the Ohio River Valley.

The Clean Air Mercury Rule (CAMR) was subsequently promulgated by EPA in 2005 and established the first U.S. regulation to control mercury emissions from coal-fired utility boilers (10). CAMR uses a cap and trade approach under which utilities can buy and sell credits in a national emissions market. Under CAMR, an interim national cap of 38 tons y^{-1} becomes effective in 2010 and a final cap of 15 tons y^{-1} becomes effective in 2018. The 2010 interim cap is based on mercury reductions expected to be achieved as a co-benefit from the EPA Clean Air Interstate Rule, also promulgated by EPA in 2005, which requires utilities to install controls to reduce NO_x and SO_2.

The relative importance of domestic coal combustion sources to atmospheric Hg deposition in the U.S. and the efficacy of the CAMR cap and trade approach to decrease Hg in fish is the topic of an ongoing debate in the scientific community. At the center of this debate is the question of the relative importance of Hg emissions from domestic coal-fired utility boilers to atmospheric deposition into sensitive aquatic and terrestrial ecosystems. As part of the CAMR development process, EPA used the Community Multi-scale Air Quality model (CMAQ), an Eulerian dispersion model, to estimate the impact of domestic mercury sources on atmospheric deposition for CY2001. While extremely useful, all contemporary deterministic models (e.g., CMAQ) are currently limited by the large uncertainties in emission inventories, atmospheric Hg chemistry, and wet and dry deposition parameterizations. Receptor models differ from deterministic models in that they only rely upon speciated wet deposition samples collected at a location or receptor. Deterministic and receptor modeling source apportionment approaches are independent and complementary.

Multivariate statistical receptor models, such as principal component analysis (PCA), have been successfully used to apportion the sources of Hg deposited in South Florida (11) and the sources of other chemical compounds elsewhere (12). More recently, statistical approaches such as Unmix (13) and positive matrix factorization (PMF) have been developed which improve upon the earlier techniques by using uncertainties in the data matrix (14, 15) as well as through constraining the solutions to non-negative values. Both techniques have the advantage of not requiring prior measurements of source

profiles or emission inventories. In this study, PMF and Unmix are applied to the precipitation chemistry data collected at the Steubenville, Ohio site to determine the sources contributing to Hg in wet deposition. In addition, meteorological analysis is performed to provide insights into the probable sources of Hg deposition.

Methods

Measurement Site

An enhanced Hg monitoring site was established in October 2002, in Steubenville, OH on the campus of the Franciscan University (40.379 N, 80.620 W; 306 m above msl) overlooking the Ohio River. This monitoring site was selected because of its proximity to numerous anthropogenic air pollution sources in the Ohio River Valley and because of the human health impacts shown to be caused by these sources during the Harvard Six-City Study (16). There are five large coal-fired utility boilers within a 50 km radius of the site and seventeen within 100 km. Figure 1 shows the location of the site as well the location of coal-fired utility boilers within a 100 km radius.

Event Deposition Sampling

Collection of wet deposition on a daily event basis rather than longer duration integrated sampling (e.g., weekly, monthly) is essential for receptor modeling and meteorological analysis (11, 17, 18, 19). The automatic wet-only event precipitation sampling system used for this study is described in detail by Landis and Keeler (19), and has been successfully deployed in the field for more than a decade (8, 20, 21). Precipitation sampling for this study began in October 2002 and will continue through December 2006. Results are reported here for samples collected in CY2003 and CY2004.

For this study, the volume of each precipitation sample was determined gravimetrically, the precipitation depth was calculated by dividing the precipitation volume by the funnel area, and all events ≥ 0.1 cm provided sufficient volume for analysis. A heated tipping-bucket precipitation gauge provided a continuous record of the precipitation received at the site and was used to calculate precipitation depths when the 1 L sample bottles were insufficient for containing the entire event and sample overflow occurred (6 events).

All field and analytical supplies used in the collection and analysis of Hg and trace element samples were prepared using an eleven-day acid-cleaning procedure (18,19). The Teflon sample bottles were further prepared by an internal 1% BrCl solution (v/v) soak for a minimum of 24-hours. Standard operating procedures included bottle blank determinations for each batch of cleaned bottles to ensure that sampling bottles were essentially Hg-free before they were deployed into the field (median<MDL; 5 ± 14 pg $bottle^{-1}$(mean ± std dev); n=151).

Analytical Methods

Precipitation samples were sent back to the University of Michigan within 24-hours of collection and were processed and analyzed in a Class 100 clean room to avoid potential contamination. Clean room suits and particle-free gloves were worn at all times during preparation and analysis of samples.

Mercury Mercury samples were oxidized with concentrated BrCl to a 1% solution (v/v) and stored in the dark in a cold room for at least 24 h (19). Mercury in precipitation was purged from solution in a Hg-free nitrogen stream after reduction of BrCl with NH_2OH and reduction of divalent Hg by $SnCl_2$ to Hg^0, and concentrated onto a gold-coated bead trap. Total Hg was then quantified using a dual amalgamation technique followed by cold-vapor atomic fluorescence spectrometry (CVAFS) (19, 22). In a previous study, collocated total Hg samples collected using identical samplers and protocols as those used at Steubenville gave an absolute mean difference in the samples of 8.1% (19). The Method Detection Limit (MDL) for total Hg during this study was determined to be 0.23 ng L^{-1}; determined using EPA method 200.8 (23). Analytical precision of laboratory replicate Hg analysis during this study was 97.3% (n=51).

Trace Elements Precipitation samples for trace element analysis were acidified with concentrated HNO_3 to a 0.2% solution (v/v) in the sample bottle and stored in a dark cold room for a minimum of 14 days before analysis to provide adequate time for optimal leaching (24). Precipitation samples were then analyzed for a suite of trace elements using a Finnigan MAT Element magnetic sector field high-resolution inductively coupled plasma mass spectrometer using a method similar to that previously described (25). Trace element isotopes were analyzed in low, medium, or high resolution depending on

the potential of impact of isobaric and/or polyatomic interferences (25). The sensitivity of the Element decreases approximately by a factor of 10 with each successive increase in resolution so elements quantified in high resolution had significantly higher MDLs (See Table S1, Supporting Information).

Ion Chromatography Precipitation samples were analyzed for major anions using a Dionex (Sunnyvale, CA) Model DX-600 ion chromatography system equipped with an IonPac® AS14 Analytical and AG14 Guard and running a 1.8 mM Na_2CO_3/1.7 mM $NaHCO_3$ eluent solution. Precision based on replicate analyses was 95.5% and 93.2%, for nitrate and chloride, respectively.

Multivariate Statistical Receptor Models

In this work, two fairly new multivariate receptor modeling approaches were employed: EPA PMF 1.1 (26) and EPA Unmix 5.0 (27). Both PMF and Unmix provide the source compositions, source composition uncertainties, and source contributions to each sample based only on the measured data. These two models use different algorithms and input data with PMF using a combination of concentration and uncertainty data and Unmix using only concentration data. For both models, the sample Hg source contributions were calculated by multiplying the Hg profile value by its source contribution estimate. All samples with sufficient volume from October 2002 through December 2004 were included in the PMF and Unmix analysis (n=162).

EPA PMF couples a graphical user interface with analysis software that implements the PMF 2 model through the Multi-linear Engine 2 (ME-2), and provides block bootstrap uncertainty estimates (26). All analyses were conducted using the default model specifications, and the results are reported for the run with the lowest Q robust value from 20 random starting points, with random seeds. One hundred bootstrap runs were used to calculate the uncertainty distribution.

EPA Unmix 5.0 includes both a graphical user interface and analysis tools. All analyses were run using the default model specifications and one hundred feasible solutions from a blocked bootstrap were used to calculate the uncertainty distribution (27).

One potential advantage of the PMF model is the ability to weight individual data points using measurement uncertainties and other analytical details such as the elemental MDLs. Here, an objective approach was used to calculate a total deposition uncertainty (U) associated with each data point (each analyte in every sample) for use in PMF by propagating the uncertainty of sample collection (SC), analytical measurement (AM), and precipitation depth (PD) measurement uncertainties (Equation II.1).

$$U_{Dep} = MDL + \sqrt{(SC)^2 + (AM)^2 + (PD)^2} \quad \text{(II.1)}$$

where, MDL=method detection limit; SC = 10%; AM= (standard deviation of 3 replicate analysis); and PD=5%.

Meteorological and Trajectory Analysis

Air mass transport to the Steubenville site was estimated using the Hybrid Single-Particle Lagrangian Integrated Trajectory (HYSPLIT) Model Version 4.6 (28). HYSPLIT 72-h back trajectories were calculated using input data from The National Weather Service. The hour of maximum precipitation intensity from each event was used as the start time for the trajectory calculation and the starting height for each trajectory was calculated as one-half the mixing height, as determined from upper-air soundings. Surface and upper air meteorological maps obtained from the National Weather Service were used to explore the validity of the calculated trajectories and to better understand the type of precipitation and meteorological patterns that influenced the deposition events.

Results and Discussion

Concentrations and Deposition Data

The two-year record of Hg in event precipitation at Steubenville is the only such record collected in Ohio. The volume-weighted mean (VWM) Hg concentration was 13.7 ng L^{-1} for the two-year period, with little difference between the years (14.0 and 13.5 ng L^{-1} for 2003 and 2004, respectively). The range in the event Hg concentrations recorded over the two-year period in Steubenville was 4.0-78.9 ng L^{-1}, similar to the range of Hg concentrations observed in a highly industrialized area in southeast Michigan during the same time period (21). However, the distribution of the Hg concentrations

observed in Steubenville was quite different than measured at rural sites in Michigan and Vermont using identical samplers (20,21). The minimum or baseline Hg concentration observed at Steubenville was ~4 ng L^{-1}; about 4 times higher than the baseline concentrations recorded during the same period at rural sites in Michigan and at Underhill, VT.

The Hg wet deposition recorded at the Steubenville site was 13.5 and 19.7 μg m^{-2} y^{-1} in 2003 and 2004, respectively. Table 1 shows a comparison of the 2003 VWM concentrations and the annual deposition reported for three sites in Michigan with that at Steubenville (21). The Hg wet deposition observed at Steubenville in 2003 was ~10% greater than that received at Dexter, MI and ~2.5 times that recorded at the northern most site located in Eagle Harbor, MI. The pattern observed in 2003, with a south to north Hg deposition gradient across Michigan, has been observed consistently over the past decade through collection of event precipitation samples at several sites in Michigan (8,18,21). The higher Hg deposition observed at the Steubenville site was not unexpected, because of the density of Hg sources in the upwind region such as coal-fired utility boilers, iron-steel manufacturing, incinerators, and other non-ferrous metal processing industries (9). The Hg deposition recorded at the Steubenville site in 2004 was 19.7 μg m^{-2} $year^{-1}$, 46% greater than the previous year.

The VWM concentrations for the 2003-2004 period for the trace elements used for source apportionment are provided in the supplemental information (Table S1).

PMF Model Results

PMF solutions with 6 and 7 sources were evaluated, and species contributions to sources were considered significant if the 5^{th} percentile of the bootstrap uncertainty distribution was greater than 0. The results from the six-source solution are presented based on the ability to identify the sources and the bootstrap uncertainty results. The six source solution was composed of iron/steel production (V, Cr, Mn, Fe), oil & incineration (V, Ni, Zn, Cd, Pb), crustal (Mg, Al, Sr, La, Ce), coal combustion (S, Se, NO_3^-), phosphorous (P, Mg, Mn, Fe, Sr), and molybdenum (Mo, Cu). The 7 source solution separated out one additional crustal source (La, Ce, Mg) and the Hg contributions from coal for the 6 and 7 source solutions were similar with 73 and 70%, respectively. Three

sources contributed significant amounts of Hg: iron/steel production (6%), coal combustion (73%), and phosphorous (2%). The results determined from the six source solution are presented in Table 2.

While PMF was able to separate out six sources, the source identified as coal combustion was clearly dominant in terms of explaining the Hg deposition. Atmospheric Se is often associated with the burning of fossil fuels such as coal (29,30), and Se in the absence of significant Ni and V was determined to be an appropriate tracer of coal combustion in Steubenville (31). There are several large steel manufacturing facilities in the Steubenville, OH –Wheeling, WV area as well as plants to the east in Pittsburgh, and iron-steel production was found to be a minor contributor to Hg deposition in this study. An unidentified phosphorous source was also found to be significant small contributors to Hg deposition. The elements Zn, Pb, Cu, and Cl have been used to identify municipal waste incinerator emissions (11,32), and the elements Ni and V are commonly used tracers to identify oil combustion (33,34). Two other sources of trace elements were identified in the event deposition data using PMF: a crustal source (24,35) and a molybdenum source. The molybdenum source may be production of Mo which is used in the steel industry. However, neither was found to be a significant contributor to Hg wet deposition during the study period.

The model (sum of the calculated source contributions) does an excellent job of reproducing the observations except for several of the top deposition events over the two years of record. The regression results of the PMF predicted versus measured Hg had a slope of 0.70, an intercept of 0.05, and a coefficient of determination of 0.85 (n=162). Figure 2a depicts the time series of the predicted deposition from coal combustion versus observed Hg wet deposition at Steubenville using the PMF six-source model solution, showing the clearly dominant impact of coal combustion.

Unmix Results

Unmix identified one influential Ni data point and its value was replaced using the Missing Data Algorithm (Ni on 04-07-2003, measured = 364.15 ng m^{-2}, replaced = 8.44 ng m^{-2}). A reduced number of species was used in the Unmix run: Hg, Cd, La, Ce, Mg, Al, P, S, V, Cr, Mn, Fe, Ni, Se, and NO_3 because using less species improved the stability

of the uncertainty estimate. The source profiles for a feasible six source solution produced by Unmix are given in Table 3 and species contributions to each source were considered significant if the 5th percentile of the bootstrap uncertainty distribution was greater than 0. Identification of the sources was performed in a similar way to that with the PMF solutions. The Unmix model found 6 sources which were identified as phosphorous, incinerator, nickel, iron/steel production, crustal and coal combustion sources. Only three sources contributed significant amounts of Hg including incinerator (12%), nickel (12%), and coal combustion (69%). The regression results of the Unmix predicted versus measured Hg had a slope of 1.00, an intercept of -0.02, and a coefficient of determination of 0.86 (n=162).

Comparison of Unmix and PMF

Both models tracked the measured values closely but under-predicted the peak concentrations. Two high deposition Hg events occurred on 08/29/2004 (1.53 μg m^{-2}) and 09/08/2004 (1.69 μg m^{-2}) shown in Figures 2a and 2b as events 146 and 147 in the time series. The Unmix and PMF Hg results for these two events were 1.08 and 1.40 μg m^{-2}, and 0.85 and 1.08 μg m^{-2} respectively. Table 4 shows that Unmix over-predicted the total measured Hg deposition by 13 and 5%, while PMF under-predicted by 7 and 11% in 2003 and 2004, respectively.

Confidence intervals (CI) were calculated for those sources identified by Unmix and PMF as a measure of the uncertainty associated with their contribution to Hg deposition. The 95% confidence interval (CI) was calculated using the 5th and 95th percentiles of the source profile uncertainty distributions. Total coal Hg contributions were 23.7 μg m^{-2}, with a CI of 16.7 to 38.4 μg m^{-2} for PMF, and 26.8 μg m^{-2}, with a CI of 16.4 to 39.1 μg m^{-2} for Unmix for the study period. Two additional PMF sources had significant Hg contributions: phosphorous total of 0.6 μg m^{-2} with a CI 0.3 to 1.5 μg m^{-2}, iron/steel production total of 1.9 μg m^{-2} with a CI 0.1 to 3.4 μg m^{-2}, and iron/steel production total of 1.9 μg m^{-2} with a CI 0.2 to 4.3 μg m^{-2}. In addition, Unmix also had two additional sources with significant Hg contributions: incinerator total of 4.6 μg m^{-2} with a CI 0.1 to 10.2; and nickel total of 4.5 μg m^{-2} with a CI 0.4 to 7.1. The lack of agreement between Unmix and PMF for these small Hg sources may indicate that these sources contribute

too little to be accurately quantified. Average results from both PMF and Unmix are well within the confidence intervals stated for both model estimates; and this wide range of uncertainties will be reduced as additional samples are included in the analysis at the conclusion of this study (CY2006).

As clearly stated in Poirot *et al.* (35), receptor models, such as PMF and Unmix, start with the assumption that the source compositions are constant and unique, and that source contributions vary over time. These assumptions may not be well met when attempting to apportion sources that emit species that undergo atmospheric transformations and form secondary species such as sulfate aerosols. Mercury chemistry may be even more complicated than that of sulfur as a larger fraction of the emissions are emitted in the oxidized forms that deposits more quickly than the Hg^0 form that is emitted concurrently. While this limitation is also acknowledged here, the use of multiple receptor models together with the meteorological analysis provided below offer independently consistent results and findings.

Climatology, Meteorology, and Sample Variability

Investigations using relatively short meteorological records, e.g. two-years, need to place the shorter record into a larger climatologically relevant context. While significant differences in the Steubenville wind speed and direction were not expected nor observed, for the CY2003-2004 period from the long-term norm, differences in temperature and precipitation were thought to be more likely. In fact, while the CY 2003 rainfall total was representative of the Steubenville climatological norm, significantly more rain than normal fell in CY 2004, with 10 of 12 months above average and the majority of the excess rainfall occurring in September. CY 2003 was a unique year for eastern Ohio in terms of frozen precipitation; snowfall totals were well over twice the climatologically expected amount. These facts help explain the large deviation between the annual deposition totals (13.5 and 19.7 $\mu g\ m^{-2}$) despite annual VWA Hg concentration similarities, because snow in temperate latitudes appears to be much less efficient at capturing Hg via wet deposition (8). In addition, the long-term study of event precipitation collected in Vermont over eleven-years found average surface temperatures were highly correlated with the monthly-averaged temperatures at that site (20).

However, the average surface temperatures for CY 2003 and 2004, did not significantly deviate from the climatological norm.

Individual precipitation events can contribute significantly to the annual Hg deposition total at individual sites (20,21). This was clearly seen in the Steubenville record as the top five Hg deposition events (1.69, 1.53, 1.19, 0.82 and 0.77 $\mu g\ m^{-2}$ seen in Figures 2a and 2b as events 148, 147, 43, 129 and 149, respectively) all had above average Hg concentrations as well as precipitation depths. While one of these (sample 43) contained precipitation from more than one distinct event, and therefore cannot be clearly categorized meteorologically, the other four samples corresponded to discrete summer-time events. Two of the discrete events were associated with remnants of September hurricanes (Frances and Ivan; samples 148 and 149), one was associated with a warm sector squall line (sample 147) and the fourth (sample 149) occurred in a series of intense precipitation events associated with outflow boundary cells preceding a stationary front. The origin of feed air for these types of precipitating systems is fairly unique; the vertical structure of a strong mid-latitude cyclone dynamically allows exceptional local entrainment and wet deposition, cleaning out the atmospheric boundary layer as the storm sweeps through. Sample 141 was associated with a squall line that formed in the warm sector of a low pressure system only hours before it reached Steubenville, indicating that the entrained air was from within a relatively short distance of the site, as outflow boundaries force lift and condensation on a local scale. Surface winds associated with the two hurricane events were primarily from the northeast, while the other events experienced weak surface winds primarily from the south-southwest which are both areas that contain a high density of coal-fired utility boilers. Three-day back trajectories also indicate air masses with origins northeast or south-southwest of the Steubenville site for these four events (See Figures S3a-e, Supporting Information). The observation of local stagnation prior to large Hg deposition events was also observed at a site in Chicago, IL during the Lake Michigan Mass Balance Study (8). Weak surface winds prior to the precipitation events in Chicago lead to higher observed Hg deposition at that site, but at rural sites in South Haven and Sleeping Bear Dunes, MI local stagnation did not lead to elevated deposition. At these rural sites the highest Hg concentrations, and wet deposition, were observed after relatively fast transport from the Chicago/Gary area.

Lastly, the average rainfall rates for these events were approximately three times the 2-year average (5.7 and 1.7 mm h^{-1}, respectively) and four of the top five events had maximum rainfall occurring in late night/early morning hours when the boundary layer is relatively shallow. Maximum rainfall times for the two-year period did not, on average, show a preference to any particular time of day.

The influence of local and regional sources is also evident when comparing the Hg concentrations of event samples collected at different sites following the path of hurricane Frances, Steubenville's highest deposition event of the two year record. The center of the low for this system moved northward into the Mid-Atlantic States and then towards the northeast, while winds prior to and during the precipitation period at Steubenville were out of the northeast. The Hg concentration at Steubenville for this event was 18.7 ng L^{-1}, the concentration found in samples with similar volume collected during Hurricane Frances at a site in Underhill, Vermont was less than half that at Steubenville (9.1 ng L^{-1}) and that collected at a site in Tampa where the feed air was primarily of oceanic origin was 4.1 ng L^{-1}.

The large temporal variability and range of concentrations among the event samples in Steubenville during this study (4.0 to 78.9 ng L^{-1}) also indicates a strong local and regional source influence. Only 9.5% of the variability in concentration could be accounted for by precipitation amount alone. In addition, a large range was found in Hg concentrations among samples with a similar precipitation depth: 4.3 to 78.9 ng L^{-1} for low precipitation depth samples (< 1 cm) and 4.2 to 22.1 ng L^{-1} for high precipitation depth samples (>5 cm). Previous studies have shown that a large range in concentration for similar rainfall amounts can be attributed to variability in impacts by local sources and to the variation in distance between the sources and the receptor site (8, 36, 37).

The results of the multivariate statistical analysis (~70% of the Hg in the wet deposition at Steubenville as originating from local and regional coal combustion sources), and meteorological analysis (highlighting the importance of local sources), consistently point toward the dominant influence by local and regional coal-burning sources.

Acknowledgements

The United States Environmental Protection Agency through its Office of Research and Development funded the research described here through cooperative agreement R-82971601 with the University of Michigan. It has been subjected to Agency review and approved for publication. We thank Jim Barres, and Ali Kamal (UMAQL) for managing laboratory support operations and data processing; Dr. Khalid Al-Wali for trajectory calculation and plotting; Dr. Frank Marsik for meteorological measurements and interpretation; Dr. James Slater (Franciscan University) for on-site logistical support; and Dr. Ron Henry (USC) and Shelly Eberly (EPA) for receptor modeling support. We would also like to thank the reviewers for their insightful comments and suggestions.

Supporting Information Available

MDLs and volume-weighted mean concentrations for all of the trace elements in Table S1. Scatter plots of PMF and Unmix modeled versus observed Hg deposition in Figures S1a-b. Three day back trajectory plots for high deposition events in Figures S2a-d.

Table II.1. Volume-weighted Average (VWA) Hg concentrations and total deposition calculated from event samples collected using identical UM samplers in 2003.

Site	N	Precipitation Depth (cm)	VWA Hg (ng L^{-1})	Deposition (μg m^{-2} y^{-1})
[1]Dexter, MI	60	89.6	11.9	10.7
[1]Pellston, MI	43	78.7	9.4	7.4
[1]Eagle Harbor, MI	58	64.5	8.3	5.2
Steubenville, OH	77	94.8	14.0	13.5

[1]Keeler and Dvonch (21).

Table II.2. PMF Source Profiles for Steubenville Event Precipitation Data.

Analyte	Source 1	Source 2	Source 3	Source 4	Source 5	Source 6
	Iron/Steel Production	**Oil & Incineration**	**Crustal**	**Coal Combustion**	**Phos-phorous**	**Molyb-denum**
Mg	187	*	558	*	101	*
Al	51	80	355	37	*	52
P	7.8	*	*	*	63.8	*
S	*	*	642	11299	197	*
Cl	267	20480	*	584	*	771
V	2.9	1.1	*	*	*	*
Cr	2.5	*	*	*	*	*
Mn	54.4	*	34.1	*	15.4	*
Fe	344	102	17	37	27	*
Ni	*	3.19	*	*	0.68	*
Cu	1.8	14.0	*	18.4	2.7	7.0
Zn	4.0	44.1	6.1	10.7	5.3	15.6
As	*	0.81	0.10	0.49	0.05	0.27
Se	*	0.97	*	1.73	*	1.30
Rb	*	0.25	0.15	0.20	0.29	0.08
Sr	0.48	3.30	5.64	0.95	1.61	*
Mo	*	*	*	*	*	4.02
Cd	0.09	0.27	*	0.31	0.02	0.23
La	*	0.13	0.63	*	*	0.04
Ce	0.02	*	1.23	*	*	*
Hg	0.01	*	*	0.15	< 0.01	*
Pb	1.10	6.59	0.59	3.62	0.36	1.13
NO_3	*	8639	1501	4532	314	*
% Hg	**6**	*	*	**73**	**2**	*

* = Not Significant at 95% confidence interval

Table II.3. Unmix Source Profiles for Steubenville Precipitation Data.

Analyte	Source 1 **Phosphorous**	Source 2 **Incinerator**	Source 3 **Ni**	Source 4 **Iron/Steel Production**	Source 5 **Crustal**	Source 6 **Coal Combustion**
Mg	103	*	*	120	869	*
Al	*	*	37	*	482	*
P	73.0	*	*	5.4	*	*
S	*	1069	1754	*	*	10494
V	*	*	0.85	3.16	*	1.35
Cr	*	*	*	3.2	*	0.4
Mn	18.5	*	*	50.9	50.3	*
Fe	33	*	55	356	70	93
Ni	*	*	11.75	0.74	*	*
Se	*	*	*	0.87	*	4.26
Cd	*	0.93	0.08	*	*	0.23
La	*	*	0.07	*	0.76	*
Ce	*	*	0.15	*	1.44	*
Hg	*	0.03	0.03	*	*	0.16
NO_3	*	*	*		1860	7518
% Hg	*	12	12	*	*	69

* Not Significant at 95% confidence interval

Table II.4. Comparison of Measured Total Hg Wet Deposition ($\mu g\ m^{-2}$) at Steubenville, OH Site to PMF and Unmix Coal Combustion Contribution Estimates.

Year	Total Measured Hg Wet Deposition	PMF Estimated Hg		Unmix Estimated Hg	
		Coal	Total	Coal	Total
2003	13.5	9.1	12.2	9.9	14.8
2004	19.7	13.1	17.6	15.5	21.1

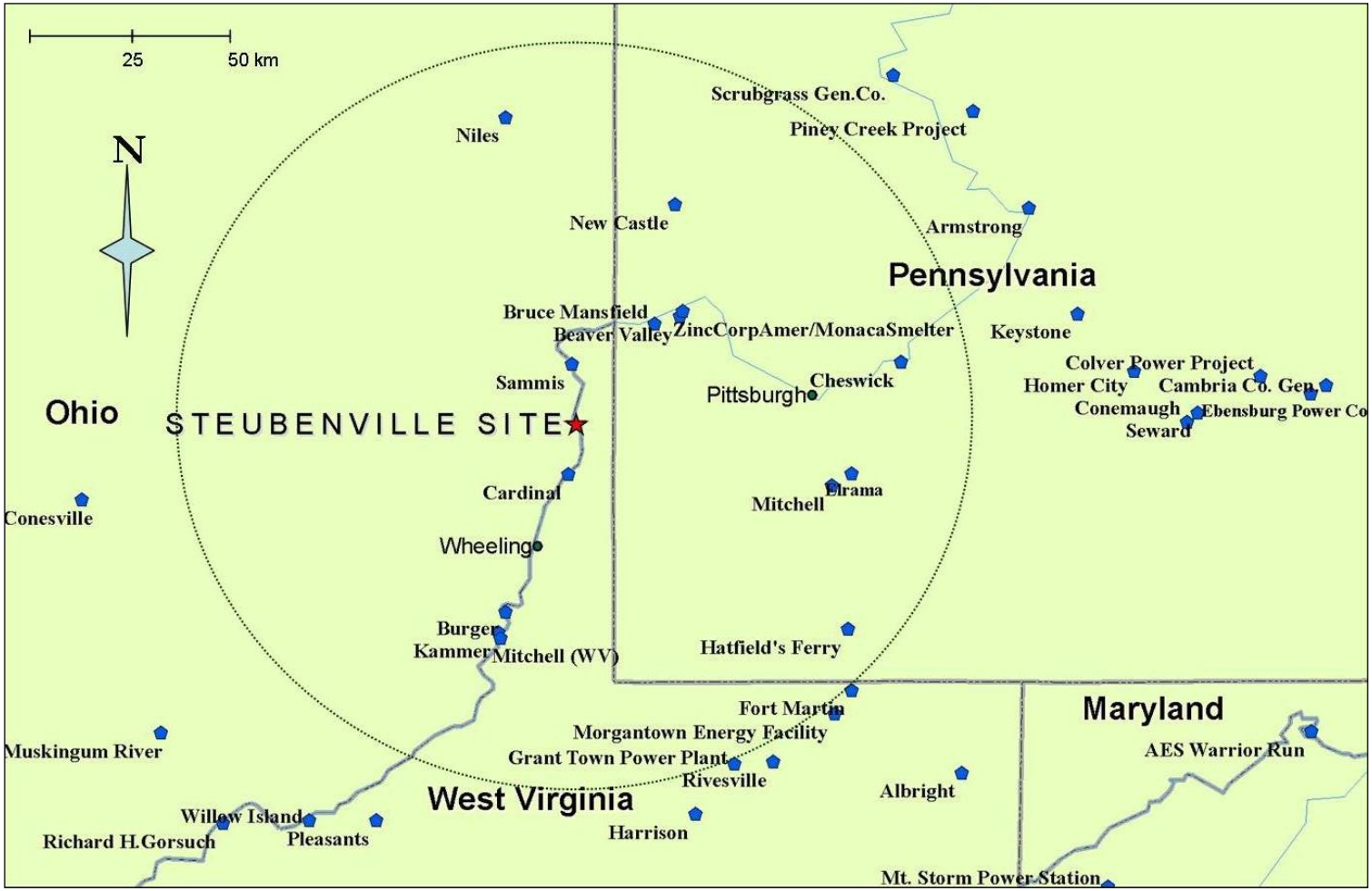

Figure II.1. Location of the Steubenville site in southeastern Ohio, surrounding coal-fired utility boilers, and a circle with a 100 km radius centered on the site.

Figure II.2a. PMF Predicted Deposition from Coal Combustion versus Measured Deposition of Hg at Steubenville, OH (2003-2004).

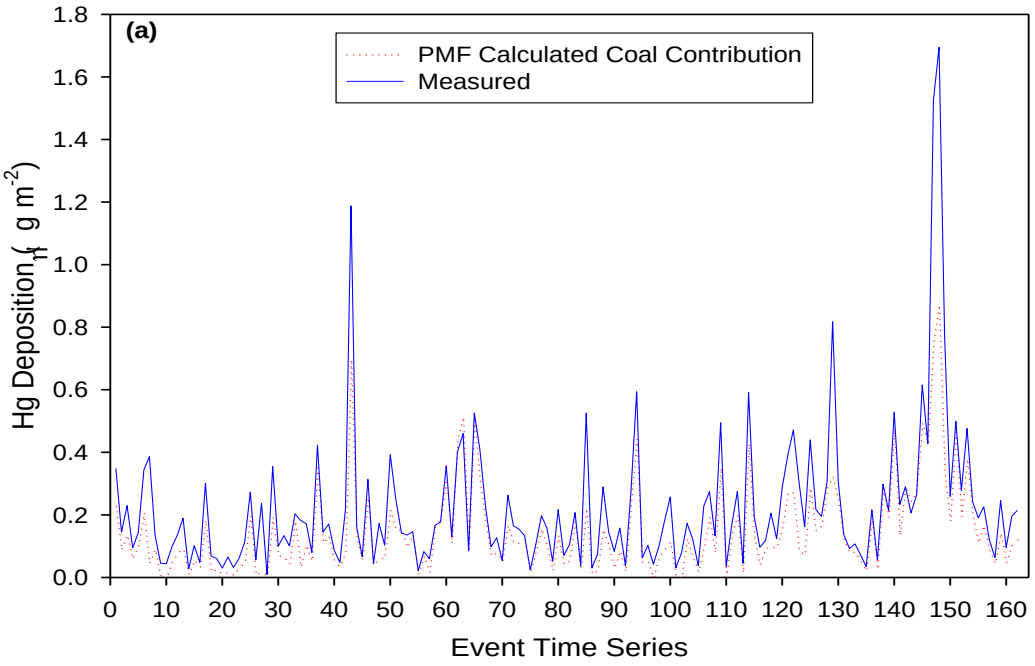

Figure II.2b. Unmix Predicted Deposition from Coal Combustion versus Measured Deposition of Hg at Steubenville, OH (2003-2004).

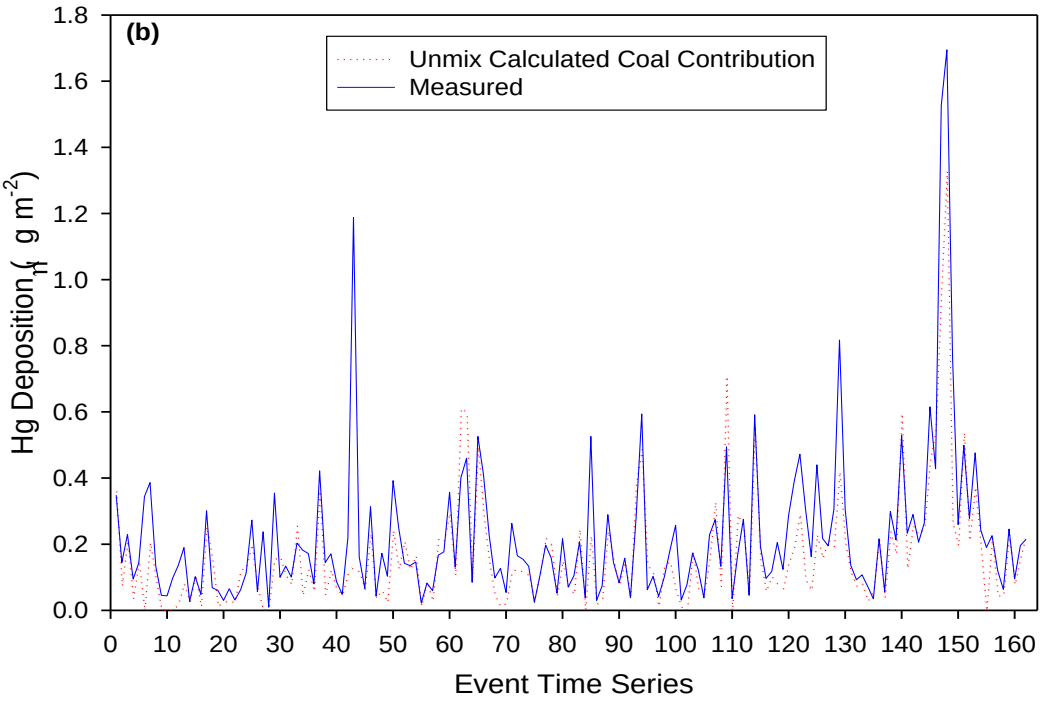

CHAPTER II: Supplemental Information

Table II.S1 provides the MDLs and analytical precision for each trace element quantified by the Element and retained for source apportionment modeling. The MDLs were calculated as the relative standard deviation of seven replicate analyses assuming the Student's t value for a 99% confidence interval and a 1-sigma estimate with n-1 degrees of freedom (3.14 for seven replicates) according to EPA method 200.8 (1). The volume-weighted mean concentrations are also shown and are more than ten times the MDLs for all elements given. The low detection limits and excellent precision obtained using the Element, as well as its ability to definitively exclude polyatomic interferences, make it an excellent analytical tool for receptor modeling applications.

Table II.S1. MDL and precision for each trace element analyzed by HR-ICPMS (N=162).

Element	Isotope	Resolution	2003-2004 VWA (ppb)	MDL (ppb)	*Precision (%)
Mg	24	MR	72.71	0.49	3.5
Al	27	MR	39.5	3.5	6.9
P	31	MR	4.88	0.14	4.7
S	32	MR	997.3	6.8	3.8
Ti	47	MR	2.17	0.08	3.7
V	51	MR	0.328	0.0045	2.8
Cr	52	MR	0.21	0.009	2.9
Mn	55	MR	7.28	0.070	4.9
Fe	57	MR	34.34	0.97	6.6
Co	59	MR	0.032	0.001	5.9
Ni	60	MR	0.681	0.081	3.6
Cu	63	MR	3.75	1.48	4.0
Zn	66	MR	7.19	1.06	3.9
As	75	HR	0.115	0.018	9.0
Se	77	HR	0.314	0.035	10.7
Rb	85	LR	0.078	0.003	3.7
Sr	88	LR	0.790	0.011	3.6
Mo	95	LR	0.270	0.030	4.3
Cd	111	LR	0.079	0.025	4.9
La	139	LR	0.054	0.001	3.4
Ce	140	LR	0.107	0.001	3.3
Sm	147	LR	0.010	0.0002	12.0
Pb	208	LR	0.89	0.03	3.2

*Based on replicate analyses

Figure II.S1a. PMF Predicted Deposition (All Sources) versus Measured Deposition of Hg at Steubenville, OH (2003-2004).

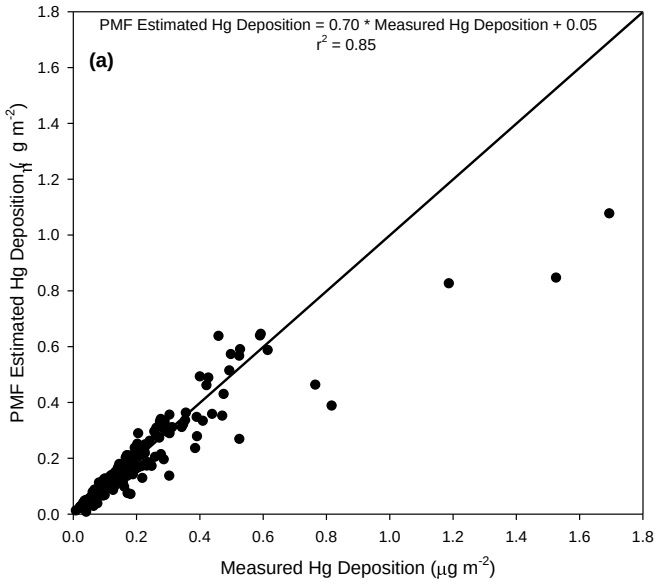

Figure II.S1b. Unmix Predicted Deposition (All Sources) versus Measured Deposition of Hg at Steubenville, OH (2003-2004).

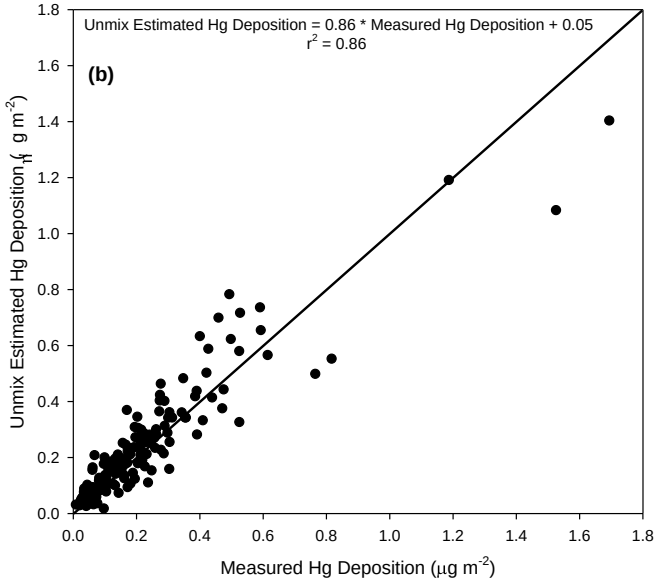

Figure II.S2a-d: Three day back trajectory plots for 2004 high deposition events (Sample IDs 141,159,160,161).

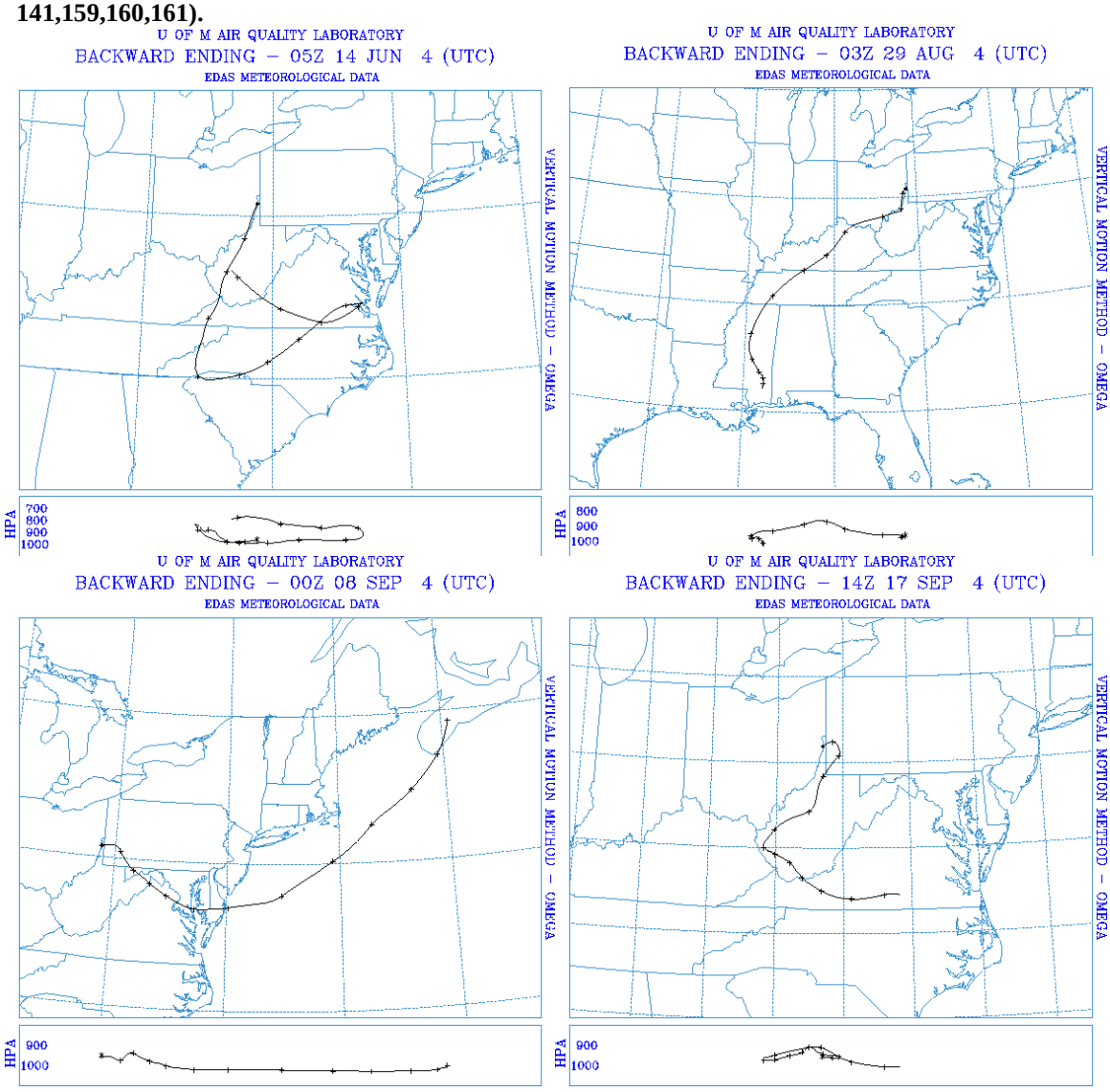

CHAPTER II: References

(1) Landis, M. S.; Keeler G.J. Atmospheric mercury deposition to Lake Michigan during the Lake Michigan Mass Balance Study. *Environ. Sci. Technol.* **2002**, 36, 4518-4524.

(2) Rolfhus, K.R.; Sakamoto, H.E.; Cleckner, L.B.; Stoor, R.W.; Babiarz, C.L.; Back, R.C.; Manolopoulos, H.; Hurley, J.P. Distribution and fluxes of total and methylmercury in Lake Superior. *Environ. Sci. Technol.* **2003**, 37, 865-872.

(3) Nriagu, J. Global metal pollution: poisoning the biosphere. *Environment* **1990**, 32, 28-32.

(4) Expert Panel on Mercury Atmospheric Processes (EPMAP). *Mercury Atmospheric Processes: A Synthesis Report*. EPRI/TR-104214, **1994**.

(5) Keeler, G.; Glinsorn, G.; Pirrone N. Particulate mercury in the atmosphere: its significance, transport, transformation and sources. *Water Air Soil Pollut*. **1995**, 80, 159-168.

(6) Landis, M. S.; Keeler G.J.; Al-Wali, K. I.; Stevens, R. K.; Divalent inorganic reactive gaseous mercury emissions from a mercury cell chlor-alkali plant and its impact on near-field atmospheric dry deposition. *Atmos. Environ.* **2004**, 38, 613-622.

(7) Iverfeldt, A. Occurrence and turnover of atmospheric mercury over the Nordic countries.*Water, Air, Soil Pollut*. **1991**, 56, 251-265.

(8) Landis, M.S.; Vette, A. F.; Keeler, G.J. Atmospheric Mercury in the Lake Michigan Basin: Influence of the Chicago/Gary Urban Area. *Environ. Sci. Technol.* **2002**, 36, 4508-4517.

(9) U.S. Environmental Protection Agency. *Mercury Study Report to Congress*; EPA-452/R-97-005 Office of Air Quality Planning and Standards, Office of Research and Development: Washington, DC, **1997**.

(10) U.S. Environmental Protection Agency. *Standards of performance for new and existing stationary sources: Electric utility steam generating units; Final Rule*; Federal Register Vol. 70, No. 95 May **2005**.

(11) Dvonch, J.T.; Graney, J.R.; Marsik, F.J.; Keeler, G.J.; Stevens, R.K. Use of elemental tracers to source apportion mercury in south Florida precipitation. *Environ. Sci. Technol.* **1999**, 33, 4522-4527.

(12) Anderson, M.J.; Daly, E.P.; Miller, S.L.; Milford, J.B. Source apportionment of exposures to volatile organic compounds. I. Evaluation of receptor models using simulated exposure data. *Atmos. Environ*. **2002**, 36, 3643-3658.

(13) Lewis, C.W.; Norris, G.; Henry, R. Source apportionment of Phoenix PM2.5 aerosol with the Unmix receptor model. J. of Air & Waste Manage. Assoc. **2003**, 53, 325-338.

(14) Paatero, P; Tapper, U. Positive matrix factorization—a nonnegative factor model with optimal utilization of error estimates of data values. *Environmetrics*. **1994**, 5, 111-126.

(15) Anttila, P.; Paatero, P.; Tapper, U.; Jarvinen, O. Source identification of bulk wet deposition in Finland by positive matrix factorization. *Atmos. Environ.* **1995**, 14, 1705-1718.

(16) Dockery, D.W.; Pope, C.; Xu, X.; Spengler, J.; Ware, J.; Fay,M.; Ferris, B.; Speizer, F. An association between air pollution and mortality in six U.S. cities. *The New England Journal of Medicine, 1993*, 329, 1753-1759.

(17) Ross H. B. Trace metal wet deposition in Sweden: insight gained from daily wet only collection. *Atmos. Environ.* **1990**, 24A**,** 1929.

(18) Hoyer, M.E.; Burke, J.B.; Keeler, G.J. Atmospheric sources, transport and deposition of mercury in Michigan: two years of event precipitation. *Water Air Soil Pollut.* **1995**, 80, 199-208.

(19) Landis, M.S.; Keeler, G.J. Critical evaluation of a modified automatic wet-only precipitation collector for mercury and trace element determinations. *Environ. Sci. Technol.* **1997**, 31, 2610-2615.

(20) Keeler, G.J.; Gratz, L.; Al-Wali, K. Influences on the long-term atmospheric mercury wet deposition at Underhill, Vermont. *Ecotoxicology*, **2005**, 14, 71-83.

(21) Keeler, G.J.; Dvonch, J.T. Atmospheric mercury: A decade of observations in the Great Lakes. *In:* Dynamics of Mercury Pollution on Regional and Global Scales:

Atmospheric Processes and Human Exposures around the World. N. Pirrone and K. Mahaffey Eds. Kluwer Ltd. **2005**.

(22) Fitzgerald, W. F.; Gill, G.A. Subnanogram determination of mercury by two-stage gold amalgamation and gas phase detection applied to atmospheric analysis. *Anal. Chem*. **1979**, 51, 1714-1720.

(23) *Methods for the Determination of Metals in Environmental Samples.* U.S. Environmental Protection Agency, Office of Research and Development, Environmental Monitoring Systems Laboratory; CRC Press, Inc.: Boca Raton, FL, **1992**; pp 95-137.

(24) Graney, J.R.; Landis, M.S.; Norris, G.A. Concentrations and solubilities of metals from indoor and personal exposure PM2.5 samples. *Atmos. Environ.* **2004**, 38, 237-247.

(25) Montaser, A. 1998. Inductively Coupled Plasma Mass Spectrometry. New York: Wiley-VCH, Inc.

(26) Eberly, S. EPA PMF 1.1 User's Guide, U.S. Environmental Protection Agency, June 30, 2005.

(27) Norris, G.; Henry, R.; Vedantham, R. EPA Unmix 5.0 User Guide, U.S. Environmental Protection Agency, January **2006**.

(28) Draxler, R.R; Hess, G.D. **1997**, Description of the HYSPLIT_4 Modeling System. NOAA TECHNICAL MEMORANDUM ERL ARL-224.

(29) Biegalski, S.R.; Landsberger, S.; Hoff, R.M. Source-receptor modeling using trace metals in aerosols collected at three rural Canadian Great Lakes sampling stations *J. Air Waste Manage. Assoc.* **1998**, 48, p227.

(30) Gordon, G.E. Receptor models. *Environ. Sci. Technol.* **1988**, 22, 1132-1142.

(31) Grahame, T.; Hidy, G. Using factor analysis to attribute health impacts of particulate pollution sources. *Inhal. Tox.* **2004**, 16, 143-152.

(32) Greenberg, R.R.; Gordon, G.E., Zoller, W.H., Jacko, R.B., Neuendorf, D.W. and York, K.J. Composition of particles emitted from the Nicosia municipal incinerator. *Environ. Sci. Technol.* **1978**, 12, 1329-1332.

(33) Kitto, M.E. Trace-element patterns in fuel oils and gasolines for use in source apportionment. *J. Air Waste Manage. Assoc.*, **1993**, 43, 1381-1388.

(34) Suarez, A.E.; Ondov, J.M. Ambient aerosol concentrations of elements resolved by size and by source: contributions of some cytokine-active metals from coal- and oil-fired power plants. *Energy and Fuels*, **2002**, 16, 562-568.
(35) Poirot, R.L.; Wishinski, P.R.; Hopke, P.K.; Polissar, A.V. Comparative application of multiple receptor methods to identify aerosol sources in northern Vermont. *Environ. Sci. Technol.* **2001**, 35, 4622-4636.
(36) Moody, J. L.; Samson, P. J. The influence of atmospheric transport on precipitation chemistry at two sites in the Midwestern United States. *Atmos. Environ.* **1989**, 23, 2117-2132.
(37) Dvonch, J.T.; Keeler, G.J.; Marsik, F.J. The Use of WSR-88D Radar Data for Source-Apportionment of Wet-Deposition Measurements from the 1995 SoFAMMS. *Journal of Applied Meteorology*, **2005,** 44 1421-1435.

CHAPTER III

Spatial Variability of Mercury Wet Deposition in Eastern Ohio: Summertime Meteorological Case Study Analysis of Local Source Influences

Abstract

Extensive exploration of event precipitation data in the Ohio River Valley indicates that coal combustion emissions play an important role in mercury (Hg) wet deposition. During July-September 2006, an intensive study was undertaken to discern the degree of local source influence. Source-receptor relationships were explored by establishing a set of wet deposition sites in and around Steubenville, Ohio. For the three-month period of study, volume-weighted mean Hg concentrations observed at the eight sites ranged from 10.2 to 22.3 ng L^{-1}, but this range increased drastically on an event basis with a maximum concentration of 89.4 and a minimum of 4.1 ng L^{-1}. A subset of events was explored in depth and the degree of variability in Hg concentrations between sites was linked to the degree of local source enhancement. Samples collected at sites less than one km from coal-fired utility stacks ("near-field") exhibited up to 72% enhancement in Hg concentrations over regionally representative samples on an event basis. Air mass transport and precipitating cell histories were traced in order to evaluate relationships between local point sources and the receptor sites. It was found that the interaction of several dynamic atmospheric parameters combined to favor local Hg concentration enhancement over more regional contribution. When significant meteorological factors (wind speed at time of maximum rain rate, wind speed 24-hours prior to precipitation, mixing height and observed ceiling) were explored, it was estimated that during summertime precipitation, 42% of Hg concentration in near-field samples could be attributed to the adjacent coal fired utility source.

Keywords: atmospheric mercury, wet deposition, local source impact, Ohio River Valley, source-receptor relationships

Introduction

Mercury (Hg) is a persistent heavy metal that bioaccumulates in organisms and biomagnifies through aquatic food chains. Inorganic Hg is transformed into highly toxic, organic methyl-mercury (MeHg) by aqueous biota, and is subsequently consumed by fish. Recent studies have shown that even low exposure may be associated with neurological and cardiovascular effects (*1*). Reproductive changes associated with Hg blood levels in the North American common loon have been found to have adverse effects on this species, while individual piscivorous mammals, such as mink and otter, demonstrate reduced avoidance behavior even at low Hg blood levels (*2*). While the major concern to the general public is MeHg concentrations in top predatory fish and the subsequent consumption of such species, understanding the means by which the contaminant enters the food chain is pivotal in designing strategies for reduction efforts.

Atmospheric transport is widely recognized as the primary method of Hg distribution in the environment. Direct atmospheric deposition of Hg can often be the most significant source of this contaminant to large lakes as found during the Lake Michigan Mass Balance Study (*3,4*). The form of Hg emissions and the synoptic scale meteorological patterns strongly influence the amount of Hg that is deposited nearby the source versus transported long distances. Mercury is emitted in three forms (gaseous elemental Hg-Hg^0, gaseous oxidized Hg-Hg^{2+} and particulate bound Hg-Hg_P) from anthropogenic sources including medical and municipal waste incinerators, cement plants, crematoriums, fluorescent light production, coke ovens, metal refineries, mining facilities and fossil fuel burning power plants. Mercury is also emitted naturally into the atmosphere, primarily as Hg^0, however, anthropogenic emissions account for between 50 and 75% of total global emissions (*5,6*). The spatial scale on which Hg is deposited is also a complex function of the concentrations of co-pollutants, chemical transformations, gas-particle interactions (*7*), stack height and other local-scale meteorological parameters. Hg^{2+} and Hg_P are relatively soluble and readily undergo heterogeneous reactions, resulting in much shorter atmospheric residence times than Hg^0 (*4, 8, 9*). Speciated stack measurements of anthropogenic Hg emissions (incineration, cement kilns and coal-fired utility boilers (CFUB)) have shown a significant percentage of total Hg to be in the Hg^{2+} and Hg_P forms (*10, 11*), and due to their short atmospheric life times, this suggests these

emissions may result in enhanced local/regional deposition gradients near anthropogenic sources.

Recent studies have linked MeHg concentrations in biota to atmospheric deposition of inorganic Hg (*12, 13*). In a 2006 study, 70% of the variability in small mouth bass MeHg concentration (EPA and individual state environmental program publications) was accounted for by differences in Hg wet deposition (state averages of National Atmospheric Deposition Program Mercury Deposition Network (MDN) results) alone, with little to no correlation between fish concentration and MeHg production physiochemical factors (*14*). It is important to note that two of the 25 states analyzed were not fit well by the linear regression model as MeHg concentrations in fish caught in New Hampshire and Maine exceeded that predicted by the Hg wet deposition. It was suggested that the deposition sites, located in rural areas of the two states, were not representative of the more industrially influenced areas of the states where a large number of the small mouth bass were caught and subsequently analyzed. The inaccurate characterization of atmospheric inputs due to collection at background precipitation sites caused under-prediction of Hg fish tissue concentrations and therefore suggests a regional or local impact of wet deposition on Hg concentrations in the tissue of the sampled fish. The MDN requires monitoring site locations to be regionally representative; "and minimizes the impact of local point or area sources" (*15*). Although these criteria may allow for adequate representation of a regional loading, the near field impact of large point sources and urban/industrial areas cannot be evaluated. Large-scale interpolation maps created by MDN do not depict local gradations or deposition "hotspots" because the siting criteria preclude data collection in areas that could potentially be impacted by large anthropogenic sources.

The importance of local and regional influences on near-field wet deposition has been previously reported with significant Hg deposition gradients near industrial and urbanized areas (*7, 8, 16*). Wet deposition data collected throughout the Great Lakes over the past decade has demonstrated distinct regional variability and a robust north-south gradient in Hg concentration and deposition (*17, 18*). In south Florida the spatial and temporal patterns of wet deposited mercury were strongly influenced by local anthropogenic sources (*19, 20*). The Chicago/Gary urban area has been shown to have substantial

influence over Hg concentrations in precipitation when multiple wet deposition sites were examined concurrently; sites less than 100 km apart differed in yearly volume weighted mean Hg concentration by over 30% (*6*). Precipitation samples collected in southeastern Michigan revealed 25-35% enhancement in the VWM Hg concentration between urban sites in Detroit and a rural site (Dexter, MI) ~60 km east (*21*, *22*).

In November 2002, an enhanced air monitoring site was established in Steubenville, OH to investigate source-receptor relationships for Hg deposition in Eastern Ohio. The site overlooking the Ohio River was in close proximity to several anthropogenic point sources including numerous CFUBs (see Figure 1). It was determined that ~70% of the Hg in wet deposition was due to CFUBs and it was suggested that local sources played a significant role (*23*). The relative contribution of local sources to the elevated Hg concentrations observed in eastern Ohio is the main focus of this paper.

Experimental Methods

Measurement Sites

Event wet-deposition samples were collected at the 'primary' monitoring site in Steubenville, OH (STB) and at four "satellite" sites for the period from July through September 2006 using a wet-only precipitation sampling system (*24*). These systems were placed at the four 'satellite' sites located ~40 km north (STN), south (STS), east (STE) and west (STW) of the STB site (Figure III.1, Table III.S1). In addition, wet-deposition collectors were manually deployed at several locations including along the Ohio River (STR, minimal lateral displacement from the primary site but approximately 300 m below STB), within 1 km of Cardinal (CAR-EST1, CAR-EST2, CAR-NRT, CAR-WST, CAR-SOU) and Sammis (SAM-EST, SAM-NOR) CFUBs, here-by referred to as 'near-field' sites. The manually deployed samplers utilized identical sample trains as the automated collectors but were deployed just prior to forecasted precipitation events and samples were collected immediately following the termination of the events, to reduce any potential dry deposition to the collector. When operated in this manner the manual and automated wet-only methods were equivalent (*24*). Samples at all sites were collected on an event basis, with "event" defined as the abatement of rain for 3 hours. Event sampling was essential for receptor modeling as well as meteorological analysis,

since integrating more than one event would preclude tracking the history of the precipitating air mass and would obscure the source chemical signature.

Event Deposition Sampling and Analysis

All precipitation collectors were configured with two sample trains: one for total Hg analysis, the other for trace element and ion analysis. The collection of all precipitation samples for Hg and trace elements followed the procedures previously described by Landis and Keeler (*24*). The only deviation from the procedure was the addition of an internal 1% v/v BrCl polishing soak of the 1 L Teflon sample bottles to ensure that every bottle was Hg-free prior to sampling.

Hg samples were returned to the University of Michigan Air Quality Laboratory (UMAQL), where each sample was oxidized with a concentrated BrCl solution to 1% (v/v) and stored in a dark cold room. Analysis of total Hg was preformed in a clean room using a Tekran Instruments Corporation (Knoxville, TN) Series 2600 Automated Water Analysis System with cold-vapor atomic fluorescence spectroscopy (CVAFS). Trace element samples were acidified to a 0.2% HNO_3, 0.1% HCl v/v solution and stored in a dark cold room for over 14 days to provide adequate time for optimal leaching (*25*). A suite of 48 trace elements were quantified using a ThermoFinnigan Element2 high-resolution magnetic sector field inductively coupled plasma mass spectrometer (HR-ICPMS). Major ion concentrations were determined using a Dionex model DX-600 ion chromatograph.

Meteorological Data and Analysis

The main Steubenville site was equipped with an anemometer and thermocouple, meteorological data was integrated and recorded at 5 min intervals. Two collocated RM Young tipping buckets, measuring 0.1 mm precipitation depth increments, were used to determine event initiation, duration, intensity, total event accumulations and time of maximum precipitation. A tipping bucket was also deployed at STW. Cloud base heights were obtained from hourly surface observations in Wheeling, WV (40 km south of STB) and soundings were obtained from Pittsburg, PA for determination of atmospheric stability.

National Climatic Data Center (NCDC) archived Doppler radar (WSR-88D) data from Pittsburgh, PA (KPBZ) was used to identify path-history of precipitating cells impacting

the wet deposition sites, as well as determine the spatial scales of transport for air feeding these precipitating cells. Tracking the precipitation cells as they moved through the study area allowed us to infer which sources likely contributed to the mercury burden within a given precipitating cell. Precipitation cell history was tracked using Level II NEXRAD radar data in GRLevelX Analyst (Gibson Ridge Software, LLC), a volumetric visualization tool. Events depicted in the figures of the following sections show Level III NEXRAD radar storm total precipitation product over-lay from the Pittsburgh radar. Visual representations and shape files shown were creating using the NCDC's Java NEXRAD viewer and ArcGIS.

Hg Concentration and Deposition Summary Results

Table 1 provides a summary of the data collected July to September 2006. All samples collected at a particular near-field location were used to calculate a single volume-weighted mean (VWM), e.g., all samples collected near the Cardinal CFUB, CAR-EST1, CAR-EST2, CAR-WST, CAR-NRT and CAR-SOU were averaged as "CAR". Manual sample collection trains were deployed only under conditions when the probability of precipitation was >70% and approaching systems were observed on PBZ radar, so small or unpredicted events were not collected, and therefore total deposition and precipitation depth for manually collected samples could not be calculated and compared to totals collected at the sites with automated collectors.

Minimum Hg concentrations ranged from 4.1 to 5.8 ng L^{-1} across the sampling sites. The maximum concentration at a satellite site was 49.2 ng L^{-1}, much lower than the maximum concentration sampled at a near-field site (89.4 ng L^{-1}). The VWM concentrations across the sites ranged from 10.2 to 22.3 ng L^{-1}. Because the precipitation depth varied among the sites for the study period, a comparison between measured sample precipitation depth and that observed at the nearest meteorological station provided confidence in the variability of the amount of precipitation impacting a given site (See Table III.1).

Comparison between the samples collected during the intensive study and those from the five-year study at the STB site revealed that the intensive study period reported here

was not atypical of Hg data collected during the other summertime periods of record. The baseline precipitation Hg concentration at STB during the multi-year study was found to be 6.1 ng L^{-1} (baseline operationally defined as 5th percentile), and the 95th percentile Hg concentration was 42.0 ng L^{-1}. Overall, the STB Hg concentration baseline was twice the baseline observed at our other sites in the Great Lakes Region during the four-year period. The contrast in Hg wet deposition across the Great Lakes region can be seen in Figure III.S1 of the Supporting Information via illustrations of the total deposition and volume-weighted mean (VWM) concentrations for the last 4 years at sites in Michigan and Ohio.

The influence of precipitation amount on the concentration of Hg was determined for samples collected during the intensive study and only 7% of the variability ($p=0.001$) in Hg concentration could be explained by precipitation depth (Supporting Information, Figure III.S2), indicating that dilution of large rainfall amounts or enhancement of Hg in lower precipitation depths did not account for the large range in Hg concentrations.

Individual Event Case Study Results

Twenty-three distinct events were collected during the three-month study. Nine of the 23 events were concurrently observed with sufficient precipitation depth (all samples ≥ 1 mm) to deposit substantial precipitation volume at (i) four of five primary and satellite sites and (ii) two or more manually deployed 'near-field' collection sites. The meteorological conditions and the resultant Hg deposition were investigated in-depth for the nine events. The degree of spatial variability in rainfall Hg concentrations between concurrently collected samples was not uniform and differed by precipitation event. The Hg concentrations measured in the samples during the nine major events were classified by calculating the event Coefficient of Variation (c_v), a normalized measure of the dispersion of the data distribution, as standard deviation of Hg concentrations divided by the mean Hg concentration for the event. The events fell into three distinct categories: (1) low spatial variability, with low and high concentrations ($c_v<0.2$), (2) moderate spatial variability ($0.3<c_v<0.5$), and (3) high spatial variability ($c_v>0.5$). Table III.2 contains statistics for each of the nine events, as well as the meteorological parameters that were found to be statistically significant in relation to individual event coefficient of

variability. Other meteorological parameters associated with these events can be found in the Supporting Information (Table III.S2). Individual events from the low and high variability categories are discussed in the following section, while those that fell into the moderately variable category are left to the supporting materials (Supporting information text and Figure III.S3).

Our analyses suggest that the variability of Hg concentration in samples collected during a single event can generally be attributed to the fact that there were sources present between two receptor sites along the precipitation path, and that Hg was fed into the precipitating cloud on a local, rather than regional scale. A local deposition gradient due to near-field point sources was observed on several occasions during the three-month collection period, as indicated by the 'high variability' category. Low variability among the samples collected during a given event was associated with occurrences of either a lesser influence by local sources and/or increased atmospheric mixing. Even samples collected at sampling sites very close to each other, e.g. samples collected near the Cardinal facility with ~0.5 km spacing, exhibited sample variability of up to 62% (CAR-NOR and CAR-SOU on 8/14). Variability of this magnitude exceeded the variability observed in collocated precipitation samplers of 8.1% (*5*).

Another measure used to define the variability among Hg concentrations for a given event was percent enhancement of near-field samples, calculated using equation III.1:

$$\% \text{ Near-field Attribution} = 1-(VWM_{satellite}/VWM_{near\text{-}field}) * 100 \quad \text{(III.1)}$$

The % Near-field Attribution is the percentage of the Hg concentration collected at the near-field sites attributed to the adjacent coal fired utility. The calculated values ranged from 0 to 72% for the nine cases examined, with an average of 41%.

Another approach used to determine source proximity was the sample Hg concentration and the Sulfur/Selenium (S/Se) ratio relationship. In absence of coal-type differentiation and without prior knowledge of pollution control technology, S/Se variability can be used as a proxy for distance from coal source influence. S and Se are co-pollutants, but there is an important difference in the chemical conversion properties of the two elements. S is emitted from CFUBs as SO_2 and is converted to sulfuric acid droplets and particles relatively slowly, over distances on the order of hundreds of kilometers (*26, 27*). Se is

emitted both in the gaseous and particulate form, but the gas condenses on particulates much more rapidly than conversion of SO_2 to particulate sulfate, and concentration of Se drops off more quickly due to deposition with transport distance. The S measured in rain is primarily SO_4^{2-}, and therefore as one samples at progressive distances away from large coal fired sources, the S/Se ratio typically increases, gradually reaching steady state until another large point source is encountered along the air parcel's trajectory. Regional steady state has been previously defined as S/Se > 3000 (*28*).

Low Hg Variability: August 3, 2006. This event, while low in relative variability, exhibited high concentrations at every site (VWM = 35.5 ng L^{-1}, Figure III.2(a)). In this case, precipitation depths influenced the concentration differences, as the lowest depth corresponded to the highest concentrations (Figure III.S4(a)). Severe thunderstorms occurred in the warm sector ahead of a cold front for this event, with severe precipitation cells approaching from the west. The mixing height was 2070 m, allowing for a large volume to mix boundary layer air. Surface observations indicated a ceiling of 2100 m, consistent with the mixing height. All S/Se ratios were well above steady state values of 3000, indicating a regionally representative boundary layer. Surface winds were moderate to high from the southwest throughout the event, with 5 min sustained gusts of 6 m s^{-1}, the highest winds of the 2006 summer. The 6 h average wind speed 24 h prior to the event was 3.8 m s^{-1}. This observed strong southwesterly flow would provide the environment for the transport of pollutants up the Ohio River Valley, resulting in high rainfall mercury concentrations. Regional- transport likely resulted in significant mixing of the airmass and thus the subsequent low variability.

Low Hg Variability: September 1, 2006. Unlike the August 3 low variability event, all samples collected during the September 1 event were close to what we have considered 'baseline' for the Steubenville area, with an event VWM of 4.9 (See Figure III.2(b)). In fact, the small variability among the sample concentrations was not much higher than our collocated sample precision. Variability among the concentrations can be accounted for by sample depth, as there is a significant negative relationship between concentration and depth when the STE sample is removed as it contained 0.5 cm more rain than other samples collected during the event (r^2 = 0.4858, p=0.037, Supplemental information: Figure III.S4(b)). All Se values were below the method detection limit

(MDL) (0.012 ppb). Using five-times the Se MDL yields all S/Se ratios greater than or equal to 3000, an indication of a regional background signature for all samples collected. Northeasterly surface winds were sustained prior to and during rain, an event associated with the remnants of the western edge of Hurricane Ernesto, and winds averaged 5.6 m sec^{-1} during maximum rain. The rapid air parcel transport helped to explain the regional, well-mixed background characteristic of the sample concentrations. The ceiling was reported at 3658 m.

High Hg Variability: July 22, 2006. This event lasted from approximately 03:45 to 05:00 EST, with an average rain fall rate of 7.8 mm h^{-1}. The convective event was associated with a large low pressure system and while precipitating cell movement was from the southwest, measured surface winds indicated air transport in the boundary layer from the south-south-west during maximum precipitation intensity. Maximum Hg concentrations were collected adjacent to the Cardinal facility (58.5, 47.0 and 32.7 ng L^{-1}; CAR-EST2, CAR-WST and CAR-SOU, respectively) with lowest concentration found at STN (7.9 ng L^{-1}; Figure III.3(a)). For this highly variable event, the mixing height was only 250 m and the observed cloud ceiling was reported at 274 m. Surface winds were particularly stagnant, averaging 1.5 m s^{-1} during the event, with a 24 h average prior to the event of 1.2 m s^{-1}.

Precipitation depth varied from 1-5 cm but this did not explain the difference in Hg concentration as sites with similar depths exhibited a large range in Hg concentration, and therefore wet deposition (Figure III.S5(a)). For the July 22 event, the S/Se to Hg concentration relationship is particularly significant ($r^2 = 0.957$, $p<0.001$, Figure III.S6), indicating that distance from source is a prime driver for the Hg concentration differences.

High Hg Variability: August 14, 2006. Convection occurred along a distinct cold front late in the evening of August 14, with precipitation lasting 45 min. While all precipitation occurred along the frontal boundary, two distinct cells seemed to contribute to the rain, with all but the northern most site receiving rain from a southern cell (Figure III.3(b)). The observed rainfall depth was not correlated to Hg concentrations (See Figure III.S5b). For example, identical rainfall depths were observed at STN and STE, with concentrations of 7.8 and 19.8 ng L^{-1}, respectively. On an even smaller spatial

displacement (<0.5 km), samples collected at sites CAR-EST2 and CAR-SOU (depths of 0.67 and 0.64 cm) differed by 21.7 ng L^{-1}. The large difference between these near-field collected sample concentrations was likely due to the combination of surface winds and sample collection placement. Namely, with surface winds from the south shifting to west, the stack plume from the Cardinal facility was observed directly overhead of the CAR-EST2 and CAR-NOR sample sites during the rain event, with the plume directed *away* from the CAR-SOU site. It appears the rain 'scrubbed' the CFUB's plume in two of the three cases, possibly scavenging the reactive gases and some particles. Of the nine samples collected during this event, four contained S/Se ratios below 'steady state,' indicating that a coal combustion point source had influenced the precipitation chemistry between the receptor sites, and these corresponded to the samples with the four highest Hg concentrations (STE, CAR-SOU, CAR-NOR, CAR-EST2).

The boundary layer mixing height was 593 m, while the observed ceiling was during 457 m during thundershowers with fog. Severe weather cells moved through the Ohio River Valley along a southwest to northeast trajectory. Relatively calm (1.9 m s^{-1}) southerly surface winds prior to the event shifted to westerly during the course of the storm, with wind speeds at 1.2 m s^{-1} during maximum rain intensity. It is of importance to note the degree of local stagnation as surface winds measured at Steubenville averaged 0.6 m s^{-1} 24 h prior to rainfall, as all things remaining equal, post-release ambient concentration of pollutants emitted from a stack will be higher if emitted into slow wind conditions.

High Hg Variability: September 28, 2006. High variability during this event is accentuated once again by the large difference between near field samples; with westerly surface winds dominating during the rain event, the sample collected just east (SAM-EST) of the Sammis facility contained precipitation with Hg concentrations more than twice that collected to the north (SAM-NOR) of the stacks (26.8 and 12.0 ng L^{-1}, respectively), suggesting that rain had fallen through the plume, resulting in a washout of pollutants. Samples collected near the Cardinal facility did not exhibit a similar level of variability, but it can be seen in Figure III.3(c) that the large variability in Hg concentration during this event is enhanced by these near field samples. Only three samples exhibited S/Se ratios below 'background' – three of the four near-field samples,

with the exception of SAM-NOR – indicating that wind direction can have a distinct effect on the degree to which a collection site might be locally enhanced by point sources.

Rain occurred along a distinct cold front that was moving west to east across the Northeastern U.S. The most intense portion of the precipitation field passed through the Ohio River Valley in late morning on September 28. The cloud base was reported at 1128 m during heaviest rain, with a mixing height of 500 m. The majority of the rain fell in 4 h, from 07:00 to 11:00 EST, the most intense rain was observed at 10:00 with winds at 1.9 m s^{-1}. There was no significant relationship between precipitation depth and concentration (See Figure III.S5c)

Case study implications

Overall, precipitation depth was found to account for only 7% of concentration variability and a strong depth/concentration relationship was observed only during events that exhibited regionally well-mixed characteristics and low between-site variability, it was concluded that, for the period studied, local source emissions had a greater impact on concentrations than precipitation depth differences for near-field sites within the Steubenville area. Unlike larger scale regionally representative Hg deposition collection, concentrations could not be spatially interpolated due to exceptionally tight gradients, invalidating the basic assumptions of spatial interpolation.

The Coefficient of Variance and Near-field Attribution of the Hg concentrations observed concurrently at the sites were somewhat correlated (r^2= 0.62, p=0.012). Differences between the two descriptive parameters were due to spatial anisotropy in the events; directionality of winds, airmass transport and precipitating cell movement cause satellite sites that are downwind of point sources to be higher in Hg concentration, while the near-field attribution calculation was determined only by the absolute distance from coal combustion point sources, not direction.

The nine case studies examined highlighted four distinct meteorological conditions that influenced the degree to which Hg concentration is enhanced on a local scale during a particular precipitation event. The most significant factor in determining the degree of spatial variability and near-field attribution of Hg concentrations was surface wind speed during the period of maximum rain rate. When relatively low wind speeds were observed

during these periods of maximum rain rates, we suggest that boundary layer mixing was reduced, resulting in tight deposition gradients. A linear regression analysis exhibits these relationships in supplemental material Figure III.S7(a) (both significant at $p<0.05$). It was also found that low boundary layer heights coincided with reduced vertical dispersion and consequently local deposition patterns, while a higher boundary layer coincides with lower variability among concentrations collected as indicative of regional influence. The nine events studied are compared in the supplemental material Figure III.S7(b), and a relationship can be seen between mixed layer height and both the coefficient of variability in Hg concentration and the percent attribution to the near field site concentrations. The other two meteorological factors that demonstrated relationships were the 6 h average of wind speeds 24 h prior and the lowest observed ceiling during precipitation, these relationships can be seen in the supporting information Figures III.S7(c) and (d). When the four meteorological factors are examined in aggregate using multivariate linear regression (MLR), the significance of the relationship increases, with 95% of the variability in Coefficient of Variance explained by meteorological parameters ($p=0.008$). The MLR was slightly less statistically significant when the four meteorological parameters were regressed against Percent Attribution ($R^2 = 0.826$, $p=0.08$), most likely due to the lack of segregation between upwind and downwind Hg concentrations in the Percent Attribution calculation.

One of the major goals of this work was to determine the overall degree of individual source influence at near-field locations, as current wet deposition collection networks do not include near-field source sampling sites. Using the statistical model for the MLR, percent attribution and coefficient of variability were estimated for an additional 14 events during the three month period. It was found that for July, August and September 2006, there was a predicted average near-field source attribution of 42%, and that 19 of the 23 events were moderately or highly spatially variable (coefficient of variation > 0.3) in Hg concentration for the region studied. Of all precipitation from CY2003 through CY2006 at Steubenville, Ohio, 29% fell during the summer months of July, August and September. While we cannot use the equations of fit to extrapolate to cold weather months because of the difference in atmospheric chemistry, meteorology and cloud properties (i.e., ice, mixed or water-only), the results from the summer evaluation

indicate that coal-fired utility boiler near-field contribution to Hg concentration is significant and greater than previously estimated. Given that our study results suggest that meteorological parameters explain greater than 80% of the variability in local Hg deposition gradients during the study period, it is evident that local sources play a significant role. This work therefore establishes the need for longer-term multi-seasonal near-field wet deposition collection for discernment of an accurate local scale gradient of Hg wet-deposition in the vicinity of point sources.

Acknowledgements

This work has been funded wholly or in part by the U.S. Environmental Protection Agency Office of Research and Development through cooperative agreement R-82971601-0, and Student Services Contract EP07D000572. It has been subjected to Agency review and approved for publication. Mention of trade names or commercial products does not constitute an endorsement or recommendation for use. We thank Jim Barres and Ali Kamal (UMAQL) for managing laboratory support operations; Dr. James Slater (Franciscan University) for on-site logistical support; Brie Van Dam, David Reed, Naima Hall, and Lynne Gratz (UMAQL) for sample preparation and collection support. Additional thanks to Daniel Walls of Belmont Co. Sewer, Clarence Thompson and Tim Vittori of the Allegheny Co. Parks Department, Todd Metz of the Ohio DNR, and Todd Davis of FFA Camp Muskingham.

Table III.1: Sample site summary statistics. STB-STW are primary and satellite sites, CAR and SAM represent Cardinal and Sammis coal fired utility boiler near-field sample collection respectively. While samples < 1 mm were included in VWM calculations, these were not considered when determining maximum sample concentrations. The primary and satellite site statistics are found at the top of Table 1, with manually collected samples below the solid line.

	Site	N	Min event [Hg] ($ng\ L^{-1}$)	Max event [Hg] ($ng\ L^{-1}$)	VWM [Hg] ($ng\ L^{-1}$)	Three Month Hg Deposition ($\mu g\ m^{-2}$)	Three Month Precip. Depth (cm)	Met. Station Precip. Depth (cm)
Automatic	**STB**	23	4.8	34.2	11.8	2.9	27.4	29.3
	STN	20	4.8	45.9	10.2	2.8	29.6	27.5
	STE	17	4.4	49.2	12.8	2.5	21.5	22.2
	STS	21	5.8	30.1	12.9	2.1	18.0	21.7
	STW	24	5.1	29.4	10.6	2.9	28.3	32.4
Manual	**STR**	13	5.0	41.7	10.9			
	CAR	15	4.8	89.4	22.3			
	SAM	4	4.1	18.5	13.8			

					Event VWM† [Hg] (ng L^{-1})			Windspeed (m sec^{-1})			
	Date	Coeff of variation	% Near-Field Enhancement	Range (ng L^{-1})	All Sites	Satellite Sites	Near-Field Sites	During max rain rate	24 hours prior	Mixing Height (m)	Ceiling (m)
Low Variability	9/1 (low conc)	0.12	0%	0.4	4.9 ±0.4	5.0±0.4	4.8±0.4	5.6	2.5	806	3658
	8/3 (high conc)	0.19	20%	19.1	35.5±2.8	33.7±2.7	42.2±3.3	4.6	3.8	2070	2134
Moderate Variability	7/12	0.31	48%	6.7	6.5±0.5	5.9±0.5	11.5±0.9	4.1	1.8	602	884
	7/28	0.44	45%	20.5	18.3±1.5	12.6±1	22.9±1.8	4.0	2.5	702	518
	8/19	0.28	28%	13.2	15.0±1.1	13.9±1.1	19.4±1.6	3.9	1.6	1119	1494
	9/18	0.35*	66%	9.5	13.3±1.1	8.5±0.7	25.3±2.0	2.8	1.2	493	1463
High Variability	7/22	0.69	72%	50.6	24.3±1.9	12.9±1.0	46.96±3.8	1.6	0.9	250	274
	8/14	0.58	55%	27.3	21.0±1.7	12.7±1.0	28.3±2.3	1.2	0.6	593	457
	9/28	0.58	43%	21.1	12.9±1.0	8.0±0.6	14.1±1.1	1.9	2.3	497	1128

Table III.2 Individual statistics on the variability of Hg concentration across the sampling field and significant meteorological parameters for 9 precipitation events studied during the summer of 2006. See Table S2 for additional event statistics. *In this calculation, one sample has been removed due to exceptional high concentration as explained by direct plume hit; coefficient of variation equals 1.44 if this sample is included. See supplemental text for further explanation. †Volume weighted mean Hg concentration.

Figure III.1. Locations of precipitation collection sites and coal fired utility boilers in the Steubenville vicinity.

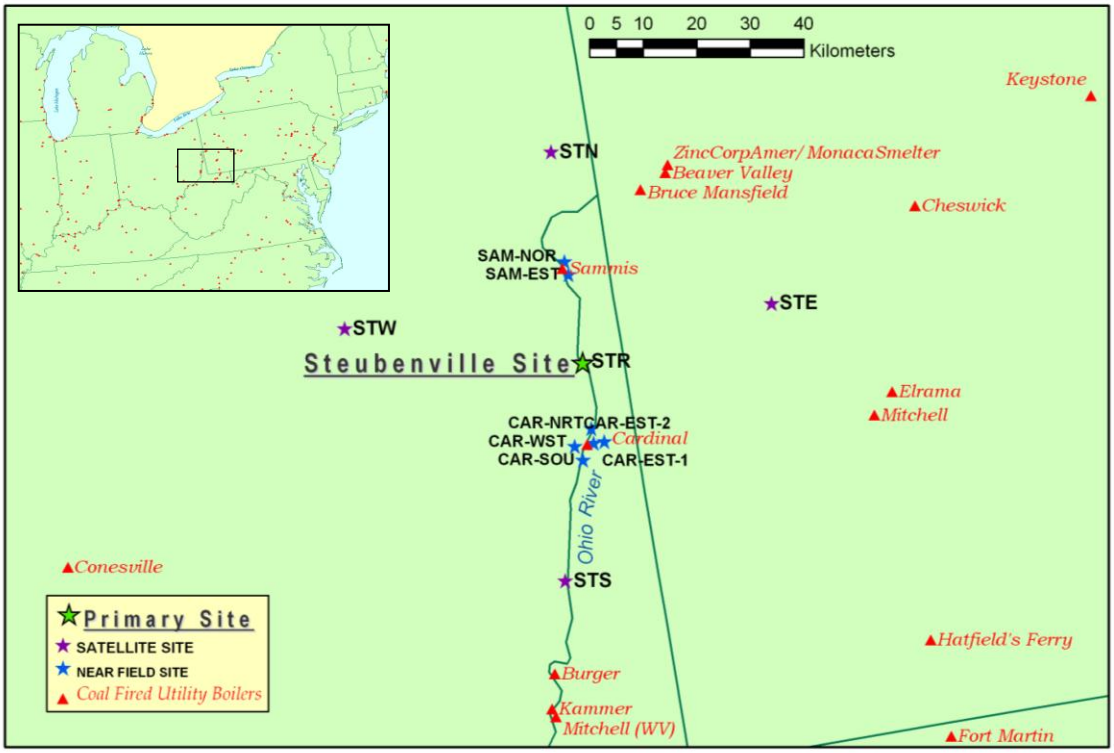

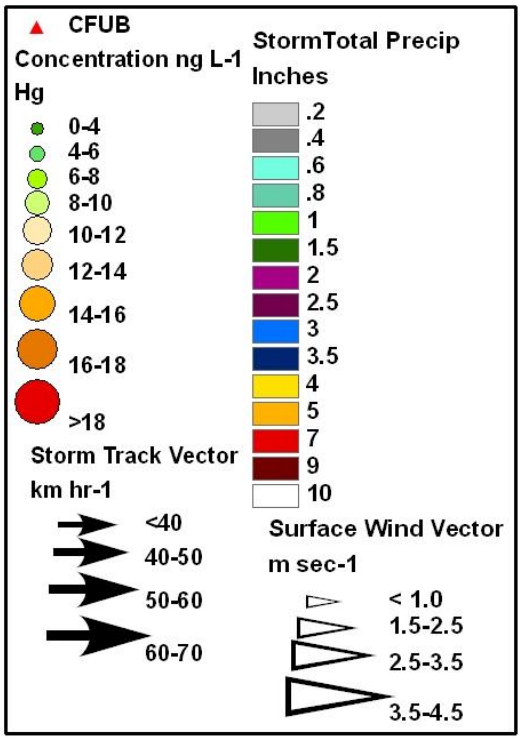

Legend for Figures III.2, III.3 and III.S3.

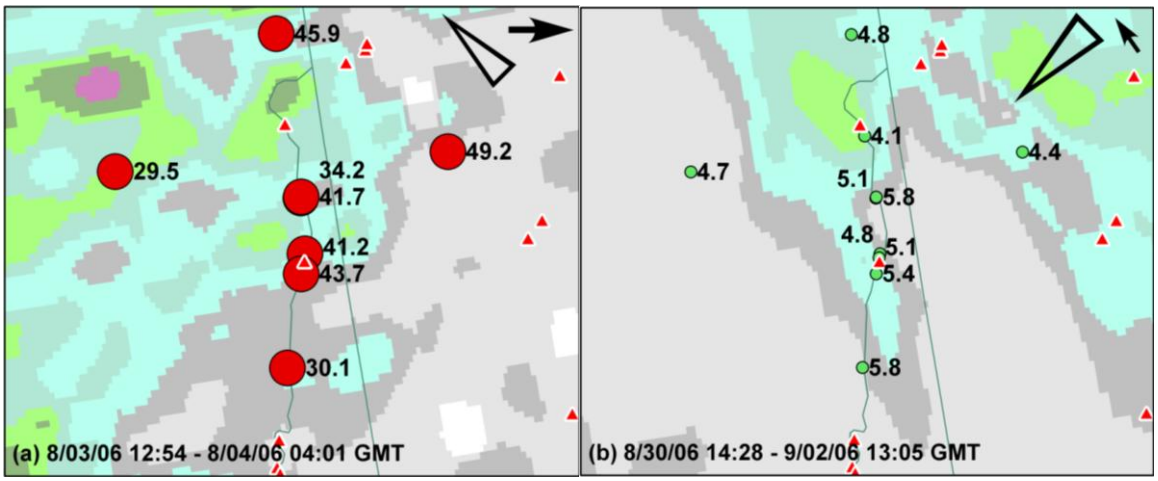

Figure III.2: Low Variability Hg concentration. Hg concentrations are depicted atop NEXRAD storm-total precipitation, with storm track and surface wind vectors in the top right hand corner. (a) August 3, 2006: High concentrations. (b) September 1, 2006: Low concentrations.

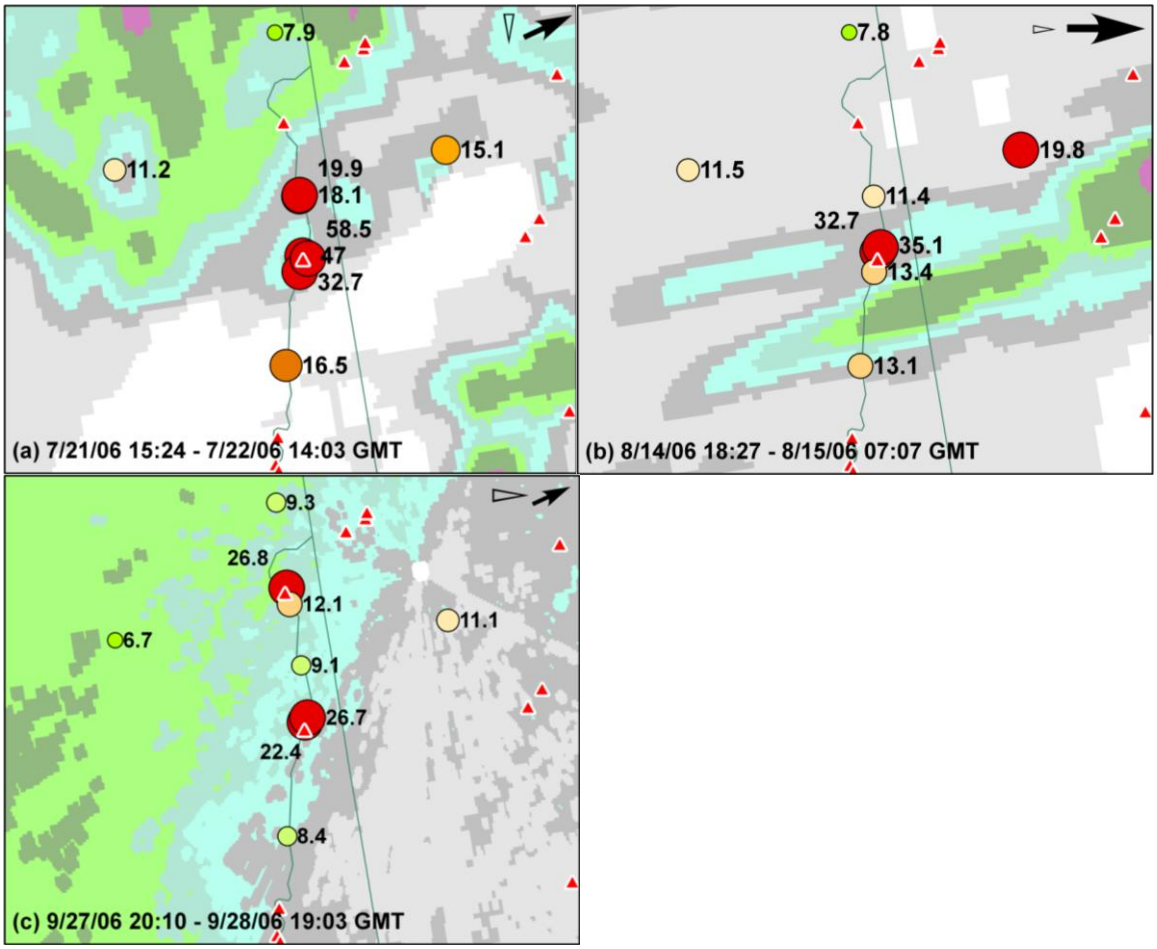

Figure III.3: Highly Variable Hg concentration. Hg concentrations are depicted atop NEXRAD storm-total precipitation, with storm track and surface wind vectors in the top right hand corner. (a) July 22, 2006. (b) August 14, 2006. (c) September 28, 2006.

CHAPTER III: Supporting Information

Moderate Variability

July 12, 2006 The nighttime rain began at STB at approximately 00:30 EST. Maximum Hg concentrations for this event (11.4, 8.1 ng L^{-1}) were collected approximately 600 m east of the Cardinal facility (CAR-EST1) and at STS, with the lowest concentrations (4.8, 5.0 ng L^{-1}) occurring at STB and the near-by STR, as seen in Figure III.S1(a). The rain came in two distinct cell lines, with a 2 h abatement between the heaviest rains, the north-south oriented cells propagated west to east at approximately 50 km hr^{-1} along an apparent stationary front. Precipitation occurred through moderate convection with a boundary layer of 602 m, cloud base at 884m during heaviest rain. Southerly surface winds at 3.7 m sec^{-1} were maintained throughout the event, helping to explain the enhanced concentration at the southerly site due to three large CFUB units 12-15 km south of STS (see Figure III.1 for CFUB placement), most likely indicating boundary layer enhancement of atmospheric Hg, because the east ward propagating cells deposited lower concentrations at the west-east situated sites of STW, STB and STE – three sites north of STS.

July 28, 2006. The affecting cell associated with this convective event moved with a southwest to north east trajectory, with the northern most edge passing just south of STN, and very little rain (0.2 cm) was deposited at the western STW site during this event, possibly resulting in enhanced Hg concentration, compared to other sites that received significantly more precipitation. There was no correlation between concentration and depth (r^2=0.004, p=0.884), indicating that concentrations variability was driven by Hg added to the precipitation in-between receptor sites. Southeasterly surface winds during this moderate intensity event may have aided in aiming the plume at the Cardinal facility to the north, explaining the Hg enhanced sample collected just north of the stacks (CAR-

NOR with 29.5 ng L^{-1}) (Figure III.S1(b)). Two samples contained a S/Se ratio below regional steady state: STE and CAR-EST2. The majority of the rain fell in approximately 30 min with an observed ceiling of 518 m and a mixing height of 700 m. Moderate surface winds were sustained through the event with 4 m s^{-1} during precipitation and 2.5 m s^{-1} 24 h prior to the event. There was significant vertical development, but no severe weather was observed due to this convection and precipitation rates were fairly moderate.

August 19, 2006. The precipitation from this event was associated with the outflow boundary of a stationary front, with sustained southerly synoptic winds. Individual cells of this event produced large hail, an indication of enhanced updrafts. While surface winds were southerly throughout, the storms themselves had a west to east trajectory. It is apparent that separate cells produced the precipitation at the different sites: the cell that first went through Steubenville seemed to merge with the cell that affected STS and the larger, combined, structure hit STE approximately 1 h later. It is likely that the cell affecting STN did not precipitate on any other site, and no precipitation was collected at STW. While the mixing height was higher than most moderately variable events, the degree of variability may be explained by a combination of relatively low surface winds 24 h prior to the event (1.6 m s^{-1}). Interestingly, it was not near field sites in this case that exhibited the highest Hg concentration, but rather the southern-most site, STS. While a slight relationship is seen between depth and concentration during this event (r^2=0.586, p=0.045), it is primarily driven by this STS sample, hypothesized to be high in concentration due to low sample depth (0.14 cm) as well as the impact of the three CFUB approximately 16 km south of STS from the southerly winds (Figure S1(c)). All other samples collected during the August 19 event were well over 0.5 cm and exhibited among themselves no relationship between concentration and depth (r^2 = 0.287, p=0.273).

September 18, 2006. Distinctly cold frontal, this event lasted approximately 1 h in the late evening of September 18, with synoptic winds shifting from southeast prior to frontal passage to westerly during and after the event. The north-south oriented linear cell structure moved through the Ohio River Valley with a south-west to north-east trajectory,

with surface winds from the south west during the rain. While the overall variability was moderate, one sample stood out during this event, CAR-EST2, with a concentration of 89.4 ng L^{-1} in 0.36 cm of rain. (Figure III.S1(d)). Validity of this enhanced Hg concentration has been affirmed by repeated sample analysis and comparison to other pollutants of coal origin, Se was also elevated in this sample. Samples collected to the north of the Cardinal and Sammis facilities did not exhibit such enhanced concentrations, and this distinct variability may be due not only to the wind direction, as the southwesterly surface winds may have directed the plume towards the CAR-EST2 sampling site, but may have also been a direct result of the site's position on a tall cliff on the eastern side of the Ohio River, a prime location for direct interception of the Cardinal plume. Units 2 and 3 were 1.2 km west of the sampling location, while Unit 1 was 2 km southwest. Cardinal's stack height is reported at 273m (in river valley,) the sampling location was at 172 m above the river. The shallow boundary layer of 493 m and relatively calm surface (2.8 m sec^{-1}) winds cause reduced volume in which the plume can mix as well as few turbulent eddies to aid in mixing with surrounding air, and cause a concentration of pollutants along the plume trajectory. While there was a slight relationship between depth and concentration, the negative slope of this relationship was very small, especially when the enhanced sample at CAR-EST2 was included. This enhanced sample was also the only sample collected during this event that contained a S/Se ratio less than background, also aiding in reinforcing the local enhancement characteristic of this sample.

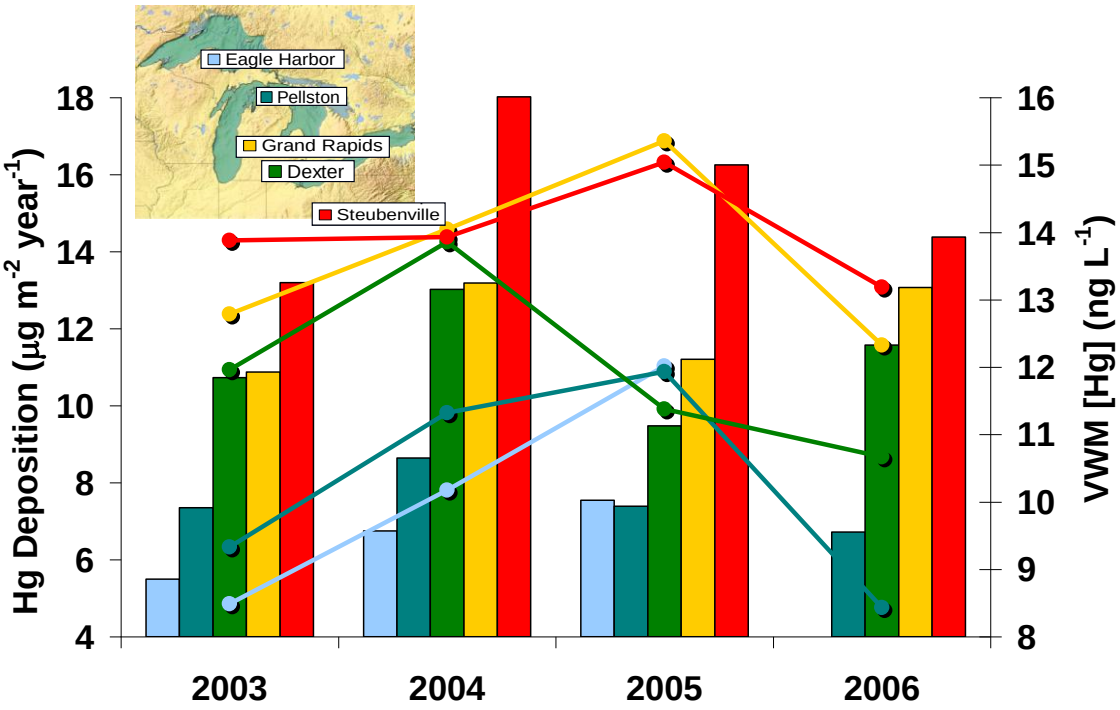

Figure III.S1. Great Lakes region Hg in wet deposition. North-south gradient is consistent over the long term in both volume weighted mean Hg concentration (depicted by lines) and Hg deposition (bars).

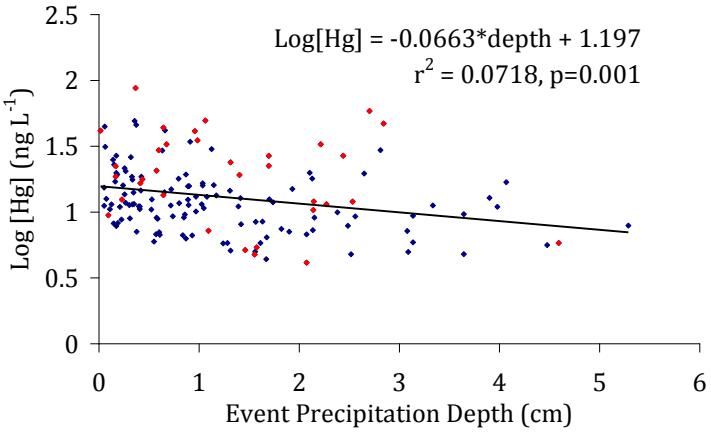

Figure III.S2: Sample Hg concentration versus depth: all samples collected during the three month period at all sites. Near-field samples are red, all others in blue.

Table III.S1: Locations of precipitation collection sites.

Site Location	Site abbreviation	Latitude	Longitude
Steubenville, OH	STB	-80.620	40.379
Beaver Creek State Park, OH	STN	-80.613	40.791
Belleville, OH	STS	-80.741	40.042
Settler's Cabin State Park, PA	STE	-80.161	40.422
Leesville Lake, OH	STW	-81.157	40.491
Ohio River, below STB	STR	-80.618	40.380
East of Cardinal CFUB, in Ohio River valley	CAR-EST1	-80.642	40.250
East of Cardinal CFUB, cliff above Ohio River	CAR-EST2	-80.634	40.265
North of Cardinal CFUB	CAR-NRT	-80.624	40.274
West of Cardinal CFUB	CAR-WST	-80.639	40.258
South of Cardinal CFUB	CAR-SOU	-80.655	40.226
East of Sammis CFUB	SAM-EST	-80.623	40.541
North of Sammis CFUB	SAM-NOR	-80.622	40.507

						Rain Rates (mm hr^{-1})		Average Temperature (°C)		Wind Direction		
		Coeff of Variation	% Near-Field Enhance	System Type	Storm track Velocity (km hr^{-1})	Ave	Max	During rain	24 hours prior	Synoptic prior	Synoptic during	Surface during
Low Variability	9/1 (low conc)	0.12	0%	HR	35	1.4	3.1	14.8	19.1	NE	NE	NE
	8/3 (high conc)	0.19	20%	WS, S	55	3.5	4.6	23.5	30.3	SW	SW	SE
Moderate Variability	7/12	0.31	48%	SF	50	3.5	9.9	22.8	24.9	S	S	S
	7/28	0.44	45%	C	70	3.2	3.2	24.4	26.8	S	S	SW
	8/19	0.28	28%	SF, S	55	3.6	5.7	28.2	26.4	S	S	SW
	9/18	0.35*	66%	CF	60	1.9	4.1	20.7	22.1	SE	W	SW
High Variability	7/22	0.69	72%	C	45	7.8	8.8	21.3	25.8	SW	NW	N
	8/14	0.58	55%	CF, S	65	1.2	1.2	24.2	23.8	S	W	W
	9/28	0.58	43%	CF	35	2.1	6.1	14.8	18.4	SE	NW	W

Table S2: Statistics on the variability of Hg concentration across the sampling field and additional meteorological parameters for individual events. *In this calculation, one sample has been removed due to exceptional high concentration as explained by direct plume hit; coefficient of variation equals 1.44 if this sample is included. System types abbreviated as follows: HR: Hurricane remnants, WS: Warm Sector, S: Severe, SF: Stationary Front, C: Convective, CF: Cold Front.

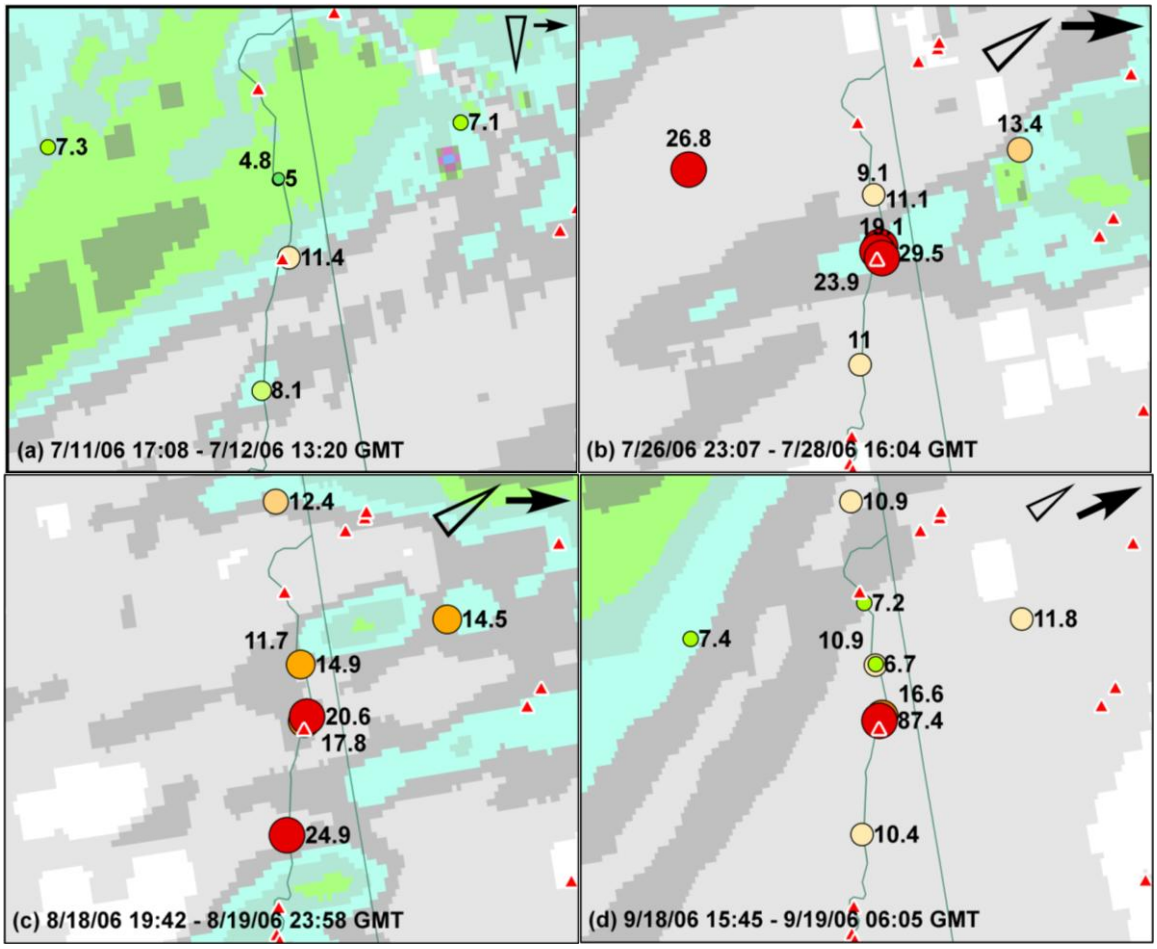

Figure III.S3: Moderately Variable Hg. Hg concentrations are depicted atop NEXRAD storm-total precipitation, with storm track and surface wind vectors in the top right hand corner. (a) July 12, (b) July 28, (c) August 19, (d) September 18.

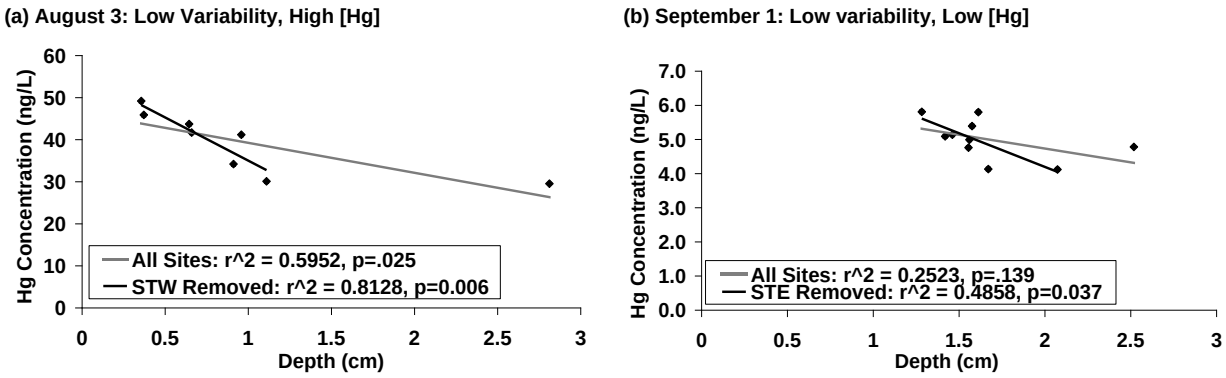

Figure III.S4: Low Variability Events: Hg concentration versus Sample Depth. (a) August 3, High Hg Concentrations, (b) September 1, Low Hg Concentrations.

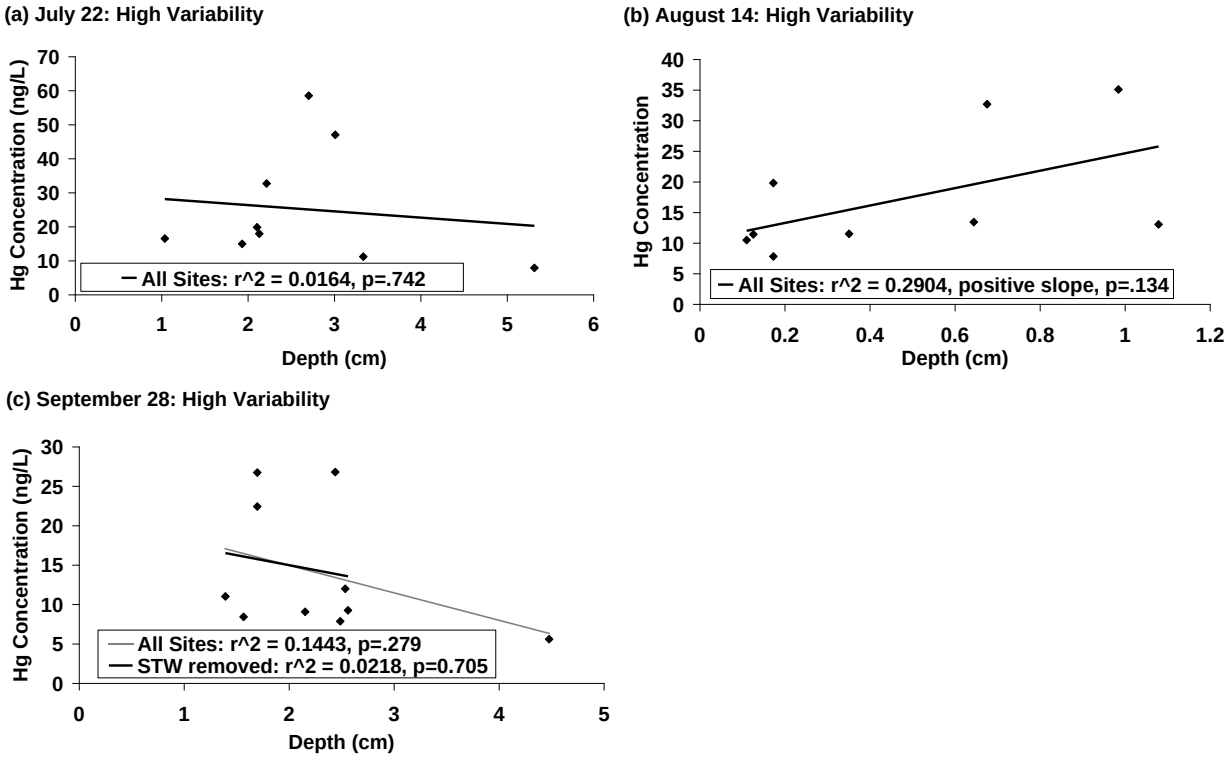

Figure III.S5: High Variability Events: Hg concentration versus Sample Depth. (a) July 22 (b) August 14, (c) September 28.

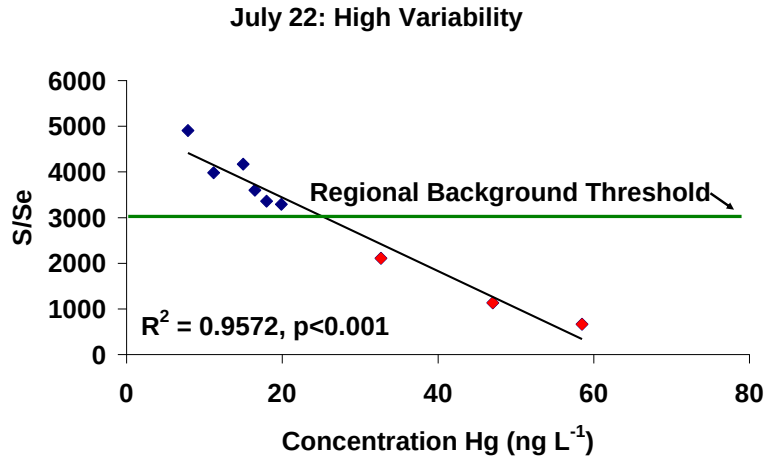

Figure III.S6: Relationship between S/Se ratio and Hg Concentration on samples collected during the July 22, 2006 event, red diamonds represent near-field samples, all others in blue.

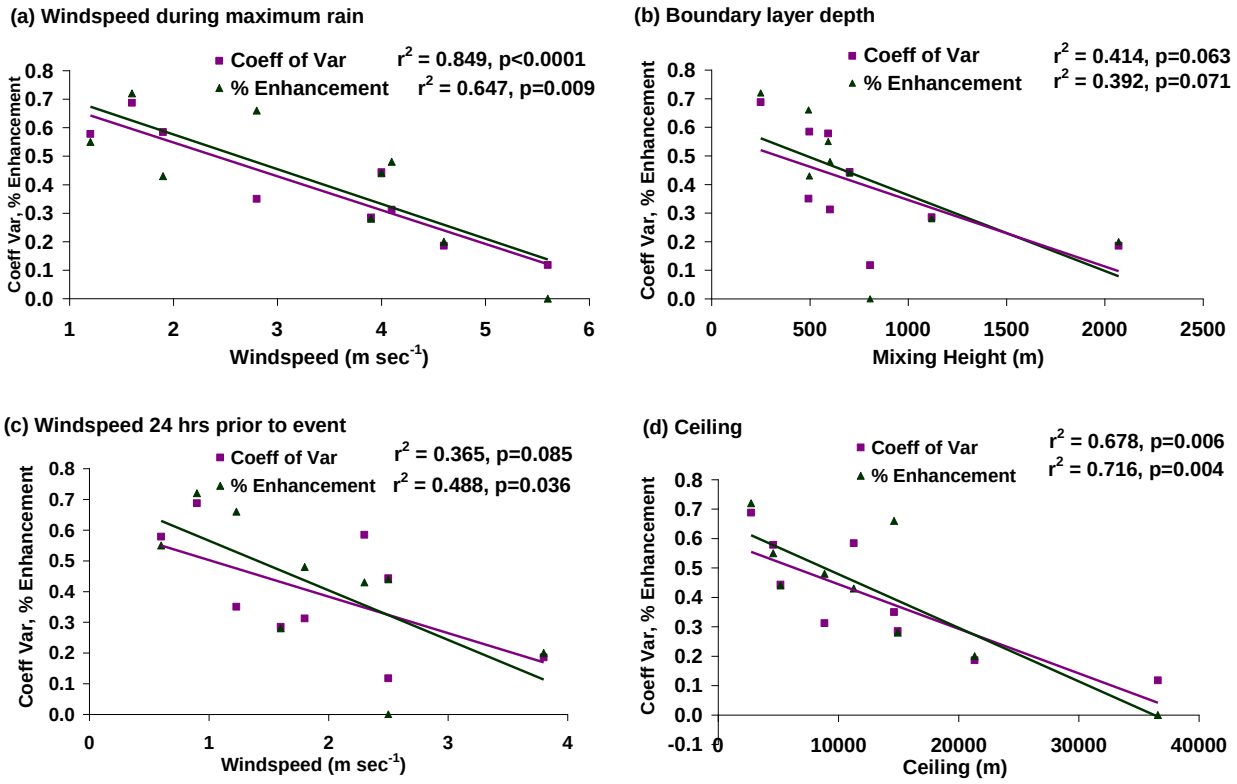

Figure III.S7: Linear regression analysis of meteorological parameters versus event Coefficient of Variability and Percent Near-field Enhancement.

CHAPTER III: References

(1) Jewett, S.C.; Duffy, L.K. Mercury in fishes of Alaska, with emphasis on subsistence species. *Sci. Tot. Environ.* **2007**, *387*, 3-27.

(2) Scheuhammer, A.M.; Meyer, M.W.; Sandheinrich, M.B.; Murray, M.W. Effects of Environmental Methylmercury of the Health of Wild Birds, Mammals and Fish. *AMBIO* **2007**, *36*, 12-18.

(3) Landis, M. S.; Keeler, G. J. Atmospheric mercury deposition to Lake Michigan during the Lake Michigan Mass Balance Study *Environ. Sci. Technol*. **2002**, *36*, 4518-4524.

(4) Landis, M.S.; Vette, A.F.; Keeler, G.J. Atmospheric mercury in the Lake Michigan Basin: Influence of the Chicago/Gary Urban Area. *Environ. Sci. Technol*. **2002**, *36*, 4508-4517.

(5) Electrical Power Research Institute. *Expert Panel on Mercury Atmospheric Processes: Mercury Atmospheric Processes: A Synthesis Report. TR-104214.* EPRI: Palo Alto, CA, **1994.**

(6) Lin, C.; Pehkonen, S.O. The chemistry of atmospheric mercury: a review. *Atmos. Environ.* **1998**, *33*, 2067-2079.

(7) Hedgecock, J.; Forlano, L.; Pirrone, N. J. Role of ambient aerosol characteristics in the speciation of atmospheric mercury. *Aerosol Sci.* **1999,** *30*, S463-S464.

(8) Lindberg, S.; Bullock, R., Ebinghaus, R., Engstrom, D., Feng., Fitzgerald, W., Pirrone, N., Prestbo, E., Seigneur, C. A Synthesis of Progress and Uncertainties in Attributing the Sources of Mercury in Deposition. *AMBIO* **2007**, 36, 19-31.

(9) Sumner, A.L.; Spicer, C.W.; Satola, J.; Mangaraj, R.; Cowen, C.A.; Landis, M.S.; Stevens, R.K.; Atkeson, T.D. In *Dynamics of Mercury Pollution on Regional and Global Scales,* Pirrone, N. and Mahaffey, K.R. Eds.; Kluwer Academic Publishers: New York, **2005.**

(10) Stevens, R.K.; Zweidenger, R.; Edgerton, E.; Mayhew, W.; Kellog, R.; Keeler G.J. Source Characterization in Support of Modeling the Transport of Mercury Emissions in South Florida. Presented at *Measurement of Toxic and Related Air Pollutants Symposium*, May 7-9, Research Triangle Park, NC, **1996.**

(11) Seingneur, C.; Lohman, K.; Vijayaraghavan, K.; Jansen, J.; Levin, L. Modeling atmospheric Mercury deposition in the vicinity of power plants. *J. Air & Waste Manage. Assoc.* **2006**, *56*, 743-751.

(12) Hammerschmidt, C.R.; Fitzgerald, W.F. Methylmercury in Mosquitoes related to atmospheric mercury deposition and contamination. *Environ. Sci. Technol.* **2005**, *39*, 3034-3039.

(13) Evers, D.C.; Kaplan, J.D.; Meyer, M.W.; Reaman, P.S.; Braselton, W.E.; Major, A.; Burgess, N.; Scheuhammer, A.M. Geographic trend in mercury measured in common loon feathers and blood. *Environ. Toxicol. Chem.* **1998**, *17*, 173-183.

(14) Hammerschmidt, C.R.; Fitzgerald, W.F. Methylmercury in freshwater fish linked to atmospheric mercury deposition. *Environ. Sci. Technol.* **2006**, *40*, 7764-7770.

(15) Bigelow, D.S.; Dossett, S.R.; Bowersox, V.C. *Instruction Manual NADP/NTN Site selection and Installation*. **2001.**

(16) U.S. Environmental Protection Agency. *Mercury Study Report to Congress,* EPA-452/R-97-005; Office of Air Quality Planning and Standards, Office of Research and Development: Washington, DC **1997.**

(17) Hoyer, M. PhD thesis, Wet Deposition of mercury in Michigan: Meteorological associations and spatial variability. University of Michigan, Ann Arbor, MI, **1995.**

(18) Keeler, G.J.; Dvonch, J.T. In *Dynamics of Mercury Pollution on Regional and Global Scales,* Pirrone, N. and Mahaffey, K.R. Eds.; Kluwer Academic Publishers: New York, **2005.**

(19) Dvonch, J.T.; Graney, J.R.; Marsik, F.J.; Keeler, G.J.; Stevens, R.K. An investigation of source-receptor relationships for mercury in south Florida using event precipitation data. *Sci. Total Environ.* **1998**, *213*, 95-108.

(20) Marsik F.J.; Dvonch J.T.; Keeler G.J.; Landis M.S.; Graney J.R. The use of WSR-88D radar data for source-apportionment of wet-deposition measurements from the 1995

SoFAMMS. *Conference Proceedings from American Meteorological Society, Third Conference on Atmospheric Chemistry*, February 2-7, Long Beach, CA, **1997.**

(21) Gildemiester, A.E. PhD thesis, Urban Atmospheric Mercury. University of Michigan, Ann Arbor, MI, **2001**.

(22) Hall, N.L.; Keeler, G. J.; Landis, M.S. Personal communication.

(23) Keeler, G.J.; Landis, M.S.; Norris, G.A., Christianson, E.M.; Dvonch, J.T. Sources of mercury wet deposition in Eastern Ohio, USA. *Environ. Sci. Technol*. **2006**, *40*, 5874-5881.

(24) Landis, M.S.; Keeler G.J. Critical evaluation of a modified automatic wet-only precipitation collector for mercury and trace element determinations. *Environ. Sci. Technol.* **1997**, *31*, 2610-2615.

(25) Graney, J.R.; Landis, M.S.; Norris, G.A. Concentrations and solubility of metals from indoor and personal exposure $PM_{2.5}$ samples. *Atmos. Environ.* **2004**, *38*, 237-247.

(26) Pinto, J.P.; Stevens, R.K.; Willis, R.D.; Kellogg, R.; Mamane, Y.; Novak, J.; Santroch, J.; Benes, I.; Lenicek, J.; Bures, V. Czech air quality monitoring and receptor modeling study. *Environ. Sci. Technol.* **1998**, *32*, 843-854.

(27) Altshuller, A.P. Seasonal and episodic trends in sulfate concentrations (1963 – 1978) in the Eastern United States. *Environ. Sci. Technol.* **1980,** *14*, 337-1349.

(28) Tuncel, S.G., Olmez, I., Parrington, J.R., Gordon, G. E., Stevens, R.K. Composition of fine particle regional sulfate component in Shenandoah Valley. *Environ. Sci. Technol.* **1985**, *19*, 529-537.

CHAPTER IV

Source Type and Region Attribution for Wet Deposited Hg in Eastern Ohio, USA

Abstract

The Ohio Mercury Monitoring and Modeling Study in Steubenville, Ohio produced a robust 5 ½ year event based (N=389) wet deposition database. Both mercury (Hg) deposition and Hg concentration were found to be enhanced over other Great Lakes regional sites. Hg deposition was explored through receptor-based models, with both multivariate statistical source profile attribution and meteorologically based air mass trajectory ensemble methods. Run concurrently, Positive Matrix Factorization and Unmix models produced similar five source type solutions, with coal combustion predicted to contribute 71% and 60% of the Hg deposition, respectively. No trend was observed in the percent source attribution over the course of the study. Seventy-two hour back-trajectories were calculated for each precipitation event, and clustered by endpoints to produce similar transport regimes. It was found that intra-cluster Hg concentration variability was maximized when trajectories were clustered by 12-24 hour endpoints, indicating that variability was due to local sources. Synoptic meteorological assessment of the clusters suggested situations that led to enhanced Hg deposition. It was found that while local stagnant conditions led to moderately high volume-weighted mean Hg concentrations and the majority of Hg wet deposition flux, and over 70% was modeled as due to coal combustion, moderate transport from areas with known emission point sources also led to high Hg concentrations, but did not contribute significantly to the overall Hg deposition.

Introduction

Classified in the 1990 Clean Air Act (CAA) as a Hazardous Air Pollutant (HAP), mercury (Hg) is a bioaccumulative neurotoxin that is spatially distributed via atmospheric transport of emissions, whether natural or anthropogenic. Hg deposition to the surface and subsequent methylation by biota allows for uptake into the food chain. Anthropogenic combustion processes account for approximately 50 - 75% of atmospheric Hg emissions (1, 2, 3). The first federal mandate to reduce mercury emissions, The Clean Air Mercury Rule (CAMR), promulgated in 2005, was struck down by the US Court of Appeals in February 2008 due to its violations of the Clean Air Act of 1990. It was found unlawful to a) implement a cap and trade program for the HAP, citing the section 112 requirement for application of best available control technology to achieve maximum reductions in emissions, and b) delist coal- and oil- fired electric utility steam generating units, therefore invalidating CAMR's regulatory approach (4). On February 6, 2009 the United States executive administration dismissed any standing Supreme Court appeal efforts by the precious administration, citing a need for more stringent controls. The U.S. is also beginning negotiations that would create a legally binding international treaty to reduce Hg emissions around the world (5). Policy decisions and developments must be aided by improved understanding of the chemistry and dynamics of atmospheric Hg source – receptor relationships.

For any given receptor site, deposition of Hg to that point is a complex mix of locally, regionally and globally transported atmospheric Hg. The complexity of source region attribution stems from the characteristic intricacies of Hg physicochemistry: Hg is observed in the atmosphere in three inorganic forms, elemental Hg (Hg^0), divalent Hg (Hg^{2+}) and particulate bound Hg (Hg(p)), which maintain different physicochemical properties. Hg^{2+} and Hg(p) have a high affinity for surface reactions and are hydroscopic, while elemental Hg is widely recognized as a global pollutant, with loss due mostly to oxidation to Hg^{2+} and subsequent deposition. Hg is emitted from coal- and oil-fired utility boilers, municipal and hospital waste incinerators, iron and steel production facilities, nonferrous metal production, cement production, coke production processes, copper and zinc smelters, petroleum refineries and mobile sources (3, 6, 7, 8, 9,10) with a significant fraction in the divalent form. Wet deposition of Hg is generally recognized as

originating from either in-cloud Hg^0 oxidation by O_3, gas-phase oxidation via OH or O_3 followed by droplet uptake, or direct scavenging of Hg(p) or Hg^{2+}, the later process enhanced in the vicinity of sources of these species (3).

The Ohio Mercury Monitoring study intended to investigate the impact of coal combustion on the chemistry, transport, and deposition processes of Hg. A cooperative agreement between the U.S. Environmental Protection Agency (U.S. EPA) and the University of Michigan Air Quality Lab (UMAQL), established an enhanced monitoring site that began operation in October 2002 in Steubenville, Ohio. When compared to previous studies and concurrently collected precipitation at other less industrially influenced sites, levels of Hg were elevated two and a half- to three-fold. (7, 11). Receptor models Positive Matrix Factorization (PMF) and Unmix were applied to the initial two years of event precipitation data (November 2002 to December 2004, N=162) to discern source type attribution to Hg deposition (7). It was found that ~70% of the Hg deposited was of coal combustion origin. Additional meteorological case study analysis of local, spatially distributed, concurrently sampled summertime precipitation in the Ohio River Valley indicated that a significant percentage of wet deposited Hg was from local sources (11).

Here, multivariate receptor models are applied to an additional three years of wet deposition samples for a more robust source attribution and characterization analysis. Because such models rely exclusively on deposition chemistry input, meteorological parameters are investigated through trajectory transport cluster analysis to aid in interpreting the multivariate receptor model results and identify the most common origins of the identified sources.

Methods

Sample Collection. Event precipitation was collected in Steubenville, Ohio at the advanced air monitoring site on the campus of Franciscan University of Steubenville (40.379 N, 80.620 W; 306 m above MSL) from October 2002 through March 2008 (n = 389). A map with site location and Hg point sources ($>10^{-6}$ tons $year^{-1}$, 2002 National Emissions Inventory) in the vicinity is depicted in Figure IV.1, locations of nationwide sources can be found in Appendix C. An RM Young tipping bucket at the Steubenville site was used to determine precipitation onset and rate. Event collection was conducted

using the UM-B modified MIC-B wet-only deposition collector, with two sample trains, one for Hg concentration determination, the other for ions and trace elements (12). The clean techniques employed, collection method, sample train configuration and material used, sample processing and analytical methods were identical to those previously described (12, 13, 7, 11). Hg analysis was performed using Cold Vapor Atomic Fluorescence Spectroscopy (CVAFS), ions were determined via ion chromatography (Dionex) and a suite of 42 trace elements were determined on the Thermo Finnigan Element 2, with inductively coupled plasma mass spectrometry (HR - ICPMS).

Data treatment Event deposition was calculated as the product of the measured sample concentration times event precipitation depth, where depth was determined by sample volume divided by funnel collection area. In the event of sample bottle overflow, tipping bucket data was utilized to calculate event depth. The total number of samples collected over the study period was 389; however, samples missing major ion or trace element species concentration determinations due to low sample volume were excluded from multivariate statistical analysis, therefore n = 368 for PMF and Unmix model input. All analytical data was thoroughly quality assured through an extensive Quality Assurance Quality Control (QAQC) procedure: for all (CVAFS, IC, HR-ICPMS) analysis runs, check standards, NIST standards and sample replicates were analyzed every 6 samples. Analyte concentrations were flagged as estimated (EST) if the accompanying check standard was greater than 15% off, the NIST was 20% outside of actual or the replicate was 20% different. Sample concentrations were considered not valid (NV) if any of these deviations were greater than 50%. While several elements from the analyzed suite were dropped due to these criteria, the most notable analyte dropped for this investigation was Mo (42% NV, 35% EST). Sulfur determined by ICP-MS was used rather than the IC SO_4^{2-}, ($S=0.4413*SO_4^{2-} + 538.8$, $r^2 = 0.9855$.)

Hour of maximum precipitation rate for each event was determined through exploration of tipping bucket data, radar images (NCDC) and Wheeling, WV observations. The three methods were also used in conjunction in order to determine if more than one precipitating event was collected in a single sample bottle. 'Event' was operationally defined for the meteorological and trajectory analysis as abatement of rain for more than 3 hours, and > 75% of total depth in the sample from a single, continuous rain. This definition too stringent to be feasible for the study period, as collection was performed on a 'daily-event' basis, i.e. collection of samples at 8 AM if there had been precipitation in the previous 24 hours. Therefore, of the 389 samples collected during the study, 72 contained more than one event. (When these samples were removed for the multivariate statistical receptor model analysis, overall results did not change, and the uncertainty robustness remained equivalent. It is hypothesized that a balance was reached between 'pure event' only, versus additional data for model input. The models, often used for ambient integrated 24 hour PM source attribution, assume a mixture of source impact.) To maintain normal meteorological distribution of events, the partial years (late 2002 and early 2008) were also removed from the ensemble trajectory analysis, as were samples associated with Hurricanes Ivan and Frances, due to exceptional meteorological conditions. The resultant 293 sample dataset was divided into two distinct trajectory analysis categories, one for rain only and one for snow and mixed precipitation, as different precipitation types were shown to exhibit variable scavenging rates.

Multivariate statistical receptor models Multivariate statistical receptor models seek to solve the general mixture problem. An original data matrix (*M*) is developed, through receptor sampling, as *i* by *j* dimensions, where *i* is the number of samples, *j* is the chemical species measured. In our case, *i* is a precipitation date. The models aim to decouple this matrix as:

$$M_{ij} = \sum_{k=1}^{N} C_{ik} F_{jk} \qquad \text{(IV.1)}$$

where *N* is the number of sources *k* contributing to *j* species, *C* is the source's (*k*) contribution to each sample, and *F* is the factor score matrix: source type by *j* species. C_{ik} maintains the original matrix units, while F_{jk} is a dimensionless 'score.' Model output

identifies the number of discernable sources with significant influence on deposition variability and the composition of these sources. A large advantage to receptor based modeling is that the only input is known concentration data, and that no prior measurements of source profiles or emission inventories are necessary. It follows that the end user characterizes the resultant factor profiles through subjective comparison to known measured source profiles.

Decoupling the sample matrix is an ill posed problem, as there are an infinite number of solutions. Receptor models differ by the method used for solving this problem. PMF, as described in detail in Paatero (1997) (14), uses a weighted least squares approach, utilizing operator defined, sample and analyte specific uncertainty estimates to derive the weights, and weighs each data point by the inverse of the measurement error (15). Uncertainties for PMF input were calculated as in equation 2.

$$U = \sqrt{(SC)^2 + (AM)^2 + (MDL)^2 + (PD)^2} \qquad \text{(IV.2)}$$

where, SC = 10% (Sample Collection uncertainty); AM= standard deviation of 3 replicate analysis (Analytical Measurement uncertainty); MDL = Method Detection Limit for the particular analyte; and PD= 5% (precipitation depth uncertainty). Method detection limits for this analysis are published in Keeler et al. (2006) (7). One advantage to the use of uncertainty is the ability of the model to use, as input, concentrations that were below detection limit or even negative, allowing for inherent variability of the data set to remain intact. While negative input is allowed, PMF results are constrained to a non-negative solution, such that no sample can have a negative contribution. Unlike earlier factor analysis methods that use analyte correlations to calculated source profiles, PMF can produce factors that are primarily one element (16). Uncertainties and variability in the solution are estimated by bootstrapping techniques and PMF version 3.0 was used for this analysis.

Unlike PMF, Unmix (17) does not does not use samples in which any analyte concentration was less than zero. Four events were dropped in the model analysis: (1) 8/29/03, Ba <0, (2) 9/13/03, Se < 0, (3) 9/15/2003, Se<0, and (4)10/17/03, Ni < 0. Unmix uses ‘self-modeling curve resolution,’ or scatter plot ‘edges,’ between elements to

define individual factors. The edges are, in some sense, assumed to be defined by 'pure' (or with very small contributions by other sources) source contributions (15). A detailed and comprehensive description of Unmix model can be found in Lewis et al. 2003 (18). For this evaluation, EPA Unmix version 6.0 was used.

Both receptor models were run concurrently for this study. Identification of elements with low signal to noise ratios (<0.2) were dropped from analysis via PMF and were therefore not run with Unmix. In PMF, the number of factor profiles was chosen based on the ability to identify all factors, the robust Q values, the ability of the model to replicate measured results, minimization of discrete difference percentiles, and bootstrap results. Unmix chooses the number of factors based on a balance of the minimum coefficient of determination and maximum signal to noise ratio and its ability to produce feasible results. The following composite source tracers aided the user in source identification of the modeled factors.

Ensemble trajectory analysis. Previous work on categorizing continental US synoptic systems and their relation to air pollution parameters, involving comparisons between wet deposition chemistry at a given receptor site to categories of storm type, found that it may not be possible to select a few 'typical' synoptic situations that produce enhanced events (19). Therefore, more objective methods are necessary to investigate longer term, larger data sets of deposition data as opposed to individual case studies. One semi-objective method of classification is the use of wind-directions or trajectories to determine the origins of airmasses arriving at a receptor. While Eularian methods that use receptor site wind speed and direction data to determine source regions are appropriate for pollutants that vary on relatively short small time steps, such as gases and particle concentrations, a Lagrangian approach must be used to describe more synoptic scale events, such as precipitation. The area surrounding the receptor is divided into spaces that can be thought of as quadrants, and the trajectories grouped as 'clusters', where concentrations and depositions tend to be stratified by transport sector. The cluster analysis divides the data set into groups of similar meteorological flow regimes, in an attempt to reflect the underlying structure present in the trajectories (20). Such grouping therefore categorizes not only by direction, but also distance which is a direct measure of wind speed. Past work at rural receptor sites typically shows that the largest pollutant

loadings occur when air parcels pass through urban or industrial areas (20, 21, 22, 23). Such modeling assumes that the air parcel 'picks-up' pollutants proportional to air parcel residence time in a particular area.

One difficulty in applying cluster analysis to trajectories originating in a highly industrialized area, however, is the pollution influence from every direction. This leads to the corollary that if the receptor site is indeed influenced heavily by local sources, the highest concentrations would be a result of local stagnation, as pollutants would be allowed the residence time to accumulate.

Seventy-two hour HYSPLIT back trajectories were calculated using meteorological data inputs from the EDAS 40 km model output. The calculation originates at the receptor site and arrives at the next 'endpoint' one hour prior, for a user specified number of hours. The line connecting the endpoints represents the most probable vector of travel for the air parcel, the center of a Gaussian spatial distribution, providing a Lagrangian path. All trajectory model runs initiated at half the mixing height. The uncertainties in trajectory calculations increase during periods of changing synoptic situations and with distance from initiation location (20). Clusters of the resulting trajectories were calculated using the SAS cluster function, which uses Ward's method to minimize within-group variance of the Euclidian distance between end points.

Results

Concentration and Deposition Event Hg wet deposition for Steubenville 2002 – 2006 compared to other concurrently collected samples in the Great Lakes region has been previously published (7, 11). A significant enhancement of Hg deposition at the Steubenville site was observed over other, more rural Midwestern receptor sites, indicating at least a regional influence. The distinct gradients were apparent in CY 2007 Hg data as well. Weekly integrated wet deposition results for Athens, Ohio, a site with a similar, industrially influenced air shed in the Ohio River Valley, were consistent with those collect for the current study in background concentrations, volume-weighted mean concentrations, maximum concentrations, and total deposition for March 2004 to March 2005 (24).

A distinct seasonal trend can be observed when the event Hg volume-weighted mean (VWM) concentrations and depositions are aggregated by month, with summer and spring dominating for both parameters (see Figure IV.2). A similar seasonal trend has been observed at rural sites in Michigan (21,13, 25) and Vermont (26) as well as at more industrially influenced receptor sites (21, 23). CY 2004 remains a unique year for Hg deposition as the remnants of Hurricanes Ivan and Frances migrated through the Ohio River Valley on September 8 and 16; high volume rains (9 and 10 cm, respectively) that were also high to moderate in Hg concentration (18.7 and 7.6) contributed 13% to the year's mercury deposition.

Trend analysis over the long term data set indicates that there was no significant overall increase or decrease in Hg concentration or deposition for the time period studied. This result may have been expected as the primary contributors to Hg deposition in the local region did not change during the period studied. Recent research for long-term wet deposition have shown both a) no long term trend at the rural Underhill Vermont site (25, 22) and b) a significant reduction in Hg deposition and concentration at the Mercury Deposition Network (MDN) site in Northeast Seattle, coincident with the closure of several local medical waste incinerators (3, 27).

PMF Model Results Twenty-three elements were used in the model analysis, seven species with signal to noise ratios of less than two but greater than 0.2 were classified as "weak," as were species with non-normally distributed residuals, prompting the model to triple the associated uncertainty. Solutions with five, six, and seven factor profiles were evaluated, the five factor solution was chosen based on the criteria mentioned in the methods section.

The five factor solution yielded 1) coal combustion (S, Se), 2) phosphorus, 3) incineration (Cl, NO_3, Pb, Zn), 4) iron and steel manufacturing (V, Cr, Mn, Fe), and 5) crustal or fugitive dust (La, Ce, Mg, Al) sources. The source contributions are given in Table IV.2 and were considered significant if the 5^{th} percentile uncertainty was greater than zero. The coefficients of determination were greater than 0.75 for all elements evaluated with the exception of Cd ($r^2 = 0.29$) and Ni ($r^2 = 0.03$). The solution was bootstrapped with a model suggested block size of 16 samples, and the lowest discrete

difference parameters were for Hg and S on the coal factor. Only 1.5% of the factors were unmapped, indicating a stable result.

While four of the sources were distinctly and conclusively identified, the phosphorus source was initially unidentified as it was difficult to associate with a specific industrial type. One feature of to the PMF model is the aggregated contribution output, a parameter that may help the user define sources and evaluate contribution trends. Temporal trends may be due to source usage, for example motor vehicle contributions that peak on weekdays, and wood burning that probably peaks in the winter. The patterns may also be due to physiochemical analyte properties or seasonal meteorological variability; photochemistry, ambient temperatures and precipitation state will result in varying lifetimes and scavenging rates of pollutants. The 'unidentified' phosphorus source yielded a distinct temporal pattern, peaking in the spring and increasing for the last 4 years. This seasonal trend may indicate some relationship with a spring thaw, as phosphorus is associated with fertilizer. Peaks in P in the individual event time series occur every year in April, with possible coincidence to agricultural disking for field preparation.

To further investigate the possible P source, PMF was run with identical parameters as above, but with P as a 'weak' element. With sources 3 - 5 remaining relatively intact, the crustal source was split onto a second factor, a factor that still remained heavily loaded with phosphorous. This second crustal factor exhibited similar temporal patterns as the P source, and maintained nominal crustal ratios: La/Ce: 0.5 Rb/Sr: 0.12 Mg/Al: 0.48. This relationship with a distinctly crustal source indicates a wind blown dust factor as the most likely source attribution. Indeed, the five factor solution with P as a strong variable and P as it's own factor profile exhibits, while the absolute contribution is relatively low, crustal elements in the appropriate ratios. If a six factor solution is modeled with P as a strong variable, profiles 2-4 remain intact, with crustal splitting into two factors. One possible explanation to the splitting of the crustal factor is the potential influence of several clay, ceramics, brick and tile manufacturers in the Steubenville area. Production of PM composed of elements similar to upper continental crust by these manufacturers may yield a crustal type signature that has no temporal pattern. From the PMF modeled results alone, we conclude that the P-source is

crustal in origin, while further discussion of the source of this factor is further investigated in following sections through trajectory and meteorological source region attribution.

The non-manufacturing crustal P source, however, has significant contributions from some elements not typically considered soil tracers, such as S, and As. It is possible that the P was mined from an area with these trace contaminates were present, and the S may be due to potassium sulfate depending on the fertilizer composition. It is thought that due to the location of the site in such an industrially influenced area, wind blown dust is made up of both naturally occurring soil elements and a significant amount of fugitive dust. The S and As on this factor are most likely due to historical PM deposition to the surface, mixed with soil and re-suspended. Area iron and steel manufacturing also reported P emissions, but because of the distinct clarity of the iron and steel factor profile and the absence of significant P attribution, it is not thought to be the source of the phosphorous profile.

Hg is heavily loaded on the coal factor, with 70.9% of the study total deposition attributed to this source. This is consistent with results from the previous two-year Steubenville source attribution (7). The other factors with significant contributions to Hg deposition were iron and steel production (4.2%), the phosphorous source (7.9%) and crustal (4.2%). Again, it is possible that the Hg is linked to the P and crustal sources due to particle deposition after coal combustion emission and subsequent re-suspension.

The model was able to reproduce Hg deposition, as seen in Figures IV.3(a) and IV.4(a). The largest deposition events were the most difficult to model, while lower deposition events, as seen near the origin in Figure IV.3(b) were more precisely reproduced. Statistically this is understandable as multivariate models try to define coefficients that give the best fit to the data on average, and therefore extremes are underrepresented. Another explanation may be due to the unusual meteorological conditions that favored enhanced scavenging, such as low mixing heights, low winds combining to produce exceptionally stagnant conditions or wind directions that caused affecting source plumes to directly impact the receptor site (11). The most notable under prediction was associated with the hurricane remnants in September of 2004. Overall, the regression of PMF predicted versus modeled Hg deposition had a slope of 0.75, an

intercept of 0.03 and a coefficient of determination of 0.82, and under predicted total study deposition by 11%. Aggregate coal factor contributions showed no significant trend over the study period (Table IV.3).

Unmix model results Unmix was run on the identical data set and element list as in above PMF profile listing, and no feasible result was found. Based on the default longitudinal and transverse spread, 0.05 and 10, respectively, 33 observations (one sample point for the scatter plot of element x versus element y) were deemed influential (as falling outside the upper and lower estimations of the edge if this point was removed). Of the 33 influential observations, 9 were removed based on the criteria that the original edge resolution was less than 0.6 (0 represents an undefined edge, 1 is perfectly resolved) and was improved by the removal of the influential point. These influential observations cause significant shifts in the edges of the scatterplots, and the missing data algorithm replaces them with the geometric mean (17). Prior to replacement of the influential points, Unmix suggested excluding Cl, Cd, Cr, Ni and Cu due to high specific variances (SV) among these species. Replacement of the 9 influential data points however, reduced the SV scores, such that Ni was the only remaining analyte with $SV > 0.5$ and was subsequently removed from analysis.

Unmix produced a five factor solution: Smelting source (Cu, Zn and Ni fit), Phosphourus source, Iron and Steel production (Pb, V, Mn, Fe), crustal (Sr, La, Ce, Mg and Al) and a coal combustion source (NO_3, S, As, Se). The source profiles are given in Table VI.4, a contribution was considered significant if the fifth percentile of the bootstrap uncertainty distribution was greater than zero. 60% of Hg was attributed to the coal factor, 6% on the Phosphorus source, 16% was attributed to the incineration and smelting, with an additional 12% attributed to windblown soil. Slope of predicted Hg depositions versus modeled was 0.77, with an intercept of 0.06 and coefficient of determination of 0.79. One distinct advantage to Unmix is the option to easily fit a species that has not been selected for model evaluation, this option was implemented for Ni, and it was primarily attributed to the incineration/smelter source.

Model comparison The Unmix modeled deposition was less precise than PMF for small deposition events, as seen by the scatterplot distribution in Figure VI.4 (a) and (b), but did a better job at predicting large deposition events. This lead to the overall

excellent modeled total Hg deposition, Unmix modeled 82.9 versus actual measured 81.6 $\mu g\ m^{-2}$. Unmix seemed to have an inherent ability to be more variable in source attribution on event, and therefore aggregated longer term, basis, whereas PMF percent predicted source contributions were less variable. General source profiles were consistent between the two models with the exception of incineration and smelting sources, while the PMF incineration source was distinct, and defined substantially by the Cl tracer, this factor was dominated by Cd in the Unmix solution. Cd is an indicator of tire burning, the National Emissions Inventory lists Stark County Landfill (aprox. 30 km NW of receptor site) as 'solid waste and tire' source, as seen in Figure VI.5. Based on the discrete difference parameter at 95% for both models, the coal contribution to Hg was not significantly different. Both models predicted slightly higher contributions from coal combustion for 2005, but this increase was not statistically significant. When compared to Keeler et al 2006, the results are consistent, both in source profiles and % of Hg attributed to the coal factor. This suggests a consistency in the source contributions over time, as well as confirms the robustness of the model calculations.

Trajectory analysis

Cluster analysis was performed repeatedly in an attempt to obtain the lowest within cluster and consequently highest intra-cluster variability among VWM Hg concentration. Four parameters were considered in the optimization of the cluster analysis: the coefficient of variability among VWM Hg concentrations between resultant clusters, the significance of the variation based on the non-parametric Kruskal-Wallis test Chi-square, and the number of clusters need to reach a minimum variance sill of 0.75, and the variance gained in producing the final cluster. When precipitation type and month were included as variables in the cluster analysis, the most robust Hg concentration intra-variability was found, but including these variables distorted the clear directionality and speed of the air mass transport, therefore all snow and mixed precipitation were split into a separate analysis. The optimization series of cluster variable selection found that 12 and 24 hour endpoint groupings resulted in the most significant intra-cluster concentration variability.

For the analysis presented in the following section, trajectories were clustered by endpoints every other hour, back 24 hours, as the optimization process above indicated

that additional endpoints (up to 72 hours) diluted the signal and made the amoung cluster variability less significant, an indication that sources impacting the Hg concentration in precipitation were within 24 hours of the receptor site. Because atmospheric flow patterns and speed vary dramatically, it should be noted that 'within 24 hours' represents a 'local' to 'regional' airshed, and in this case represents approximately 500 km (± 300 km.) While the variability of VWM Hg concentration between clusters is statistically significant, the coefficient of variability (0.2) is low compared to other precipitation studies. It is hypothesized that this is due to the large number of sources in the immediate vicinity, impacting the receptor site no matter the air parcel trajectory. Because grouping the events by the 3 day endpoints did not result in any significant intra-cluster variability, it can be assumed the location of the air parcel 3 days prior to precipitation had little impact on the resultant event precipitation.

One reason it may have been difficult to increase intra-cluster variability is the large number of trajectories in which southerly flow dominates, as 40-60% of trajectories were from the southwest. This fact was due to the primary synoptic situation that brings precipitation to the eastern continental US; the middle latitude cyclone. Development of this system type begins along the polar front, the boundary between warm moist Gulf air (maritime tropical) and cool dry (continental polar) air masses. If upper level dynamics align to produce divergence (trough exit) and/or warm air advection (trough exit through short wave coincident with planetary trough) aloft, the surface low will deepen and a wave cyclone results. The polar jet stream is the strongest and farthest south in the winter, supporting well developed lows over the mid to northern United States, while the slower upper level winds of the more northern spring and summer polar jet stream position encourages cyclone sustainment over the northern United States and eastern Canada (28, 29). The common migration pattern of these wave cyclones cause our receptor site in Eastern Ohio to be affected by the quadrants to the south of main low, often the site is situated south of occlusion as well. In a general sense, winds preceding the warm front will typically be from the south east, warm sector winds will be southerly, and surface winds behind the cold front will vary from north to north west to west. All three of these regions of the wave cyclone can produce precipitation, and depending on

the coincidence of the site position within the system at the time of maximum precipitation, air mass back trajectories will represent that particular flow.

Based on Donora Pennsylvania smog disaster of 1954, the standard definition of stagnation is 4 days of sustained geostrophic winds of 8 m sec^{-1}, corresponding to surface wind speeds of less than 4 m sec^{-1}, with an additional 10% windspeed if an inversion existed below 850 mb (30). It should be noted that this type of definition pertains to events with no precipitation, as the purpose of the definition is to warn of enhanced PM and ambient gas concentrations, and precipitation would washout potential pollutants of concern. In the current investigation however, precipitation is always present, and therefore associated with much higher windspeeds. Here, because events are being categorized based on Lagrangian calculations and not local measurements, wind speeds are based on trajectory length for a given period of time at half the mixing height, which varied from 10 to 2,083 m. Because absolute heights do not translate directly to pressure surfaces, wind speeds were standardized as

$$score = \frac{\overline{WS}_{cluster} - \mu_{WS}}{\sigma_{WS}} \qquad \text{(IV.3)}$$

and binned as categorically stagnant, moderate or rapid. This calculation was performed separately for rain and snow/mix so as not to produce seasonal bias, as winter winds are, on average, significantly faster.

The trajectory cluster figures depict 72 hour most probable air mass path in grey, with 12 hour endpoints highlighted in red, 24 hour endpoints shown in violet. Nine rain clusters are labeled (a-i) in Figures IV.6 and IV.7, five snow and mixed precipitation clusters are labeled (a-e) in Figure IV.8, with Tables IV.5 and IV.6 and text discussion referring to the individual clusters as R1-R9 and S/M1-S/M5 for rain, and snow and mixed precipitation, respectively. Appendix C contains the Pearson Correlation Matrix for all events and clusters. The correlations are calculated for individual event Hg concentration against several trace elements (S, Fe, Cl, La, Pb, P and Se), mixing height and a series of wind speeds divided into three hour increments along the trajectory path. Table IV.7 utilizes PMF and Unmix daily source contributions as calculated from the entire data set to attribute the percent of Hg in each cluster to each source type. Each

cluster is evaluated in detail to understand the synoptic dynamics and flow regimes that lead to particular source-receptor relationships and deposition patterns.

R1 By far the most dominate cluster in terms of number of events, total precipitation, and Hg deposition, Rain Cluster 1 (Figure IV.7.a) occurs with the southerly flow preceding a cold front, in the warm sector, often times to the south of occlusion, of a typical mid-latitude wave cyclone. The low propagates eastward, the northern Great Lakes region location of the surface low coinciding with the more northern summertime location of the polar jet, with summertime, primarily July events (Table IV.6), falling into this transport situation. As the primary low passes north of the receptor site, south west surface winds pull moist air from the Gulf region, feeding the precipitating system preceding the cold front. Southwest winds in the 24 hours preceding are comparatively stagnant, leading to a high VWM Hg concentration for this cluster. The influence of several coal fired utility boilers southwest (Appendix A) of the receptor site along the Ohio river valley is evident in both the inter-cluster significant correlation with S and the highest cluster single variable linear regression significance among the clusters with Se and the model source attribution; Unmix and PMF predicting 70% and 76% of the Hg deposition due to coal, respectively. The high range of Hg concentrations (5.4-67.5 ng L^{-1}) within this individual transport cluster indicates that small perturbations in local meteorological parameters can cause enhancement. Twenty-four percent of all Hg wet deposition is associated with this meteorological situation. Five of the nine case studies evaluated in White et al, (11) fell into this cluster.

R2 13% of all wet deposited Hg coincided with this cluster as well as the highest mean deposition per event, again associated with stagnant local conditions; 12 hour flow was easterly preceding maximum precipitation**,** but 24 hour endpoints depict deviation from this general path, with trajectories coming from northeast to south (Figure IV.7.b). A far more disorganized cluster than R1, spring and fall events were more likely in this grouping, often associated with precipitating events when either the site was located just north of the early stages of a surface stationary front and/or south of a primary high pressure maximum. Some events also occurred in the region ahead of a surface

occlusion, explaining the easterly transport. Inter-cluster Hg concentrations were correlated once again with S, but also with Fe, Cl, Pb and P, with the multivariate statistical models predicting a primarily coal influence (58% and 76%), Unmix identified incineration/smelting as also having a significant impact (22%). The significance of multiple tracers, as well as the wide range inter-cluster Hg concentrations (5.0 – 78.9) indicated a large degree of varying source influence, and may possibly be explained by the disorganized structure and varying meteorological conditions that fell into this group.

R3 Stagnant southerly flow once again clustered together, with 24 hour endpoints falling almost on top of the 12 hour endpoints, all tracers with the exception of P had significant correlations. This cluster did not necessarily follow a specific transport regime and was primarily grouped due to local stagnation, a fact that caused events from all seasons to fall into this category. The summertime events that fell into this category were associated with afternoon ordinary (air-mass) thunderstorm convection, while the spring and winter-time events occurred when a system of low pressure passed almost directly over the site, with precipitation occurring just ahead of the low, both conditions leading to local stagnation. The lowest Hg concentration for this cluster was twice the baseline, indicating that the degree of stagnation, and consequently, local pollutants, consistently enhanced any background concentrations. Within this cluster, Hg was correlated with all trace elements with the exceptions of La and Se. La, a soil tracer is typically positively correlated with wind speed as higher winds pick up more particles. It is unclear why Se is not correlated with Hg, as PMF identifies 77% of the Hg due to coal. 11% of all Hg wet deposition to Steubenville falls within this cluster.

R4 Similar in synoptic situation to R1, the events in this cluster are associated with cell lines of precipitation preceding, or along, a cold frontal boundary. The low that passes north of the receptor site is somewhat deeper in this case, however, causing steeper pressure gradients and consequently moderately higher surface winds, 12 hour endpoints fall in southern West Virginia, while 24 hours prior to precipitation the air parcel was along the Tennessee/North Carolina border or in northern South Carolina. It is interesting to note that despite similar directionality of R1 and R4, the VWM

concentration for R4 is lower (12.0 vs 15.4ng L^{-1}), presumably due to degree of stagnation and air mass transport differences. S and Pb were significantly correlated to Hg concentration, and the multivariate statistical models predicted, once again, coal contributions in excess of 60%. With a slightly lower average event deposition than the previous three cluster groups, approximately 7% of the total Hg deposition is attributed to this transport type.

R5 This cluster, driven primarily once again by the summer northern location of the jet stream that leads to lows passing through the northern Midwest, is made up, almost exclusively, of cold frontal rain. With a slight western shift from R4 and significantly higher surface transport that R1, this air mass group traveled 390 ± 70 km in the 12 hour preceding maximum precipitation. Correlations are significant with S, Fe, Cl, Pb and Se, presumably because of the direct path of the last 12 hours through the Ohio River Valley, and the numerous and many types of emission sources therein. Model results indicate a primary coal influence (57 – 67%) with some possible impact from soil and phosphourus, although these tracers were not significantly correlated with Hg concentration. A moderate average deposition leads to 6% of wet deposited Hg falling into this transport category. An individual event (8/3/2006) from this cluster was thoroughly examined as a case study in White et al. (11), and local Hg concentrations were found to be minimally enhanced by the near-field source.

R6 Precipitation in this cluster occurs well behind the passage of either a cold or stationary front, leading to northeasterly flow, causing the air masses to pass through Detroit, MI, Toledo, OH and Northeastern Ohio. The wind speeds were moderate for this cluster, but calmer than average. P, La, Fe and S were correlated with Hg concentration. Mean deposition was moderately low as was mean concentration, PMF predicted some contribution from incineration sources, and is probably due to municipal waste incinerators in northeast Ohio and the Detroit area (Appendix A, Figure 3). Coal is predicted to contribute approximately 60% to the cluster deposition, measured to be 6% of total Hg deposition.

R7 The situation almost exclusively typified by precipitation and westerly flow following the passage of a cold front accounts for 7% of total Hg deposition, and is high in VWM Hg concentration at 16.4 ng L^{-1}. Twelve hour endpoints land near the Ohio/Indiana border, and wind speeds gain momentum between 12 and 24 hours, for trajectories ranging everywhere from central Wisconsin to southern Illinois, with the Chigago/Gary area being a potential contributor to this cluster's Hg. Moderate wind speeds such as these, but from a source area, lead to enhanced Hg concentrations. It is interesting that even at a receptor site so surrounded by emission sources, regional pollution transport can be observed. Significant correlations with La and P (re-suspended soil) are also understandable given the moderate to high wind speeds. 60 and 69% (Unmix and PMF, respectively) of the Hg in this cluster is still, however, predicted to be from coal sources.

R8 Somewhat similar in transport direction to R4, the interesting dynamics of this cluster lead to stagnation 12-24 hours upwind of the site. The SES air mass transport regime typically occurs ahead of a cold front or in the region to the east of the occluded portion or warm front portions of a surface cyclone. While the 12 hour distance from receptor site was 380 ± 80 km, the air mass traveled less than 150 km in the 12 -24 hour time period (24 hour endpoints at 500 ± 160 km), leading to increased residence time in Virginia and northern North Carolina. An area of relatively few point sources, transport from this region leads to an even lesser VWM than R4 at 10.0 ng L^{-1}, well below the total rain average. While PMF results indicate 75% of the Hg present is from coal, Unmix predicts a significant portion (24%) may be from incineration/smelting, and this influence is further reflected in the Hg relationship to Cl. The remnants of Hurricane Katrina (2004) fell into this cluster.

R9 Representing a unique synoptic situation, cluster 9 was rare, and accounted for less than 1% of the total Hg deposition and was extremely low in VWM concentration. These late fall and winter rain events were associated with one occurrence when 2 low pressure systems combined to form a deep low and in the other cases, perfectly aligned upper level features drove steep pressure gradients and consequent high geostrophic winds. With only 24 and 56% of the Hg attributed to the coal profile (Unmix and PMF respectively),

the other significant sources were P and soil. The high winds are expected to increase crustal influence, and the P explanation is twofold: if transport was truly on the order of 72 hours, it is possible that phosphorus production in the south eastern U.S. influenced precipitation in Steubenville, or that phosphorus as fertilizer combined with the soil was picked up with high winds. Whatever the source, it should be noted that any statistical analysis on a sample N of 3 is weak, and this cluster accounts for less than 1% of the total Hg deposition.

S/M1 The polar jet stream moves south in the winter and gains momentum, bringing upper level support to mid-latitude cyclones that propagate west to east as in the summer, but farther south. In the case of S/M1, the winter snow and mix occurs in the region just north of the surface low, with winds preceding precipitation from the east. While only slightly above average (11.7 ng L^{-1}) for VWM concentration for snow and mix, this transport pattern brings about the highest average event deposition (0.26 μg m^{-2}) of any cluster studied as the average event precipitation depth was exceptionally high (2.4 cm) for this type of precipitation. One event was over 7 cm and the three snow events that seem to drive the negative linear relationship in Figure IV.3c were contained in this transport regime. Degree of stagnation for both the last 24 hours and the 6 to 9 hour trajectory segment were significantly correlated with individual event Hg concentration within this cluster, an indication that sources affecting the concentration variability were within 215 ± 150 km (distance to 24 hours for this cluster) of the receptor site, and possibly within 120 to 170 ± 60km (distance to 6 and 9 hours.) While coal is predicted by the multivariate statistical models to play a smaller role in the mixed and snow precipitation, approximately 50% was attributed to this source, with significant contributions calculated for incineration and crustal factors as well. Significant correlations were observed between Hg and S, Pb and P concentrations.

S/M2 Averaging < 0.5 cm in precipitation depth, this cluster represented small deposition (0.08 μg m^{-2}) events with high VWM Hg concentrations (15.1 ng L^{-1}). A particular synoptic situation did not describe this regime that clustered events from primarily January and February. Stagnation in the last 24 to the SW of the receptor site leads to Hg

correlations with S, Fe and La. While PMF modeled 41% of the Hg in this cluster due to incineration, Unmix maintained that 62% could be attributed to coal. This is the highest (although not statistically significant based on discrete difference percentile uncertainties) difference between the two source attributions for any cluster and may be due to the low event depositions.

S/M3 A similar transport regime to R8, although with a slightly more easterly component, the maximum precipitation occurred ahead of a surface low or to the northeast of a developing stationary front. While winds just prior to the event were moderate to slightly stagnant, the VWM mean Hg concentration was low for this cluster, presumably due to transport from the Virginia and North Carolina region. Again, the air mass was slow moving between 12 and 24 hours, with 12 hour distances from Steubenville at approximately 300 km, while the 12 hours prior (to 24 hours back) saw the air masses being transported an average of 50 km. PMF and Unmix models agreed with coal attribution (50%) with crustal components (Unmix 33%) and incineration (PMF 24%) also playing a significant role. Se, Pb and Fe were correlated to inter-cluster Hg concentration variability, with this being a rare case where S was not significant to the single variable linear regression. This cluster contributed 4% of the total Hg wet deposition.

S/M4. Rapid south west transport was associated with maximum precipitation occurring along a cold frontal boundary with the surface low passing to the north of the receptor site, a similar situation to S1 and S5, but with stronger winter winds. Rapid, winter time transport from a region that during slower summertime wind situations is associated with high concentration and high deposition, brings about lower VWM concentrations. Slightly more of the Hg deposition than for other S/M clusters could be attributed to coal, as understandable from the southwest trajectory, and smelting/incineration also play a role. Se, Pb, Fe and S were all significantly correlated with Hg concentration in this cluster, which contributed 2% of the total Hg deposition.

S/M5 A uniquely wintertime situation, clear, cold continental polar air moves over the warmer water of the Great Lakes (this cluster predominately occurs in November when surface water temperatures are still relatively warm), picking up moisture and creating lake-effect snow and mixed precipitation, a phenomena that is predominately highly localized, usually extending a few to 50 km to the leeside of the lakes (28). Seven times during the course of precipitation collection, this lake effect snow reached the Steubenville receptor site. Because the moisture is of Great Lakes origin, the associated pollutants are most likely regional, if not local in nature. The highest bottom end of Hg concentration ranges falls into this situation, 2.5 times what is considered baseline for Steubenville. The only significantly correlated tracer is Pb, the models predict slightly less than 50% of the Hg due to coal combustion with a significant percentage due to incineration (32% PMF) and P source (28% Unmix). This meteorological situation yields less than 1% of all wet deposited Hg due to the rarity of the situation and low depth accumulation, but is high in VWM Hg concentration.

Overall, it was shown that when grouped by endpoints, the trajectories fell into specific synoptic meteorological situations. Both the direction and degree of stagnation 24 hours prior to precipitation effected the Hg concentrations, with similar directions (R1 and R4, R5 as well as S/M2 and S/M4) yielding vastly different VWM concentrations depending on the transport speed. Local stagnation led to enhancement of background Hg concentrations as indicated by high minimum concentrations in the stagnant clusters. Surface winds that were of the same magnitude (R1 and R2) but from different directions also resulted in varying VWM Hg concentrations. The middle latitude cyclone situation produced the majority of precipitation events, the cluster in which the trajectory fell determined by either the quadrant in which the receptor site fell for the particular event or the frontal region for which the maximum precipitation was associated.

Acknowledgments

This work has been funded wholly or in part by the U.S. Environmental Protection Agency Office of Research and Development through cooperative agreement R-82971601-0, and Student Services Contract EP07D000572. It has not yet been subjected to Agency review. Mention of trade names or commercial products does not constitute an endorsement or recommendation for use. We thank Jim Barres and Ali Kamal (UMAQL) for managing laboratory support operations and data processing; Dr. James Slater (Franciscan University) for on-site logistical support, Dr. Larry Oolman of the University of Wyoming for surface observations, Gary Norris for aid with the PMF and Unmix models and NOAA ARL for the provision of the HYSPLIT transport model.

Table IV.1: Source profile tracers and ratios used in identification of modeled factors.

Source	Tracers
Soil/crustal dust	Mg, Al, Se, K, Ca, Sc, Ti, Mn, Fe, Ga, Sr, La, Ce, Sm (10, 31) Upper continental crust ratios: La/Ce: 0.5 – 0.6, Mg/Al: 0.2 – 0.3, Rb/Sr: 0.1 – 0.3, Fe/Al: 0.4 (31)
Coal combustion	S, Al, Fe, Si, Ca, Se (8)
Oil combustion	S, V, Ni, Al, Ca, Fe (8) Mo (10) Ratio: La/Ce 1-2 (32) V/Ni: 2.7 ±0.1 (8)
Petroleum refinery	La, Ce, Nd
Motor Vehicles	Si, S, K, Ca, Fe, Cu, Zn, Ba (9) Ratios: La/Ce: 0.3 (32)
Smelters	Ni, Cu, As, Cd, In, Sn, Sb, Pb
Marine Aerosol	Na, Cl (10) Sr, Mg (32)
Vegetation Burning	Organic and Elemental Carbon, Cl, K, Zn
Iron/Steel Manufacturing	Mg, Cr, Mn, Fe, Co, Ni
Incineration	Cl, Zn, Ag, In, Sb (10) Pb (32)
Cement	Ca, K in absence of Si, S Ratios: La/Ce: 0.3 Mg/Al: 0.35, Fe/Al: 0.4 (10)

Table IV.2: PMF five factor source profile. Analyte in bold if representative of greater that 40% of total species deposition, replaced with "x" if the 5th percentile uncertainty for the bootstrap run was not greater than zero.

	Source 1 Crustal, no temporal trend	Source 2 Phosphorus, spring dominated	Source 3 Iron and steel production	Source 4 Coal combustion	Source 5 Incineration
Cl	x	x	413	x	**3157**
NO_3	1030	x	x	3779	**8773**
Rb	0.23	0.34	x	0.24	0.20
Sr	**5.9**	1.8	0.9	0.3	2.9
Cd	x	x	0.06	**0.56**	0.17
La	**0.56**	x	x	x	0.12
Ce	**1.08**	x	0.05	x	0.21
Pb	x	0.93	1.32	2.74	**4.66**
Mg	**388**	x	206	x	x
Al	**347**	97	62	x	x
P	x	**81**	x	x	x
S	x	1230	x	**11227**	x
V	x	x	**2.82**	1.57	x
Cr	x	0.14	**2.07**	0.68	x
Mn	21.7	x	**51.9**	x	x
Fe	x	128	**331**	x	26
Ni	0.42	x	0.81	1.09	0.86
Cu	x	x	5.2	11.4	9.2
Zn	2.9	9.7	6.6	22.3	**34.3**
As	0.11	0.26	0.02	**0.78**	0.60
Se	x	x	x	**2.86**	0.95
Ba	**8.21**	2.68	1.02	1.67	4.57
Hg	0.01	0.02	0.01	**0.14**	x
%Hg	5.9	7.9	4.2	**70.9**	x

Table IV.3: PMF and Unmix yearly coal contribution and total modeled deposition in μg m^{-2}

	Measured Hg deposition	PMF Hg deposition by coal	PMF Hg deposition total	Unmix Hg deposition by coal	Unmix Hg deposition total
2003	13.1	7.9 (67%)	11.7	8.3 (59%)	14.1
2004	19.7	12.6 (74%)	17.1	12.3 (63%)	19.7
2005	16.2	11.3 (78%)	14.5	10.4 (66%)	15.7
2006	13.2	8.9 (74%)	11.9	7.3 (54%)	13.5
2007	13.9	8.1 (65%)	12.4	8.0 (58%)	13.8
Study Total	81.6	51.3 (71%)	72.5	49.7 (60%)	82.9

.

Table IV.4: Unmix five factor source profile scores. Analyte in bold if representative of greater that 40% of total species deposition, replaced with "x" if the 5% bootstrap uncertainty is not greater than zero.

	Source 1	Source 2	Source 3	Source 4	Source 5
	Incineration/ Smelter	Phosphorus	Iron and steel production	Crustal	Coal combustion
Cl	x	x	1000	1240	**1790**
NO^3	1580	1640	x	3570	**7950**
Rb	0.10	0.45	x	0.43	0.27
Sr	0.87	1.74	0.86	**6.61**	2.07
Cd	**1.19**	x	x	x	x
La	x	x	x	**0.79**	0.06
Ce	x	x	x	**1.46**	0.14
Pb	2.59	x	3.74	2.2	3.81
Mg	x	x	160	**849**	x
Al	x	x	x	**585**	61
P	x	**98.0**	x	x	x
S	2560	1220	x	2340	**10100**
V	0.37	0.34	2.19	1.12	1.78
Cr	x	x	3.02	0.41	0.36
Mn	x	x	43	**54**	x
Fe	x	135	311	153	63
Cu	x	x	10.1	x	14.9
Zn	22.7	x	**47.9**	x	18.3
As	0.19	0.20	0.22	0.38	**0.96**
Se	x	x	0.60	x	**3.91**
Ba	1.9	1.8	x	**9.6**	5.7
Hg	0.04	.01	x	0.03	**0.14**
%Hg	16%	6%		12%	**60%**

Table IV.5: Precipitation and air mass transport statistics by cluster.

	Hg VWM (ng L^{-1})	Range	Fraction of total deposition	Mean Hg Deposition (µg m^{-2})	Standardized 12 hr WS	Standardized 24 hr WS	Classification	Direction
R1	15.4	5.4-67.5	.24	0.20	-0.68	-0.73	Stag	SW
R2	12.8	5.0-78.9	.13	0.24	-0.75	-0.77	Stag	E
R3	14.3	7.8-41.8	.11	0.20	-1.06	-1.05	Stag	S
R4	12.0	4.5-38.9	.07	0.18	-0.01	-0.09	Mod	SWS
R5	12.8	3.3-44.5	.09	0.16	0.17	0.16	Mod	SW
R6	12.7	7.5-61.2	.06	0.16	-0.47	-0.21	Mod	NW
R7	16.4	6.2-43.0	.07	0.18	0.29	0.59	Mod	W
R8	10.0	4.0-47.0	.08	0.20	0.16	-0.20	Mod	SES
R9	8.8	5.6-13.5	<.01	0.11	2.35	2.30	Rapid	S
Rain Total	13.4	3.3-78.9	0.86	0.18				
S/M1	11.7	8.4-24.3	.06	0.26	-0.81	-0.54	Stag	E
S/M2	15.1	4.3-48.6	.02	0.08	-1.14	-1.02	Stag	SW
S/M3	9.6	4.3-20.7	.04	0.14	-0.06	-0.59	Mod	SE
S/M4	10.9	4.7-32.9	.02	0.10	1.09	1.09	Rapid	SW
S/M5	16.0	10.6-36.2	<.01	0.06	0.92	1.06	Rapid	NW
Snow/Mix Total	11.2	4.3-48.6	0.14	0.13				

Table IV.6: Count of trajectories for each month, aggregated by cluster.

	jan	feb	mar	apr	may	jun	jul	aug	sep	oct	nov	dec
R1	0	0	1	3	8	8	17	10	5	5	1	1
R2	1	2	3	5	1	2	2	4	6	0	2	0
R3	2	1	2	0	4	2	5	4	0	2	1	4
R4	0	1	3	1	2	3	1	1	2	3	1	2
R5	0	0	0	4	4	1	4	5	4	3	2	0
R6	1	0	3	0	4	3	7	0	2	2	0	0
R7	0	2	2	0	3	4	7	1	2	2	2	0
R8	2	2	0	3	0	1	1	1	2	2	3	4
R9	1	0	0	0	0	0	0	0	0	0	2	0
S/M1	2	3	5	2	1	0	0	0	0	0	2	2
S/M2	5	5	1	0	2	0	0	0	0	0	0	1
S/M3	5	4	1	0	0	0	0	0	0	0	2	4
S/M4	5	3	2	0	0	0	0	0	0	0	2	1
S/M5	2	1	1	1	0	0	0	0	0	0	5	1

Table IV.7: Percentages of modeled source attribution by cluster.

	Unmix P	PMF P	**Unmix inc/smelt**	PMF inc	**Unmix iron/steel**	PMF iron/steel	**Unmix soil**	PMF crust	**Unmix coal**	PMFcoal	Fraction of total deposition
Rain 1	8	10	9	9	3	2	9	3	70	76	.24
Rain 2	6	7	22	10	6	4	8	3	58	76	.13
Rain 3	5	6	21	9	2	2	11	5	61	77	.11
Rain 4	5	7	15	11	5	5	10	4	65	72	.07
Rain 5	10	14	15	11	3	3	15	5	57	67	.09
Rain 6	9	13	13	15	6	5	13	4	58	64	.06
Rain 7	8	10	16	12	4	4	12	4	60	69	.07
Rain 8	4	5	24	12	4	4	8	4	60	75	.08
Rain 9	30	24	8	6	7	6	30	8	25	56	<.01
S/M 1	5	6	14	20	7	5	27	14	46	53	.06
S/M 2	3	7	17	41	7	9	11	5	62	39	.02
S/M 3	4	5	10	24	5	6	33	15	49	50	.04
S/M 4	5	6	22	17	10	9	12	4	52	64	.02
S/M 5	28	13	10	32	5	7	13	2	45	46	<.01

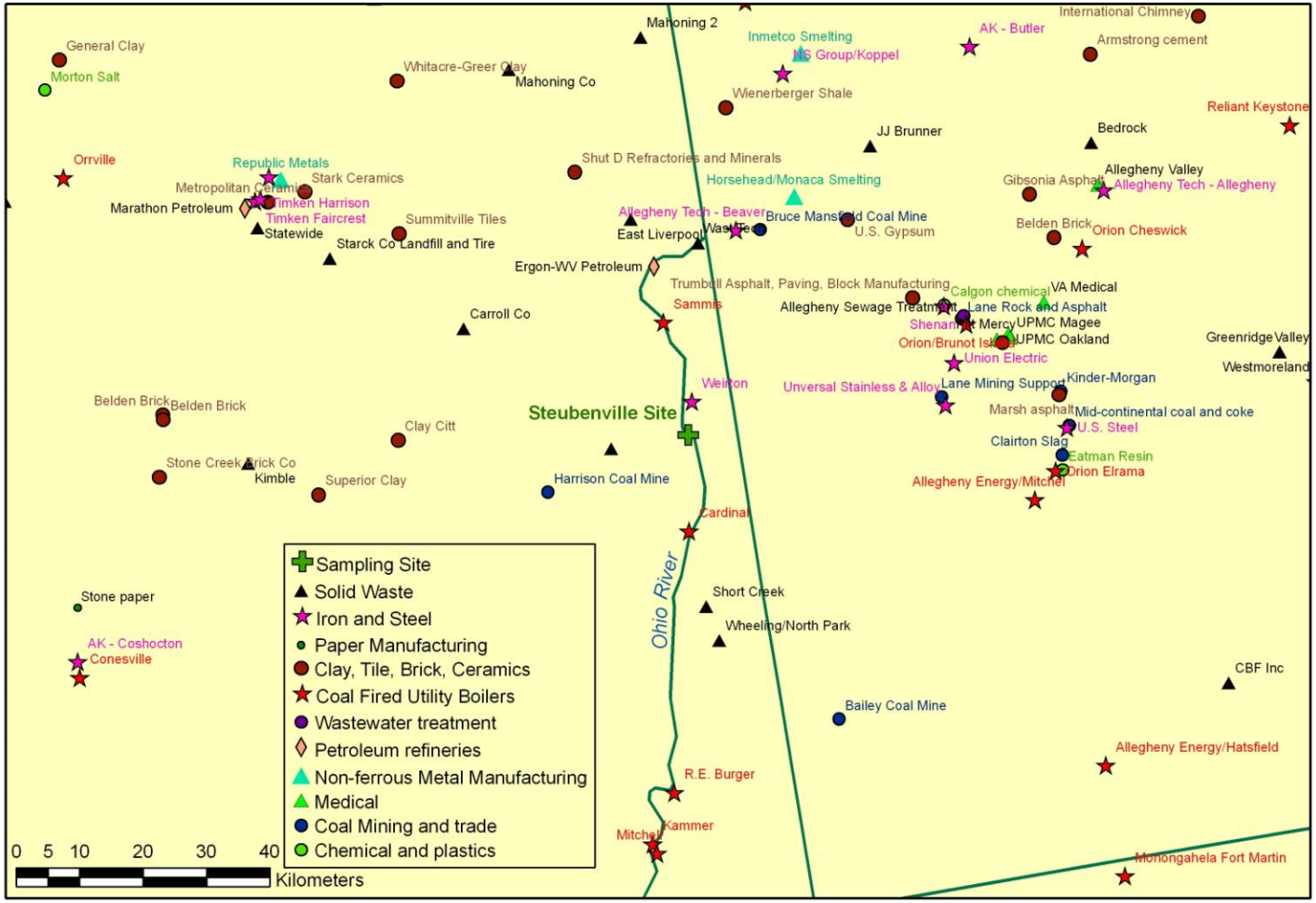

Figure IV.1: Steubenville site location and mercury point sources > $1*10^{-6}$ tons year $^{-1}$ (NEI, 2002)

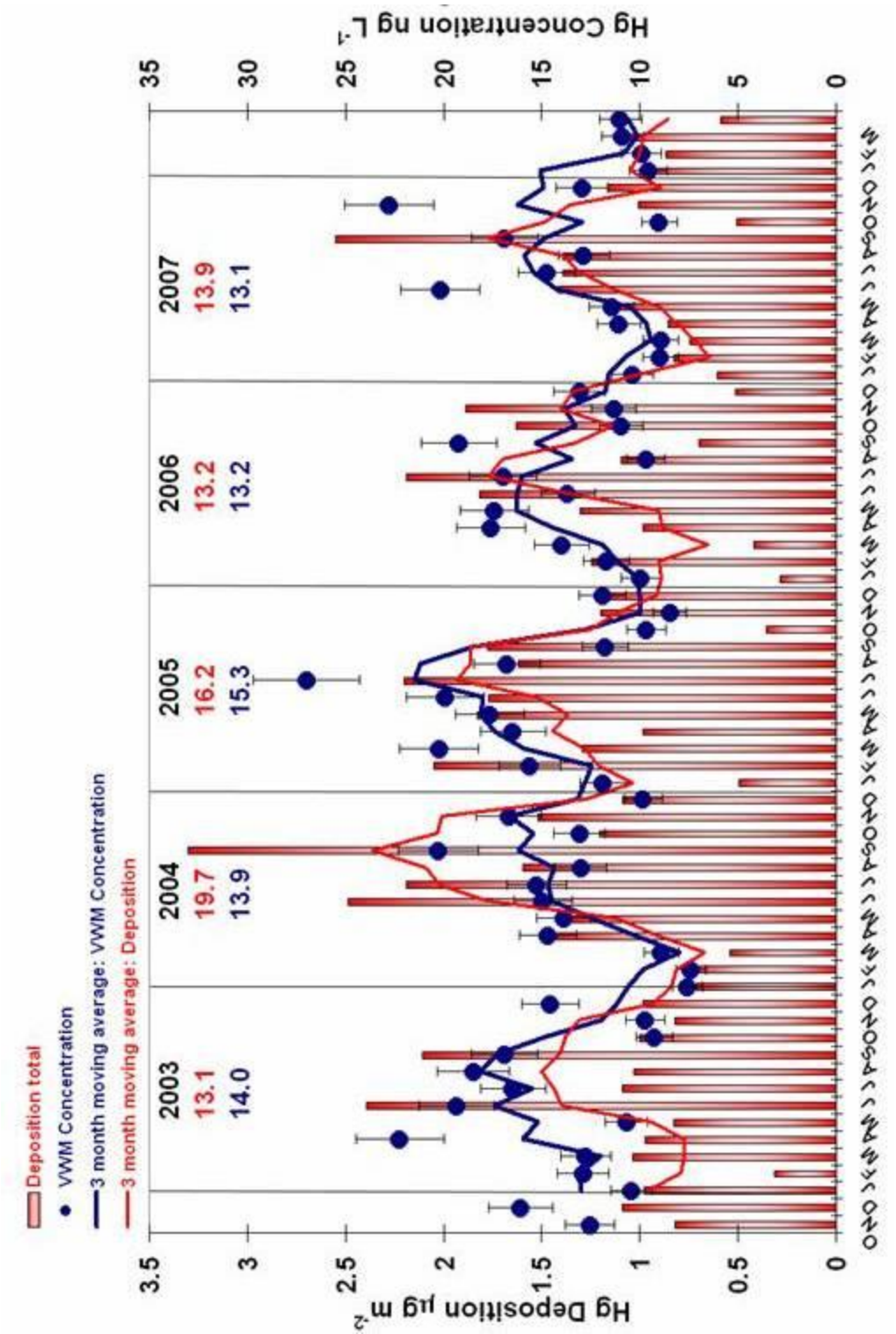

Figure IV.2: Hg wet deposition by month from November 2002 to April 2008 for Steubenville, Ohio. Yearly depositions (red) and volume weighted mean concentrations (blue) found below year label.

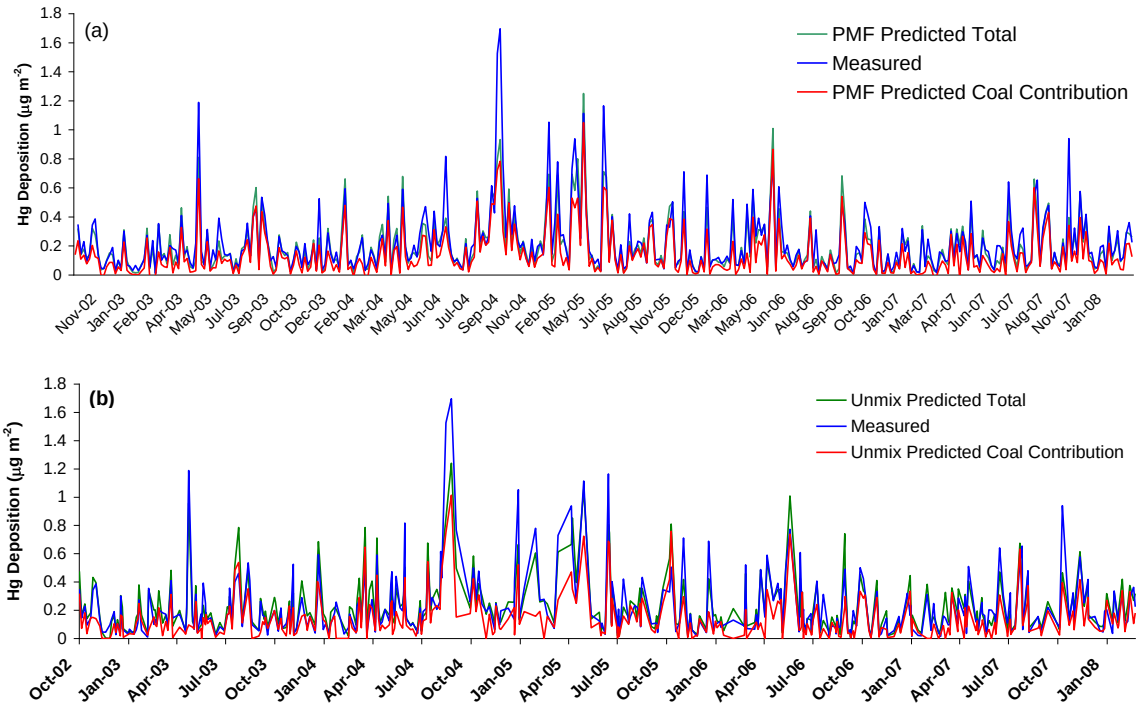

Figure IV.3: (a) PMF and (b) Unmix modeled depositions by event time series.

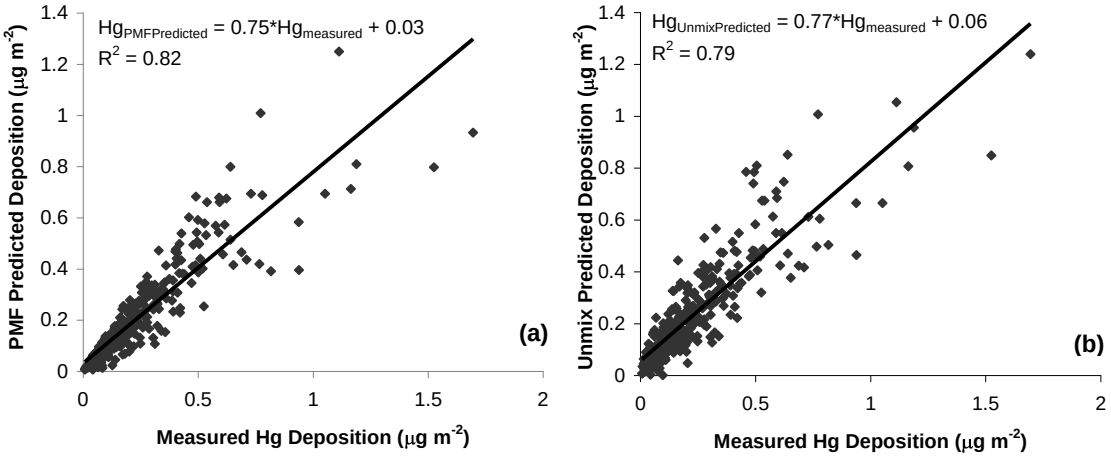

Figure IV.4: (a) PMF and (b) Unmix model versus predicted Hg deposition by event.

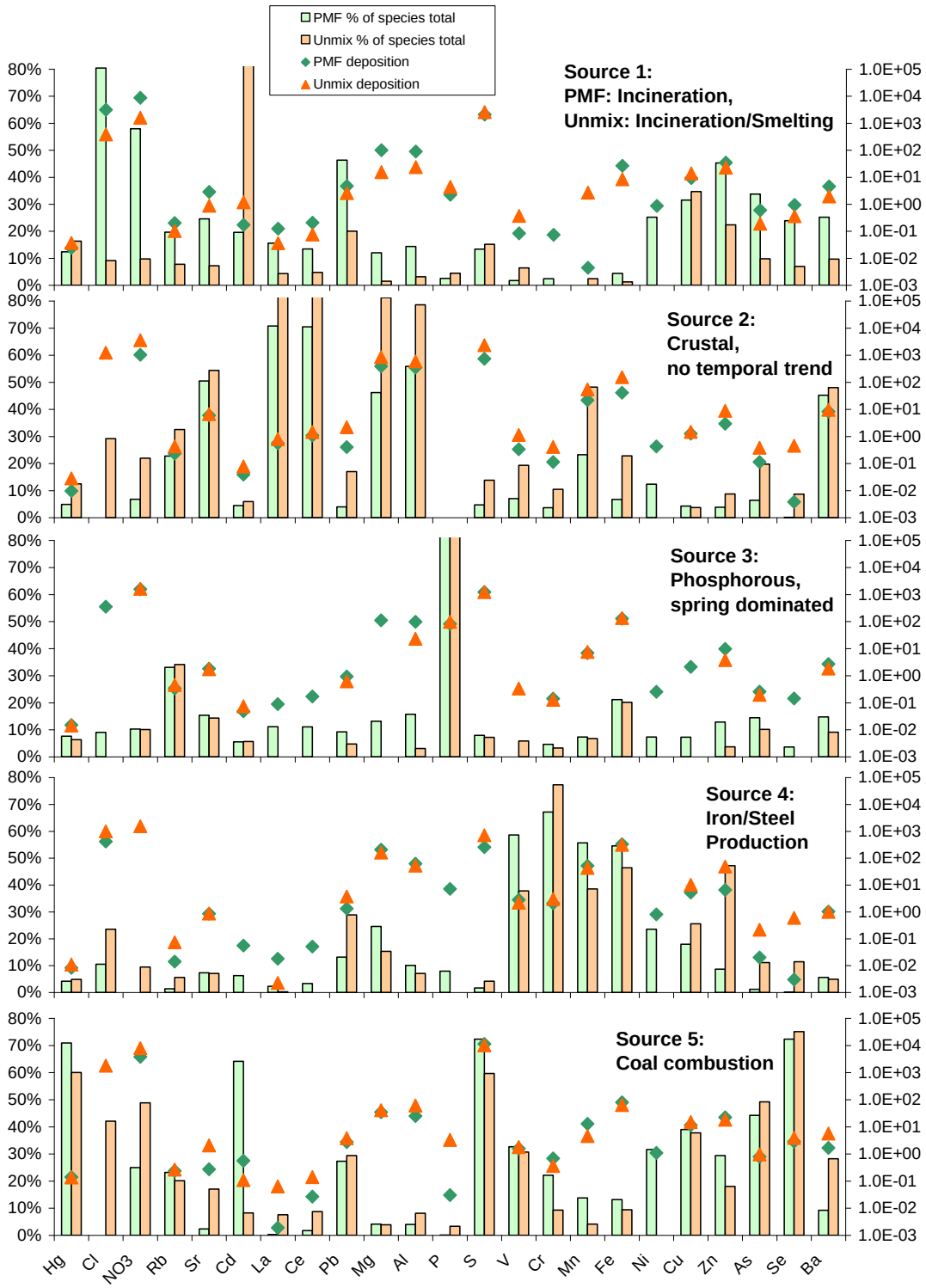

Figure IV.5: Model source profile comparisons.

Figure IV.6 (a-d) 72 hour back trajectories for rain events clustered by 24 hour endpoints. 12 hour (red) and 24 (violet) endpoints are highlighted.

Figure IV.7 (e-i) 72 hour back trajectories for rain events clustered by 24 hour endpoints. 12 hour (red) and 24 (violet) endpoints are highlighted.

Figure IV.8 (a-e): 72 hour back trajectories for snow and mixed precipitation events, clustered by 24 hour endpoints. 12 hour (red) and 24 (violet) endpoints are highlighted.

CHAPTER IV: References

(1) Expert Panel on Mercury Atmospheric Processes. *Technical Report EPRI/TR-104214;* **1994**.

(2) Lin, C.; Pehkonen, S.O. The chemistry of atmospheric mercury: a review *Atmos. Environ.* **1998**, 33, 2067-2079.

(3) Lindberg, S., Bullock, R., Ebinghaus, R., Engstrom, D., Feng., Fitzgerald, W., Pirrone, N., Prestbo, E., Seigneur, C., A Synthesis of Progress and Uncertainties in Attributing the Sources of Mercury in Deposition. *AMBIO* **2007**, 36, 19-31.

(4) United States Court of Appeals for the D.C. Circuit. State of New Jersey, et al., v. Environmental Protection Agency. Decided February 8, **2008**.

(5) Eilperin, J. Nations to Write Treaty Cutting Mercury Emissions. The Washington Post. February 21, **2009**.

(6) Keeler, G.; Glinsorn, G.; Pirrone N. Particulate mercury in the atmosphere: its significance, transport, transformation and sources. *Water Air Soil Pollut*. **1995**, 80, 159-168.

(7) Keeler, G.J.; Landis, M.S.; Norris, G.A., Christianson, E.M.; Dvonch, J.T. Sources of Mercury Wet Deposition in Eastern Ohio, USA Environ. Sci. Technol. **2006**, 40, 5874-5881.

(8) Landis, M.S., Hays, M., Beck, L., and Ryan, J., Contemporary Inorganic Source Profiles from Oil- and Coal-Fired Utility Boilers. Air Quality VI Conference, Arlington, VA. **2007**.

(9) Landis, M.S., Lewis, C.W., Stevens, R. K., Keeler, G. J., Dvonch, J. T., Tremblay, R. T., Ft. McHenry tunnel study: Source profiles and mercury emissions from diesel and gasoline powered vehicles. Atmospheric Environment. **2007**, 41, 8711-8724

(10) Keeler, G.J. A Hybrid Approach for Source Apportionment of Atmospheric Pollutants in the Northeastern United States. PhD Dissertation, University of Michigan. **1987.**

(11) White, E.M., Keeler, G.J., Landis, M.S. Spatial Variability of Mercury Wet Deposition in Eastern Ohio: Summertime Meteorological Case Study Analysis of Local Source Influences. Environ. Sci. Technol. May **2009**. Chapter III of current dissertation.
(12) Landis, M.S.; Keeler, G.J. Critical evaluation of a modified automatic wer-only precipitation collector for mercury and trace element determinations. *Environ. Sci. Technol.* **1997**, 31, 2610-2615.
(13) Hoyer, M. PhD thesis, Wet Deposition of mercury in Michigan: Meteorological associations and spatial variability. University of Michigan, Ann Arbor, MI, **1995.**
(14) Paatero, P. Least squares formulation of robust non-negative foctor analysis. *Chemometrics and Intelligent Laboratory Systems* **1997** 37, 23-35.
(15) Henry, R.C. Multivariate receptor models – current practice and future trends. *Chemometrics and Intelligent Laboratory Systems*. **2002**, 60, 43-48.
(16) Positive Matrix Factorization User Guide Version 3.0 developed for the US EPA by Lockheed Martin. June 13, **2008**.
(17) Norris, G.A.; Henry, R.C.; Vedantham, R.; EPA Unmix User Guide. October **2005**.
(18) Lewis C.W.; Norris, G., Henry,R. Source Apportionment of Phoenix PM2.5 Aerosol with the Unmix Receptor Model *J. Air & Waste Manage. Assoc*. 53: 325-338.**2003**.
(19) Fernau, M.E. Use of cluster analysis to define periods of similar meteorology and precipitation chemistry in eastern North America. PhD Dissertation, University of Michigan. **1988.**
(20) Moody, J.L. The influence of Meteorology on precipitation chemistry at selected sites in the Eastern United States. PhD Dissertation, University of Michigan **1986**.
(21) Landis, M.S, Lake Michigan Mass Balance Study. PhD dissertation, University of Michigan. **1998.**
(22) Gratz, L.E., Keeler, G. J., Al-wali, K. Lon-term Atmospheric Merucyr Wet Deposition at Underhill, VT. International Association of Great Lakes Research Conference. **2005.**
(23) Gratz, L.E. Personal communication, **2009.**
(24) Yatavelli, R. L.; Fahrni, J.K., Kim, M.; Crist, K.C.; Vickers, C.D.; Winter, S.E., Connell, D.P. Mercury, PM2.5 and gaseaous co-pollutants in the Ohio River Valley

region: Preliminary results from the Athens supersite. *Atmos. Environ*. **2006**, 40, 6650-6665.

(25) Keeler, G.J.; Dvonch, J.T. Atmospheric mercury: A decade of observations in the Great Lakes. In: *Dynamics of Mercury Pollution on Regional and Global Scales: Atmospheric Processes and Human Exposures around the World;* Pirrone, N., Mahaffey, K., Eds,: Kluwer Ltd: Norwell, MA, **2005.**

(26) Keeler, G. J., Gratz., L. E., Al-Wali, K. Long-term Atmospheric Mercury Wet Deposition at Underhill, Vermont. Ecotoxicology, **2005**, 14, 71-83.

(27) Prestbo, E.M., Leutner, J.m. and Pollman, C.D. 2006 Abrupt decrease in mercury wet-deposition concentration and annual flux in Seattle, Washington due to emission point source changes, In: *Proceedings of the International Conference on Mercury as a Global Pollutant.* Madison WI. **2006.**

(28) Ahrens, C.D. Air Masses and Fronts, Middle Latitude Cyclones, Thunderstorms. *Meteorology Today.* Ch 12-14. **2000.**

(29) Stull, R.S. Air Masses and Fronts. *Meteorology for Scientists and Engineers.* Ch 12. **2000.**

(30) Wang, J.X., Angell, J.K., Air Stagnation Climatology for the United States (1948-1998) *NOAA/ARL ATLAS No.1*. **1999.**

(31) Taylor, S. R. and McLennan, S. M. *The Continental Crust: its Composition and Evolution*. Blackwell Scientific Publication pp 46, **1985.**

(32) Dvonch, J.T., Graney, J.R., Marsik, F.J., Keeler, G.J., Stevens, R.K. An investigation of source-receptor relationships for mercury in south Florida using event precipitation data. *Sci. Total Environ.* **1998**, 213, 95-108.

CHAPTER V

Determination of Wet Deposited Hg Physicochemistry in the Ohio River Valley Through Sub-event Sampling Using the Automated Sequential Precipitation System

Abstract

Intra-storm variability and soluble fractionation was explored for summer-time rain events in Steubenville, Ohio, with the purpose of evaluating the physical processes controlling mercury (Hg) in wet deposition in a highly industrialized region. Precipitation samples were collected from July through September 2006 and analyzed for Hg and a suite of trace elements. Real-time filtration of event total precipitation revealed that 69% (±37%) of Hg in wet deposition was in a soluble form. In wet deposition, the trace elements show the following order of decreasing solubility: As > S > Zn > Na > Ca > Mn > Se > Mg > Hg > V > Cr > Fe ≥ La ≈ Ce. The Automated Sequential Precipitation Sampler II, designed by the University of Michigan Air Quality Laboratory, was shown to be effective in collecting discrete, sequential sub-event precipitation samples. Results indicated that Hg had lower 'scavenging coefficients' (the rate of Hg concentration decrease throughout the events) than the majority of elements analyzed, indicating that either (i) Hg is incorporated into rain via gas phase inclusion or particulate nucleation within cloud, (ii) or Hg is available in the boundary layer for scavenging, even in the latter stages of precipitation. The Hg scavenging coefficient was particularly low compared to S, a co-pollutant of Hg, with the highest scavenging coefficient. When compared to an upwind, regionally representative site, the scavenging coefficient of Hg for the locally influenced precipitation was significantly lower. This result indicated that continuous feed of soluble Hg may be the reason for the low scavenging coefficient. Overall, it was found that the physicochemical properties of Hg emissions result in elevated deposition rates near point sources.

Introduction

The mercury (Hg) wet deposition flux to the Eastern Ohio has been shown to be enhanced over other Northeastern and Midwestern US regions due to local and regional anthropogenic point sources (1, 2, 3). Hg wet deposition has been established as correlated to methylmercury concentrations in fish, a critical step in the bioaccumulation process of this hazardous neurotoxin (4). With current policy decisions regarding mitigation for both domestic and international Hg emissions under negotiation, the best possible understanding of biogeochemical cycling of Hg is essential.

The means by which a pollutant enters precipitation can be exceptionally dynamic, involves several possible processes, and is determined by numerous parameters. With pollutant species in both gas and particle forms, there is conversion from one form to another, and the particles on which the pollutant is bound can act directly as cloud condensation nuclei via nucleation scavenging. Soluble gases can diffuse into cloud droplets within cloud or below clouds in rain drops. Primarily coarse mode particles can also be scavenged by falling precipitation below cloud. The specific process that dominates at any one time depends on several factors: pollutant concentration, speciation, species solubility, conversion rates, moisture content, reactive gas concentrations, UV availability, temperature, and parcel height.

One way to experimentally determine removal mechanisms is to evaluate pollutant concentrations over the course of a single precipitation event. Sequential sampling of particles, major ions and total trace metals in wet deposition was explored at a rural site in Ireland in a study conducted by Lim et al. 1990 (5). This type of sampling allowed the researchers to determine the removal mechanisms of analytes. The author linked the relative cumulative deposition rates of the various constituents into three categories and was able to discern removal processes: sea-salt constituents were removed by below-cloud processes as indicated by the rapid removal rate; trace metal removal was dominated by in-cloud particle accumulation mechanisms while ammonium and non-sea salt sulfate had very low cumulative deposition rates, indicative of gas phase within-cloud scavenging of NH_3 and SO_2 gases (5). Although the solubility fractionation of heavy metals in precipitation has been discussed and deemed important both for flux

determinations as well as bioavailability properties (7, 8), there is no published literature pertaining to sequential sampling for Hg or the removal mechanisms therein.

Spatial modeling of Hg deposition fluxes is a poorly posed problem due to the complicated nature and gaps in our understanding of atmospheric chemistry and deposition processes of Hg, and the scarcity of speciated Hg measurements from emission point sources. Gaseous Hg is present in the atmosphere in two major inorganic forms: elemental Hg (Hg^0), and the divalent form of Hg (Hg^{2+}, often referred to as reactive gaseous mercury – RGM). Hg adhered to particles is referred to as particulate Hg (Hg(p)). While the global pool is >99% in the elemental form, emissions from point sources may range from 25 – 90% RGM (9). While Hg^0 is very low in solubility and therefore removed slowly due to deposition processes, Hg^{2+} is removed rapidly because of the high solubility and high affinity to surface reactions (9). Consequently, transformations between the oxidation states (Hg^0 oxidizes to Hg^{2+} in the presence of OH, O_3, and halides and it is thought that Hg^{2+} may reduce to Hg^0 in point source plumes and clouds) and emissions speciation will determine deposition rates (9).

The purpose of the following experiment was fourfold: (i) evaluate the physical processes that determine the inclusion behavior of atmospheric mercury in precipitation using sub-event sequential sampling events by comparing mercury to species with well known cloud and rain out processes, (ii) quantify the soluble and insoluble fractions of mercury to wet deposition in a highly industrial area, (iii) evaluate boundary layer removal of ambient gas and particulate pollutants during summer time precipitation events and (iv) evaluate the field deployment effectiveness of the Automatic Sequential Precipitation System (ASPS II).

Methods

Established in October of 2002, the advanced air monitoring site in Steubenville Ohio (40.379 N, 80.620 W; 306 m above MSL) was the result of a cooperative research study between the U.S. Environmental Protection Agency Office of Research and Development and the University of Michigan Air Quality Lab (UMAQL), with the

specific aim of investigating the impact of coal combustion on the chemistry, transport and deposition processes of Hg. The site was equipped with continuous ambient gas, particulate and meteorological instrumention. A listing of the instruments applicable to the current discussion, as well as the sampling interval for each measurement are listed in Table V.1.

As part of the long-term study, a summertime field intensive was conducted in July through September 2006. While several measurement methods were added to the above long term suite of measurements, only those of interest to the current experiment will be discussed here. An additional Tekran 2537a, 1130 and 1135 Hg speciation unit was employed for collocated precision calculations as well as the ability to increase data acquisition to every hour.

Precipitation collection was conducted by several different methods to evaluate both soluble and insoluble fractions as well as scavenging and washout properties of Hg. Event samples were collected under identical conditions to the long-term study, with two sample trains, one for Hg and the other for trace element determination, housed in a wet-only UM modified MIC-B precipitation collector. Detailed discussion of the event method can be found in previous literature (1, 2, 3, 10). A separate, UM modified MIC-B housed four sampling trains for event-total filtration: two co-located Hg and trace elements trains deployed to ensure sampling technique precision. In this study, the soluble fraction was operationally defined as that which passes through a 0.2 µm pore size polycarbonate filter membrane (8). The filtration was performed in real-time using vacuum chambers; sample bottles were placed inside the vacuum chambers immediately prior to rainfall, with the mouth of the bottle just below a 1 ½ inch piece of ¼ inch ID Teflon tubing fitted onto a filterpack housing the filter. The sample collection funnels were connected to the filterpacks with acid-cleaned 1cm ID c-flex. Small electric Gast pumps pulled the vacuum from a port at the bottom of the chamber. All components of the sample trains were thoroughly acid cleaned prior to deployment and funnels and bottles were prepared as described in Landis and Keeler (10).

It was noted in previous work (1, 3) that pure-event wet deposition, though integral to source apportionment modeling and meteorological evaluation, is difficult to collect on a long-term basis, due to the need for intense operator commitment. The ASPS

II was designed by UMAQL as a precipitation collection system that operates and collects precipitation according to user defined parameters. Housed in the wet-only ASPS cabinet, a system is comprised of (a) funnels, (b) funnel to rack adaptation apparatus, (c) bottle rack with computer controlled valve system, (d) data interface controller, (e) wetness sensor and (f) tipping bucket. Precipitation is collected by up to 4 removable bottle racks, each containing up to eight sample bottles. Valves (solenoid operated pinch valves) direct rainfall collected by the funnel into the appropriate bottle based on the user-defined sampling protocol. The valve keeps the bottles sealed at all times except when the currently 'active' bottle is receiving precipitation. The system consists of a rainfall collection 'controller' and data logger. The controller is mounted inside the precipitation collector and is connected to the racks. User input allows for numerous capabilities, as samples can be collected by time or total volume limitations. While the instrument's deployment in the field is for long-term precipitation collection on an event basis, for this experiment, the system was programmed to sample sequentially throughout each individual precipitation event based on volume limits, determined by depth accumulation recorded by the tipping bucket. The system records all events, such as rainfall time and amount, bottle begin and end times, temperature and lid position (open, closed or transitioning) in a comprehensive text-based format available for upload at any time via wireless internet, direct ethernet connection or remotely when the telephone line and modem option is employed.

To allow for the precipitation event to be split into several parts, a volume limit of 50 mL was set on the ASPS for each of the first 7 bottles, the eighth and final bottle collected until the end of the rain event, providing discrete, high resolution sub samples within a single storm. There were four sequential sample trains, one each to be analyzed for total mercury and trace metals and the other for soluble mercury and trace metals. To attain soluble-only sub-event samples, the valved sample tubing was connected to 50 mL polypropolene syringes that were HCl (3 M) acid cooked and BrCl (1% v/v) soaked. The user removed syringes as the system switched to the next bottle, and manually pushed the sample through a filter holder into a 125 mL Teflon sample bottle. Extensive laboratory evaluation of this method indicated less than 5pg L^{-1} contamination checks on the polycarbonate syringes, and no measurable loss of Hg to the polycarbonate surface with

exchange from syringe to Teflon bottle. Sub-event samples were collected for 3 summer months in 2006, while the filtered samples were collected for 1 ½ months as the operation of this collection type demanded operator presence at time of precipitation, see Table V.2 for specific types and dates.

In addition to the precipitation collection at the Steubenville primary site, precipitation was sequentially sampled, using the ASPS and identically programmed sampling parameters, at a more regionally representative site 40km to the west, from July 2 to August 3. This site, designated "STW", was situated in a rural area, and with primarily western flow, was to represent 'upwind' and therefore background Hg concentrations.

Event total samples[1] were collected for Hg analysis in 1 liter Teflon bottles with 20 mL of HCl preservative acid, while sub-event samples were collected in 125 mL Teflon bottles to reduce surface area and subsequent wall loss and reduce head space, with 2 mL HCl, a resultant average 10% v/v preservation. Trace element event total and sub-event samples were collected in 1 liter and 150 mL polypropolene bottles, respectively. Hg samples were oxidized to a 1% BrCl v/v solution, as determined gravimetrically, and stored in a dark cold room (5). A Tekran 2600 cold-vapor atomic fluorescence spectrometer (CVAFS) was employed for Hg concentration determination. Trace element samples were acidified to a 0.2% HNO_3, 0.1 % HCl solution and 42 elements were quantified on a ThermoFinnigan Element2 high resolution magnetic sector field inductively coupled plamsa mass spectrometer (ICPMS). Calibration check standards as well as sample replicates were run every six samples for both Hg and trace element analysis.

[1] Event total refers to samples that were collected without any processing, e.g. filtering, thus contain the soluble and insoluble fractions or were not sequentially split.

Results

Event statistics for the Ohio Mercury Monitoring Project wet deposition can be found in previous publications, but two key conclusions should be mentioned here as they have direct relevance to the current science question.

The variabilty in event total Hg concentration for the 5 ½ year study period was related to depth, with the degree of this relationship differing by precipitation type. Figures V.1(a-c) depict the negative relationship between concentration and depth, slope of the relationship an idication of washout properties. Previous studies find regionally influenced washout coefficients for rain on the order of -0.23 to -0.24, (11, 12) with lower coefficients (-0.16) in regions of local source influence (11). Here, a slope of -0.14 indicates Hg was avaible for scavenging into the later stages of precipitation, as even large precipitation amounts were high in concentration. Mixed precipitation was somewhat less efficient at scavenging with a washout coefficient of -0.08, while the relationship for snow was dominated by three large depth events, but neither relationship was significant at a $p<0.05$ level.

July and August precipitation accounts for approximately 30% of the yearly Hg wet deposition flux to the Steubenville receptor site (2).

Soluble Fraction Co-located filtered samples exhibited an absolute mean difference of 19% (1.4 ± 1.2ng L^{-1}, n=5) for Hg concentration. For the paired samples, 61% of the Hg concentration was in the soluble form, ranging from 43% for the sample collected on the afternoon of July 14, to 77% for the low Hg concentration event on July 11 (Figure V.1). Based on uncertainty estimates for the event total as 9.8% (9), the differences between the soluble and total Hg concentration are significant for all but one of the July 12 events.

In Table V.3, the solubility of other trace element are compared to that of Hg. Here, coefficients are not standardized, as both populations, the soluble and total concentration, are identical analytes and any variability between the data sets needs to remain intact for adequate representation. Analytes shown here were chosen based upon known particle properties: particles associated with combustion processes are often formed via gas to particle conversion, tend to form oxides and in the fine mode (<1 μm in

aerodynamic diameter) so they are highly soluble . Crustal elements, however, are typically course mode (>1μm) and are much less soluble (13). The elements are listed in order of decreasing solubility, based on the slope of the relationship between soluble and total concentrations, elements in bold are significant at $p<0.05$.

As hypothesized, combustion products formed via gas to particle conversion had the highest degree of solubility. Both As and S, largely products of coal combustion, were highly soluble, indicating that very little of these elements were in large particle form. The other extreme, La and Ce, which are crustal tracers, were not statistically analyzed in the same manner as the other metals because the soluble fraction in precipitation was below detection limit for all filtered samples. Method detection limits for La and Ce (0.0037 and 0.0041 ppb, respectively) were less than 10% of the event total wet deposited average concentrations for these elements (0.0529 and 0.1139 ppb, respectively, approximations in table calculated with maximum uncertainty). This indicates that a large percentage of these elements were in large particle form. The contribution of the soluble fraction to total wet deposition is greater than 50% for all metals with the exception of V, C, Fe and the crustal elements. This is in agreement with urban and industrial wet deposition heavy metals solubility work in Italy that found Cr to be only 12% soluble, and of the metals studied, Zn to be the most soluble (8). Hg falls at the lower end of the highly soluble group, indicating that while the majority of Hg in rain was incorporated either as gas phase inclusion or scavenging of small particles, large particle scavenging, perhaps fertilizer and windblown soil components may also play a significant role.

Sequential Sub-Event Fourteen of the 23 sequentially sampled events are depicted in Figure V.3.a-n, with the sub-sample Hg concentrations as a continuous line and the comparison of the volume-weighted mean for the storm splits compared to co-located event total collection Hg concentration as columns on the left. Nine events were excluded because they had fewer than 4 splits or were removed because the sample volume for one of the sub-event samples was less than 20 mL, the lower volume limit for blank contamination uncertainty. Overall, the sub-event volume-weighted means were not significantly different than the co-located event total Hg concentrations. The decrease

in concentration of Hg differs by event, for example, events a-f and h all exhibited an increase in Hg at some point in the sequence, in events g and j-n the Hg concentration decreased through-out the event. Sub-event soluble fraction Hg concentration is depicted as a blue line in V.3.b,c and e. While these 14 figures are each on a different scale, August 2 and 28 are maximized at 50 ng L^{-1}, while the July 12th AM event contained samples all below 8 ng L^{-1}, all samples have been standardized within the individual event in Figure V.4, and it can be seen that the behavior does not show an overall decreasing trend.

Every event demonstrated individual concentration trend characteristics, but a pattern seemed to emerge: earlier (July) samples deposition rates (concentration reduction over the course of an event) were lower than those for samples at the end of the study (September). Slopes for the deposition rates, while not listed because they are standardized and discussed in a subsequent section, ranged from a gain of 6.1 ng L^{-1} per sub-sample (Aug 28) to a loss of 4.2 ng L^{-1} per sub sample on September 28 (both significant at $p<0.05$). Therefore, in-depth investigations into groups of individual events from both July and September were conducted to elucidate the impact of meteorological and/or local ambient gas concentrations on deposition rates. Nine events are listed in Table V.5, with start and end times, duration, collected sample depth, wind speed and direction and SO_2 ambient gas data associated with each sub-event sample, and on the line preceding the individual sample parameters, the VWM of all sub-events, the event total Hg concentration and the wind and SO_2 averages for the 2 hours preceding the particular event. Precipitation Hg concentrations are listed for each event in Table V.5. Ambient Hg concentrations are listed for each event in Table V.6, as the Tekran Hg speciation units record in hourly increments, only averages for the 2, 6, 12, 24 hour time segments preceding and the first and last hour of rain fall are recorded here. Two event sub-sample sequences (Sept 12 and 13) and their corresponding local meteorology and ambient Hg and SO_2 concentrations are charted in Figure V.5.

Case Studies

July 4. Southerly winds were prevalent in the warm sector that produced the precipitation for this event, ahead of a cold front. The low and occlusion passed well north of the Great Lakes through central Ontario. There was a decrease in Hg concentration with the first three sequential samples, and an increase in sample concentration with sub-events four and five that did not coincide with rain rate, wind or ambient SO_2 changes. Winds shifted from north through northwest to southwest where it remained through the majority of the event, while SO_2 concentrations decreased throughout precipitation. The July 4th event does not have associated Tekran Hg concentrations due to field intensive initiation instrument calibration.

July 12. The next three sets of sequential samples were all associated with a similar synoptic situation, a long NE to SW Stationary front with preceding wind from the southwest, center of the low passing over central Michigan, but there was substantial abatement in precipitation events such that three discrete, separate events were collected. For the duration of the first set of sub-event samples in the early morning (0:19 to 1:50 EST: 7/12 early AM), Hg concentrations in rain decreased in the initial stages, but increased for samples four and five before dropping again in the last portion of precipitation (Figure V.2b, Table V.5). Wind speed, direction, rate did not change to explain the higher concentrations for sub-samples four and five, but SO_2 concentrations did increase slightly at the 5 minute interval corresponding to collection of these samples. Ambient concentrations dropped off significantly for all three Hg species throughout the course of this event.

Three hours later (4:50 EST: 7/12AM), rain began again, this time associated with slightly increased wind speeds (same direction as for prior event) and Hg concentrations in precipitation were lower and remained relatively unchanged throughout the event. It should be noted that the lowest event total Hg concentration collected at the Steubenville site for the 5 ½ year period was 3.3 ng L^{-1} (9/28/05), and baseline (operationally defined at 5th percentile) is 6.1 ng L^{-1}, while samples collected at less industrially influenced receptor sites maintained lower baselines (approximately half) and exhibited minimum concentrations less than 1 ng L^{-1}. Two of the eight sub-samples collected during this

event exhibited the lowest concentrations ever collected at Steubenville, indicating that wash-out of Hg in the earlier stages of precipitation may occur. All three species of ambient Hg concentrations were lower preceding the precipitation than for the early AM event discussed in the prior paragraph, as was the event total wet deposition Hg concentration.

The July 12 afternoon event (13:04 to 14:29 EST: 7/12 PM) exhibited an increase in Hg concentrations in the middle of the event, and was associated with decreased precipitation rate and a slight decrease in wind speeds. It was observed that the ambient particulate and divalent Hg concentrations dropped below instrument detection limit by the end of the course of the three events. SO_2 was also significantly reduced. The three separate rain events on July 12 all occurred under the same synoptic pattern. Therefore, they could be considered sequential samples in and of themselves. The significant increase in total event Hg concentration for the afternoon event as compared to the morning (based on associated error) indicates that local scale source contributions likely impacted the Hg concentrations.

July 14. Precipitation sub-event Hg concentrations increased and peaked during the middle of this event, a short evening rain associated with a stationary front. The rain did not cause a decrease in ambient RGM, however the Hg(P) dropped to below instrument detection over the course of the precipitation. SWS winds increased slightly and corresponded to the peak in sample five.

Sept 1. As discussed in White et. al. 2008, this event had low overall concentrations and was associated with the rear NW quadrant of Hurricane Ernesto. Relatively rapid NE winds brought about very low ambient Hg concentrations. Much lower rain rates than the July events were maintained throughout. A drastic reduction in SO_2 during the early stages of rain was mirrored by RGM and Hg^0, but not by Hg(p) which increased four-fold over the course of the rain. Over the eight hour period (20:38 to 5:01 EST), sub-event samples exhibited an increase in Hg concentration for the fourth sample, as well as a slight steady increase over the last 4 samples in the sequence.

Sept 12. A light rain lasted for a full 15 hours (8:00 to 23:00 EST), and was associated with southerly winds flowing into a large low that was situated over Indiana for the majority of the precipitation event. A slight wind direction change from approximately

185 to 195 degrees seemed to bring about a SO_2 concentration increase coincided with a peak in sub-event samples. Ambient Hg concentrations increased as well throughout the event, particularly RGM, which peaked at 68.6 pg m^{-3} for the hour ending at 17:00. These changes in both ambient and wet deposition Hg concentrations can be observed in Figure V.5. It is apparent that a very slight change in wind direction brought about a significant change in ambient Hg concentrations, and that the subsequent precipitation also increased in concentration at this time. After the precipitation, ambient Hg levels fell to background, but began to rise again at approximately 9:00 AM.

Sept 13. The event examined here followed the previous event and can also be seen in Figure V.5. Light, unchanging winds were observed, there was a distinct decreasing trend in Hg concentration in both ambient and precipitation over the course of the rain. This series of two back-to-back events provides evidence of both increasing Hg concentrations over the course of a rain event associated with slight perturbations in local meteorology as well as decreasing Hg concentrations over the course of precipitation when the winds did not favor additional feed of boundary layer ambient Hg.

Sept 28: Another event discussed in White et al. 2008, a cold frontal passage brought about late morning rains (5:28 to 13:05 EST) on September 28. Winds shifting from south to southwest to north throughout the event were accompanied by the most drastic Hg concentration reduction rate in the 14 events depicted in Figure V.4. A combination of wind shift and precipitation did seem to bring about decreased SO_2 over the course of the event.

Overall it was observed that local meteorological and ambient Hg may have played a role in the behavior of Hg concentration over the course of the events, and it was apparent that on several occasions Hg concentrations increased at some point over the course of an individual event. It was seen on an individual event basis that minor perturbations in wind direction and speed may bring about conditions that favor an increase in ambient Hg concentrations due to impact of local sources and subsequent increases in sub-event sequential samples in the latter stages of precipitation.

Event aggregation

To better determine the overall wet deposition incorporation behavior of Hg, the events were examined together, in aggregate, and the Hg behavior was compared to that of other metals.

Intensity Often, an inverse relationship is evident between the concentration of an element in precipitation over time and the rainfall intensity (5), and it has been suggested that rainfall rate can be a dominating factor in determining wet-deposition flux (6). For this study, rate was determined by the rain depth collected divided by the collection time, and a rate was applied to each sub-sample. Of the elements studied, only three exhibited significant relationships between concentration and rainfall rate: Se, La and Ce; and Hg displayed no correlation. This indicates that the physical or chemical properties and/or sources controlling Hg inclusion are not the same as the crustal elements. It is interesting to note, that multivariate statistical analysis has indicated that Hg deposition to this receptor site is primarily from coal combustion sources (1,3), and Se is a tracer for coal combustion, that the physical chemistry that drives the inclusion is dissimilar for the two elements. Se is hypothesized to be emitted primarily in the gas form, is rapidly transformed via gas to particle conversion, and then deposited through precipitation in the particle form.

Scavenging coefficients The relative deposition rate of sub event samples was evaluated to help elucidate the removal process: rapid reduction in concentration indicates boundary layer wash–out removal of larger mode aerosols, in comparison, a constant concentration throughout an event would be indicative of gas-phase inclusion within cloud and/or continuous feed of the element into either the boundary layer below the cloud or continuous entrainment aloft.

Both element concentrations and sequence number were standardized as in Eq. V.1 for *i* event, *k* sequence *within* each event such that the a) washout behavior was standardized without weight on absolute concentration, b) the first and last sub-event

sample were given equal and opposite weights, without regard or weighting to events with a disproportionate number of sub-events.

$$score_{i,k} = \frac{[analyte]_k - \mu_i}{\sigma_i} \qquad \text{V.1}$$

Scavenging coefficients can be found in Table V.4, and are listed in the order of rate. S, Ca, V, Se demonstrate the most efficient scavenging, but S has the highest coefficient indicating the most robust and consistent reduction trend in concentration throughout an event, behaving almost as large particle washout. We know that the majority (>90%) of S in the precipitation is in the soluble from the earlier discussion and therefore large particle washout is not the reason for the efficient scavenging behavior. Sulfur has also been modeled to be 87% attributed to coal combustion for the Steubenville receptor site (2). Unlike S, Hg is on the low end of soluble (94 and 61%, respectively). Therefore we are evaluating two species with the same source, but vastly different chemistries. The other coal tracer, Se, predicted to be 66% due to coal combustion, was moderately soluble and had a similar scavenging rate to Hg (-0.395).

The vast majority of SO_2 is transported away from the emission source and is converted to the soluble form at 4% an hour. Because SO_2 to SO_4^{2+} conversion and deposition processes are well studied and documented, comparison between S ($S=0.4413* SO_4^{2+} + 539$, $r^2 = 0.9855$, $p<0.0001$ in Steubenville precipitation) and Hg deposition may shed some light on the incorporation of Hg into rain. The difference in scavenging efficiencies between Hg and S is illustrated in Figure V.6, where the difference in slope, while not statistically significant through standard error evaluation, is evident. It is also interesting to note the difference in coefficient of determination for the scavenging rates of S and Hg; the measure values are much better estimated ($r^2=0.537$, $p<0.0001$) by the equation of fit for the S, whereas Hg is not as well described ($r^2= 0.156$, $p<0.0001$) by the linear regression model. Only 4% of sulfur in coal fired utility boiler plumes is in the soluble SO_4^{2-} form in comparison to 67 ±27% of Hg in the soluble Hg^{2+} form (12). Therefore, it is possible we witnessed a 'buildup' of sulfate particles in the boundary layer between precipitation event, which were washed out effectively and quickly, and not replenished after wash out due to the low fraction of emissions in the

soluble form. Hg, on the other hand, with the majority of emissions in the soluble form (RGM), while some washout is evident and buildup is probable, is continuously available for uptake in an area of constant supply.

To better respond to the above hypothesis and elucidate a clear answer to the question of lower scavenging rates due to continuous feed versus either RGM entrainment from aloft or gas phase cloud inclusion, Hg concentrations for identical events were compared between Steubenville and the upwind site (STW). (Note that collection only occurred at STW for the month of July, and as mentioned in the previous section, concentration fall-off through the sub-events was greater in September than in July, so the rate observed here differs from the aggregate total of -0.395.) Standardized results are shown in Figure V.7, and it can be observed visually, even prior to statistical analysis, that the Steubenville sequential samples are much less precise about the trend, high concentrations fall during the later stages of precipitation (upper-right quadrant) and low concentration samples may occur during the earlier stages (lower left quadrant). Statistically, this evaluation remains: Hg concentrations for precipitation collected at STW, the 'upwind' site, pose greater washout behavior, scavenging coefficient is -0.390 and -0.515 for STB and STW respectively, than for the STB. Therefore, by examining the same element at differing regions of source influence for the same events, and with the assumption that the underlying chemistry remains intact, it can be concluded that a soluble form of Hg is fed into precipitation on a local scale. Overall, physicochemical properties of Hg emissions result in unique deposition rates near point sources.

Table V.1: Steubenville, OH applicable continuous measurements November 2002 – December 2006

Instrument	Measurement	Increment
Ambient Gases	SO_2 (ppb), O_3 (ppb), CO (ppm), NO (ppb), NO_2 (ppb), NO_x (ppb)	Continuous, 5 minute
Meteorological	Wind Spd (m/s), Wind Dir, Temp, %RH	Continuous, 5 minute
Tekran 2537a, 1130 & 1135	Hg^0 (ng/m^3), Hg^{2+} (pg/m^3), Hg(p) (pg/m^3)	Hourly, odd hours
Radiometer	Global and UV radiation (W/m^2)	Continuous, 5 minute
MIC-B	Precipitation for Hg, Ion and Trace Elements	Daily Event

Table V.2: Wet deposition samples collected in Steubenville Ohio during the Ohio Mercury Monitoring project.

Sample Type	Dates Collected	Sample Sets
Event Total	Nov 2002 – March 2008	389
Sub-Event Sequential	July 2 2006 – Oct 1, 2006	23
Filtered Sub-Event Sequential	July 2, 2006 – Aug 18, 2006	9
Event Total Filtered	July 2, 2006 – Aug 18, 2006	7
STW Sub-Event Sequential	July 4, 2006 – Aug 4, 2006	9

Table V.3: Correlation coefficients of soluble to total species concentrations in summertime rain for Steubenville Ohio. Significant relationships are in bold, and elements are listed in decreasing order of soluble fraction.

	As	**S**	Zn	**Na**	**Ca**	Mn	**Se**	**Mg**	**Hg**	V	Cr	**La**	**Ce**	**Fe**
B	**1.477**	**0.943**	0.94	**0.851**	**0.719**	0.692	**0.682**	**0.679**	**0.605**	0.361	0.233	**<0.20**	**<0.20**	**0.044**
r^2	**0.940**	**0.988**	0.524	**0.895**	**0.912**	0.450	**0.86**	**0.968**	**0.927**	0.723	0.425			**0.813**
p	**0.006**	**0.001**	0.167	**0.015**	**0.011**	0.080	**0.023**	**0.003**	**<0.001**	0.068	0.233			**0.037**

Table V.4: Sub-event element concentration scavenging rate coefficients, all values significant at a p<0.0001 level.

	S	Ca	V	Ce	Mn	La	Fe	Zn	Se	As	Hg	Na	Mg	Cr
B	-0.733	-0.597	-0.565	-0.547	-0.536	-0.504	-0.464	-0.467	-0.425	-0.412	-0.395	-0.394	-0.388	-0.343
r^2	0.537	0.357	0.320	0.300	0.287	0.245	0.215	0.218	0.182	0.169	0.156	0.155	0.150	0..118

Table V.5: Times, winds, depths, Hg concentration and SO_2 data for individual sequentially sampled events. The VWM of all sub-events, the event total Hg concentration and the wind and SO_2 averages for 2 hours preceding a particular event is given on the line preceding individual sample parameters.

	Start	End	Duration	Depth	Hg (ng L^{-1})	VWM	Co-located		WS	SO_2
7/4						**11.25**	**8.19**	**N**	**1.10**	**3.49**
1	6:34:43	7:32:57	0:58:14	0.14	16.07			N to W to SW	2.18	3.34
2	7:34:31	7:47:53	0:13:22	0.10	9.97			SW	3.97	2.13
3	7:49:07	8:00:01	0:10:54	0.11	5.19			SW	3.13	1.74
4	8:00:39	8:15:48	0:15:09	0.10	6.29			SW	3.31	1.41
5	8:18:00	8:36:21	0:18:21	0.09	12.19			SW	3.50	1.23
6	8:38:30	9:06:56	0:28:26	0.10	14.11			SW	4.05	0.96
7	9:07:29	9:13:04	0:05:35	0.09	8.46			SW	4.07	0.83
8	9:13:04	9:56:54	0:43:50	0.80	6.90			SW	3.98	0.73
7/12 early AM						**11.81**	**15.33**	**S**	**2.85**	**4.11**
1	0:19:31	0:50:23	0:30:52	0.16	16.28			SWS	2.83	2.65
2	0:51:00	0:58:54	0:07:54	0.10	11.96			SWS	3.49	2.75
3	0:59:57	1:02:43	0:02:46	0.09	7.45			SWS	3.08	1.58
4	1:02:55	1:06:28	0:03:33	0.09	10.65			SWS	2.96	2.58
5	1:06:47	1:09:00	0:02:13	0.10	16.10			SWS	2.96	2.58
6	1:09:07	1:10:09	0:01:02	0.10	5.56			SWS	2.96	2.58
7	1:10:18	1:11:49	0:01:31	0.09	6.54			SWS	2.96	2.58
8	1:12:04	1:50:00	0:37:56	0.35	8.10			SWS	2.48	1.61
7/12 AM						**4.32**	**4.79**	**SWS**	**3.99**	**1.03**
1	4:49:55	5:06:45	0:16:50	0.21	5.24			SWS	3.83	0.84
2	5:06:59	5:07:30	0:00:31	0.04	3.28			SWS	4.19	0.84
3	5:07:42	5:09:26	0:01:44	0.11	4.95			SWS	4.53	0.76
4	5:09:35	5:12:18	0:02:43	0.13	3.68			SWS	4.55	0.60
5	5:12:54	5:19:27	0:06:33	0.11	5.32			SWS	4.74	1.06
6	5:20:24	5:24:26	0:04:02	0.12	2.48			SWS	4.67	0.91
7	5:24:57	5:28:40	0:03:43	0.11	4.61			SWS	4.24	0.60
8	5:29:34	7:15:45	1:46:11	1.16	2.83			SWS	3.89	0.75
7/12 PM						**5.97**	**6.65**	**SWS**	**3.93**	**0.97**
1	13:04:32	13:13:13	0:08:41	0.16	8.58			SWS	5.53	0.97
2	13:13:20	13:14:29	0:01:09	0.10	5.27			SW	5.18	0.84
3	13:14:35	13:15:26	0:00:51	0.12	5.44			SW	6.17	0.60
4	13:15:37	13:17:13	0:01:36	0.09	4.31			SW	5.49	0.74
5	13:17:26	13:19:55	0:02:29	0.10	3.71			SW	5.49	0.74
6	13:20:25	14:04:36	0:44:11	0.09	6.23			SW	3.98	0.58
7	14:04:51	14:08:39	0:03:48	0.10	6.74			SW	5.27	0.60
8	14:08:57	14:29:58	0:21:01	0.07	4.27			SW	4.71	0.44
7/14 PM						**12.99**	**12.50**	**SWS**	**2.42**	**0.59**
1	21:46:21	21:47:49	0:01:28	0.21	9.96			SW	2.26	0.60
2	21:47:57	21:49:03	0:01:06	0.12	9.79			SWS	3.66	1.02
3	21:49:11	21:49:56	0:00:45	0.13	12.71			SWS	3.66	1.02
4	21:50:00	21:50:37	0:00:37	0.11	11.91			SWS	3.66	1.02
5	21:50:40	21:51:20	0:00:40	0.13	21.99			SWS	6.91	0.88
6	21:51:22	21:52:46	0:01:24	0.13	9.52			SWS	6.91	0.88
7	21:53:04	21:58:29	0:05:25	0.12	9.73			SWS	6.91	0.88
8	21:58:29	22:08:24	0:09:55	0.03	7.40			SWS	5.80	0.68

	Start	End	Duration	Depth	Hg (ng L^{-1})	VWM	Co-located	WS	SO_2	VWM
9/1						**6.88**	**4.99**	**NE**	**4.80**	**7.62**
1	20:38:10	23:26:44	2:48:34	0.19	8.06			NE	3.76	4.81
2	23:26:44	0:46:00	1:20:00	0.20	9.77			NE	5.32	1.78
3	0:46:00	1:35:54	0:49:54	0.21	3.63			NEN	5.56	1.27
4	1:35:54	2:01:06	0:25:12	0.21	7.33			NEN	5.58	1.11
5	2:01:06	2:27:37	0:26:31	0.21	3.02			NEN	5.57	1.10
6	2:27:37	3:22:13	0:54:36	0.20	4.12			NEN	5.55	1.28
7	3:22:13	4:42:17	1:20:04	0.21	4.73			NEN	4.65	1.35
8	4:42:18	5:00:49	0:18:31	0.10	7.40			NEN	4.97	1.04
9/12						**15.79**	**12.80**	**S**	**2.46**	**1.99**
1	8:00:00	8:33:00	0:33:00	0.15	26.03			S	2.70	3.37
2	8:33:48	12:50:02	4:16:14	0.21	13.46			S	2.26	4.95
3	12:50:02	14:39:49	1:49:47	0.20	16.26			S	2.84	11.26
4	14:39:49	16:01:32	1:21:43	0.21	18.62			S	2.71	4.56
5	16:01:32	16:46:01	0:44:29	0.21	9.85			S	2.83	2.24
6	16:46:01	17:39:02	0:53:01	0.20	7.29			S	3.20	1.45
7	17:39:02	18:57:54	1:18:52	0.22	5.62			S	3.55	1.31
8	18:57:54	23:00:18	4:02:24	0.45	7.54			SWS	3.36	1.86
9/13						**15.89**	**9.60**	**SE**	**1.52**	**4.38**
1	19:37:20	20:08:18	0:30:58	0.23	24.66			S	1.89	1.97
2	20:08:18	20:55:08	0:46:50	0.23	19.25			SWS	1.66	1.89
3	20:55:08	22:11:38	1:16:30	0.23	14.28			SWS	0.97	2.48
4	22:11:38	22:17:32	0:05:54	0.24	7.17			SWS	2.53	3.45
5	22:17:32	22:23:16	0:05:44	0.22	9.50			SWS	1.82	2.30
6	22:23:16	22:28:11	0:04:55	0.23	2.80			SWS	2.51	3.26
7	22:28:11	22:35:05	0:06:54	0.21	2.99			SWS	3.35	3.77
8	22:35:05	23:00:18	0:25:13	1.03	6.12			SWS	1.41	3.66
9/28						**19.30**	**7.90**	**SW**	**2.66**	**3.84**
1	5:28:12	6:34:07	1:05:55	0.19	33.02			SWS	3.34	2.37
2	6:34:07	7:12:31	0:38:24	0.21	14.65			SWS	3.38	1.87
3	7:12:31	8:17:43	1:05:12	0.22	9.70			SWS	3.17	2.04
4	8:17:43	9:25:07	1:07:24	0.22	4.07			SW	3.15	1.48
5	9:25:07	9:32:07	0:07:00	0.22	5.01			W	2.00	1.12
6	9:32:07	9:36:15	0:04:08	0.21	3.60			W	2.13	1.11
7	9:36:15	10:12:59	0:36:44	0.21	3.07			NW	1.34	1.11
8	10:11:59	13:05:41	2:53:42	0.71	3.20			NW to N	1.82	0.97

Table V.6: Ambient Hg values for hours preceding and during precipitation events.

		Hg(P) (pg m^{-3})	RGM (pg m^{-3})	Hg(0) (ng m^{-3})
7/12 early AM	24 hrs prior	11.93	7.91	2.63
	12 hrs prior	5.20	9.39	1.88
	6 hrs prior	3.37	11.22	1.86
	2 hrs prior	6.90	23.68	2.38
	1st hr	4.62	4.23	2.68
	last hr	0.93	1.88	1.73
7/12 AM	24 hrs prior	9.36	7.99	2.52
	12 hrs prior	2.76	8.65	1.81
	6 hrs prior	3.08	6.76	1.93
	2 hrs prior	1.93	6.27	1.74
	1st hr	0.00	4.01	1.38
	last hr	1.16	1.47	1.61
7/12 PM	24 hrs prior	2.29	6.52	1.69
	12 hrs prior	1.05	3.70	1.56
	6 hrs prior	0.83	2.14	1.53
	2 hrs prior	0.94	3.05	1.47
	1st hr	0.00	2.20	1.20
	last hr	0.00	0.00	1.58
7/14	24 hrs prior	9.52	15.86	2.48
	12 hrs prior	9.01	29.89	2.72
	6 hrs prior	4.01	8.49	1.53
	2 hrs prior	2.28	3.65	1.51
	1st hr	1.81	6.75	1.36
	last hr	0.00	7.14	1.85
9/1	24 hrs prior	2.46	0.68	1.54
	12 hrs prior	1.80	0.91	1.28
	6 hrs prior	1.28	0.72	1.20
	2 hrs prior	1.06	0.52	1.24
	1st hr	1.48	1.15	1.42
	last hr	4.43	0.00	2.02
9/12	24 hrs prior	10.52	17.24	1.59
	12 hrs prior	12.08	15.94	1.61
	6 hrs prior	12.01	17.91	1.66
	2 hrs prior	11.71	30.02	1.45
	1st hr	13.94	14.82	1.53
	last hr	15.64	63.20	1.73
9/13	24 hrs prior	10.84	43.49	1.70
	12 hrs prior	13.96	78.24	1.74
	6 hrs prior	7.41	115.20	1.37
	2 hrs prior	4.63	81.07	1.35
	1st hr	4.03	33.60	1.34
	last hr	2.99	9.08	1.35
9/28	24 hrs prior	3.75	3.98	1.84
	12 hrs prior	1.01	1.31	1.63
	6 hrs prior	0.81	0.83	1.66
	2 hrs prior	1.42	1.17	1.74
	1st hr	1.71	0.72	1.79
	last hr	1.77	9.16	1.69

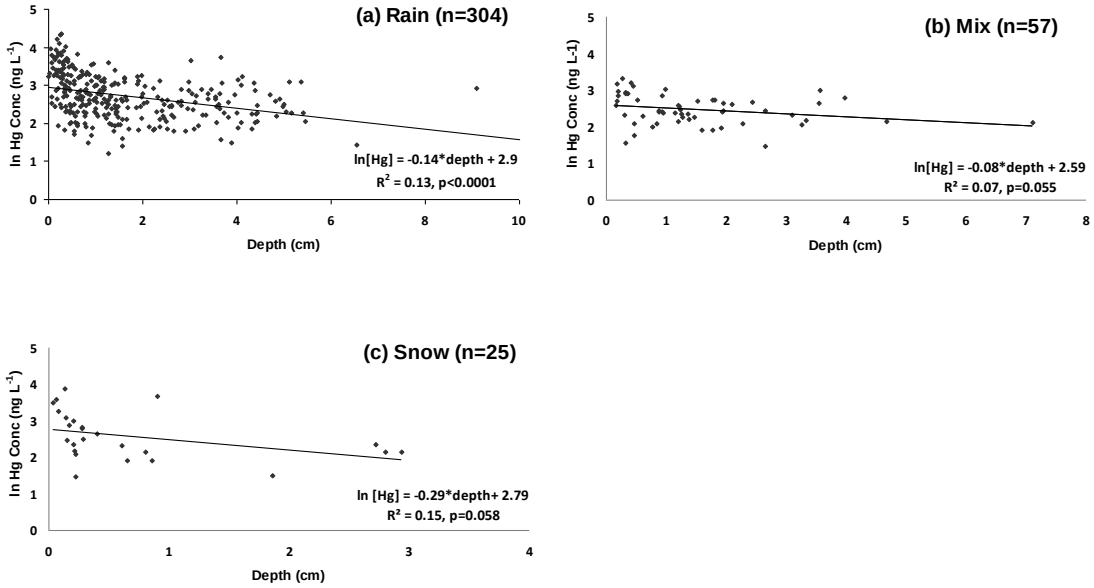

Figure V.1 (a-c) Regression plots depicting precipitation depth and Hg concentration relationship, according to precipitation type.

Figure V.2: Soluble and total Hg wet deposition concentrations.

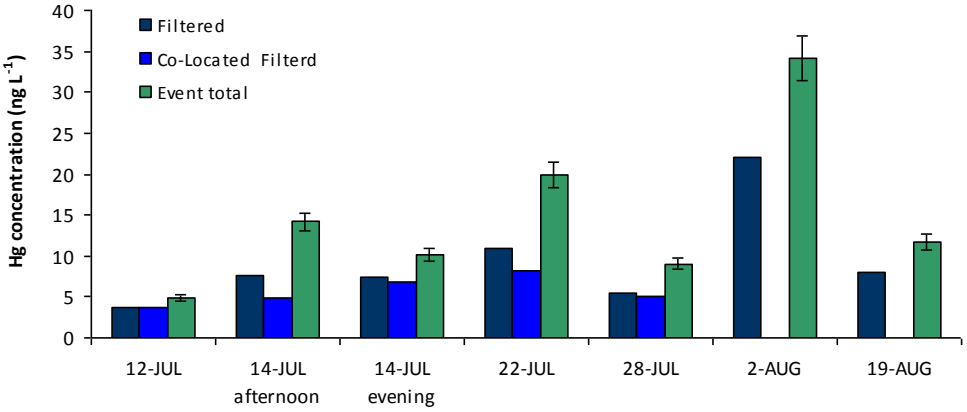

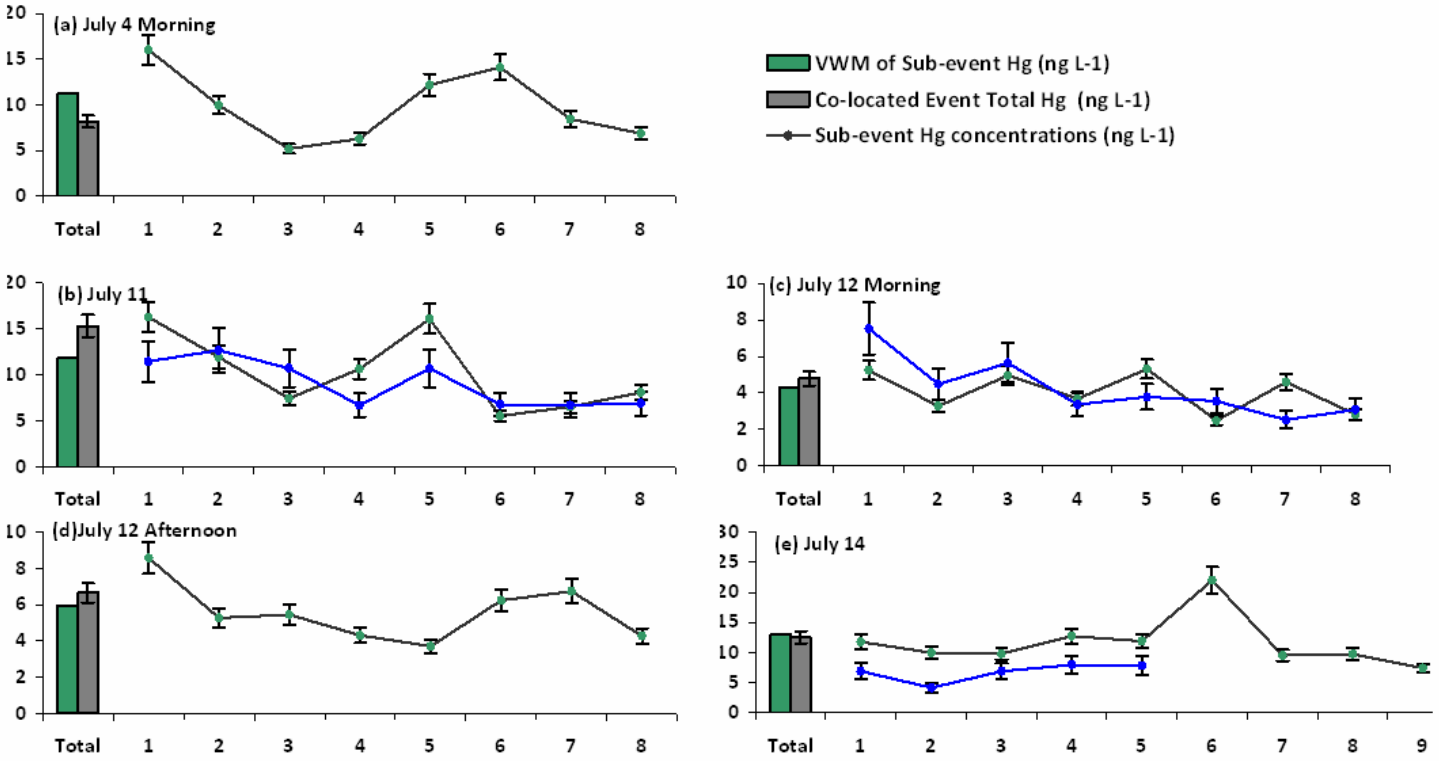

Figure V.3(a-e): Sub-event Hg concentrations in ng L^{-1}, total event concentration as columns, line represents Hg concentration through out the course of a single event as discrete sub-samples, the blue line depicting the soluble fraction of the sub-event.

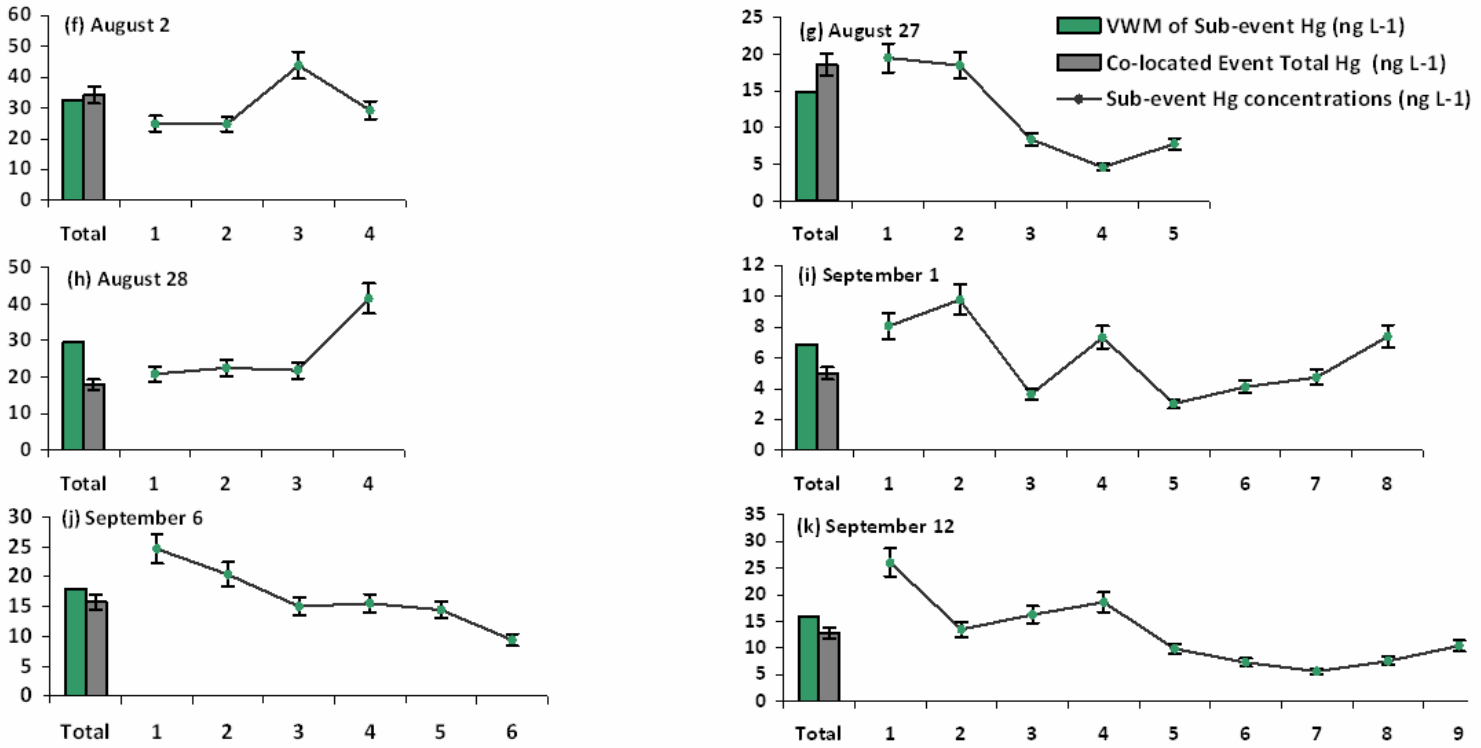

Figure V.3(f-k): Sub-event Hg concentrations in ng L^{-1}, total event concentration as columns, line represents Hg concentration through out the course of a single event as discrete sub-samples, the blue line depicting the soluble fraction of the sub-event.

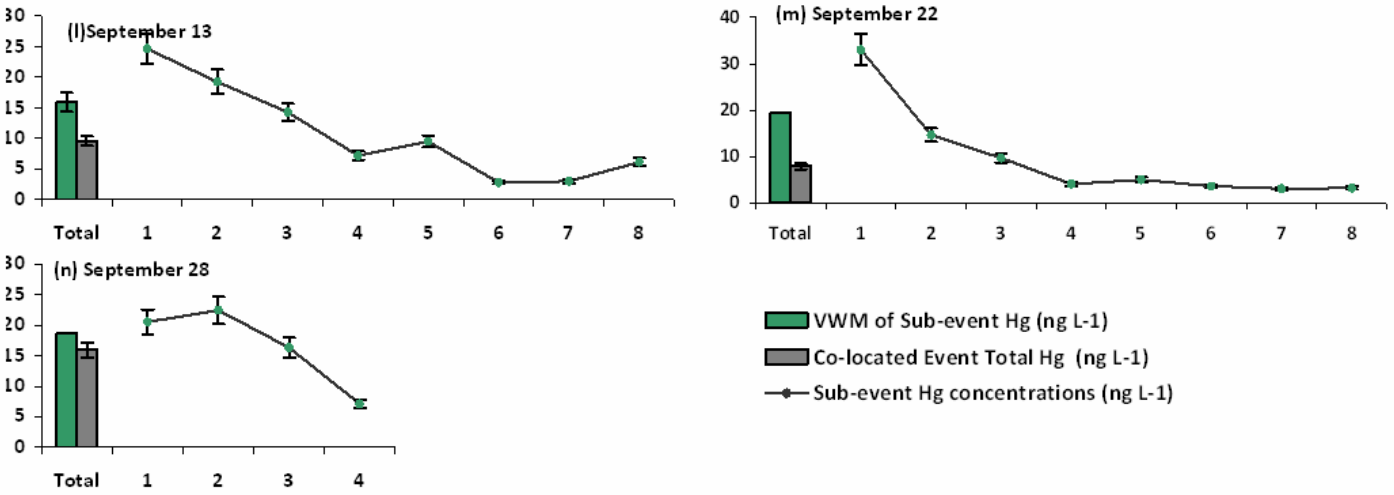

Figure V.3 (l-n) Sub-event Hg concentrations in ng L^{-1}, total event concentration as columns; line represents Hg concentration through out the course of a single event as discrete sub-samples, the blue line depicting the soluble fraction of the sub-event.

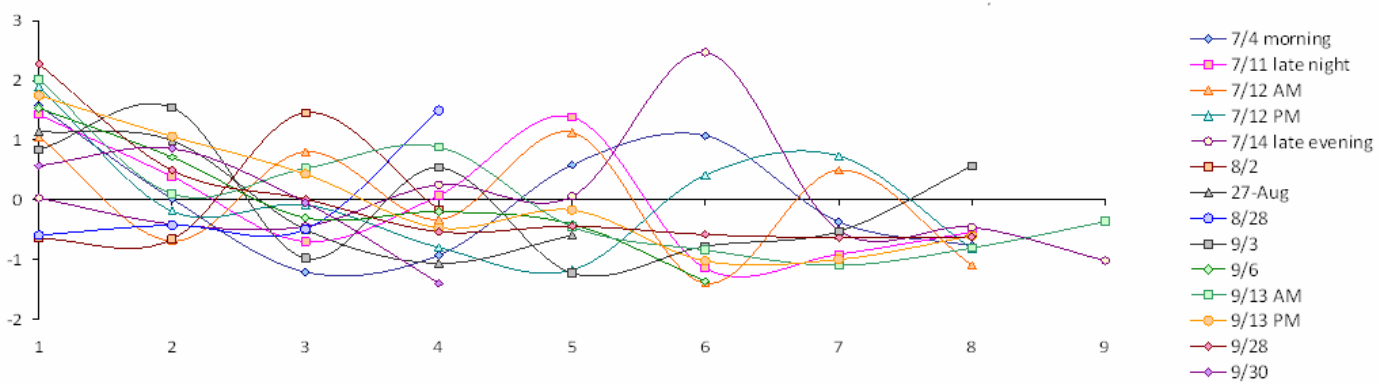

Figure V.4: Standardized sub-event Hg concentrations for all events collected.

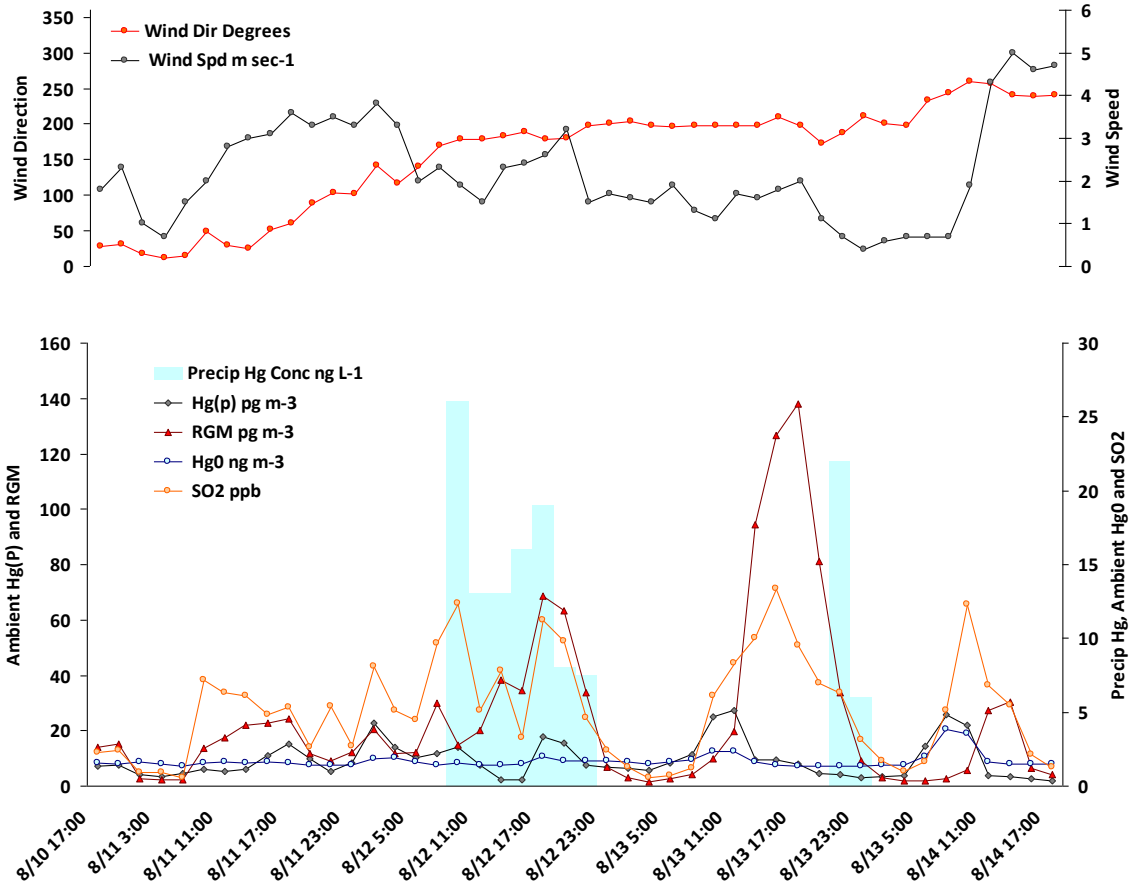

Figure V.5: Ambient gas, winds and sub-event wet deposition Hg concentrations for a four day period in September 2006.

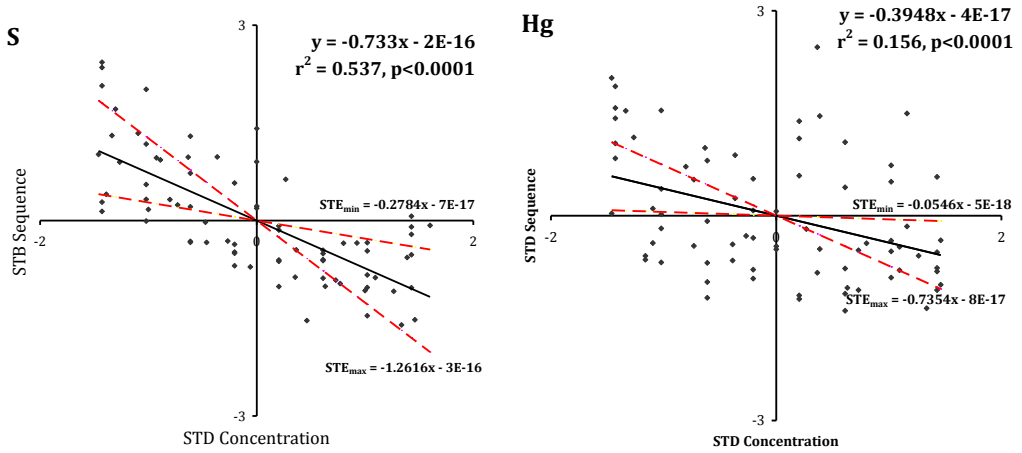

Figure V.6: Three month sub-event standardized S and Hg concentrations.

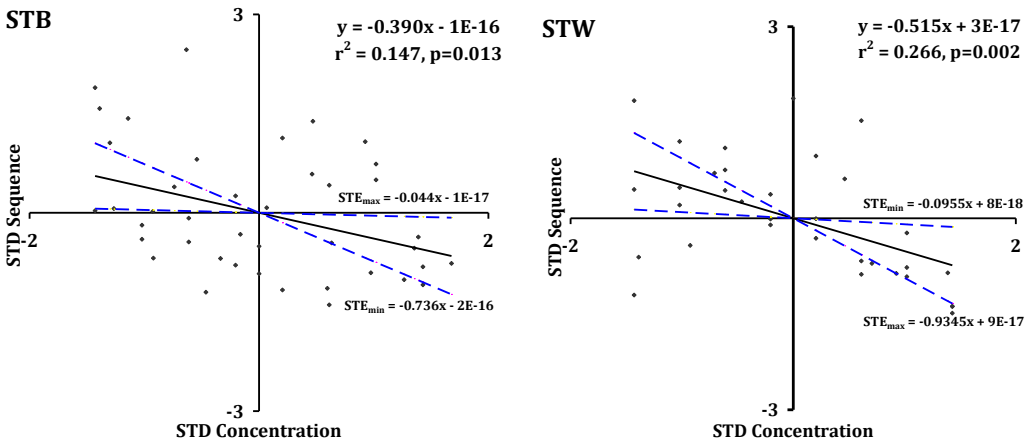

Figure V.7: July sub-event standardized Hg concentrations at Steubenville (STB) and a rural site up-wind, west of Steubenville (STW).

CHAPTER V: References

(1) Keeler, G.J.; Landis, M.S.; Norris, G.A., Christianson, E.M.; Dvonch, J.T. Sources of Mercury Wet Deposition in Eastern Ohio, USA *Environ. Sci. Technol*. **2006**, 40, 5874-5881.

(2) White, E.M.; Keeler, G.J. Landis, M.S.; Spatial Variability of Mercury Wet Deposition in Eastern Ohio: Summertime Meteorological Case Study Analysis of Local Source Influences. Submitted to *Environ. Sci. Technol.* Dec 2008, accepted April **2009.** As Chapter III in current dissertation.

(3) White, E.M.; Keeler, G.J., Landis, M.S.; Source type and region attribution for wet deposited Hg in Eastern Ohio, USA. As Chapter IV in current PhD thesis, to be submitted for publication, **2009**.

(4) Hammerschmidt, C. R.; Fitzgerald, W. F. Methylmercury in freshwater fish linked to atmospheric mercury deposition *Environ. Sci. Technol.* **2006**, 40, 7764-7770

(5) Lim, B.; Jickells, T.; Davies, T. Sequential sampling of particles, major ions and total trace metals in wet deposition. *Atmos Environ.* **1990,** 25A, 745-762.

(6) Graney, J.R.; Landis, M.S.; Norris, G.A. Concentrations and solubilities of metals from indoor and personal exposure PM2.5 samples. *Atmos Environ.* 2004, 38, 237-247.

(7) Lou, W. Wet-deposition fluxes of soluble chemical species and the elements in insoluble materials. *Atmos Environ.* **2000**, 35, 2963-2967.

(8) Morselli, L.; Olivieri, P.; Brusori, B.; Passarini, F. Soluble and insoluble fractions of heavy metals in wet and dry atmospheric depositions in Bologna, Italy. *Environ. Pollution.* 2003, 124, 457-469.

(9) Lindberg S., Bullock, R., Ebinghaus, R., Engstrom, D., Feng., Fitzgerald, W., Pirrone, N., Prestbo, E., Seigneur, C., A Synthesis of Progress and Uncertainties in Attributing the Sources of Mercury in Deposition. *AMBIO* **2007**, 36, 19-31.

(10) Landis, M.S.; Keeler, G.J. Critical evaluation of a modified automatic wer-only precipitation collector for mercury and trace element determinations. *Environ. Sci. Technol.* **1997**, 31, 2610-2615.
(11) Landis, M.S, Lake Michigan Mass Balance Study. PhD dissertation, University of Michigan. **1998**.
(12) Gratz, L.E., Keeler, G. J., Al-wali, K. Long-term Atmospheric Mercury Wet Deposition at Underhill, VT. International Association of Great Lakes Research Conference. **2005**.
(13) Sienfeld, J. H., Pandis, S.N., Atmospheric Chemistry and Physics: From Air Pollution to Climate Change. Wiley Interscience. **1998.**
(13) Burke, J., M. Hoyer, G. Keeler, T. Scherbatskoy. Wet deposition of mercury and ambient mercury concentrations at a site in the Lake Champlain basin. *Water, Air Soil Pollut.*, **1995**, 80, 353-362.
(14) Stevens, R.K.; Zweidenger, R.; Edgerton, E.; Mayhew, W.; Kellog, R.; Keeler G.J.; Source Characterization in Support of Modeling the Transport of Mercury Emissions in South Florida. Presented at Measurement of Toxic and Related Air Pollutants Symposium, May 7-9, Research Triangle Park, NC, 1996.

CHAPTER VI

Summary and Conclusions

Several temporal and spatial scales were evaluated to better understand the processes that define Hg wet deposition to Steubenville, Ohio. Because this thesis was written in manuscript form, the individual chapters were essentially independent; here, conclusions from the chapters are brought together to transcend the varying scales and tie together important findings.

Model analysis of long – term event based Hg deposition.

Chapter II combined event based precipitation samples from the first two and a half years of the Ohio Mercury Monitoring study for a multivariate statistical model source apportionment evaluation that attributed ~70% of Hg deposition to coal fired utility boilers. Model evaluation was revisited in Chapter IV with an additional three years of event precipitation data that resulted in essentially equivalent source attribution. The additional three years, however, did yield a substantial data set for synoptic scale meteorological evaluation using air mass back trajectory ensemble cluster analysis. It was found that intra-cluster volume-weighted mean Hg concentration variability was maximized when trajectories were based on between 12- and 24-hour back trajectories. Clustering the trajectories using endpoints out to 72 hours only diluted the variability, suggesting that sources most strongly affecting the receptor site were within one day's transport. Synoptic meteorological assessment of the clusters defined situations that led to enhanced Hg deposition It was found that local stagnant conditions led to moderately high volume-weighted mean Hg concentrations, a majority of Hg wet deposition flux, and over 70% was modeled as due to coal combustion. However, moderately fast transport from areas with known emission point sources also led to high Hg

concentrations, but these events did not contribute significantly to the overall Hg deposition. It was also found that stagnant conditions prior to precipitation led to increased minimum concentrations, indicating that background baseline concentrations were enhanced if air mass residence time in the local area was increased. Coal combustion played the most significant role in source type attribution no matter the speed or direction of air mass transport. The contribution of coal combustion sources was reduced for snow and mixed precipitation events as well as for extremely rapid or northerly flow regimes, contributing less than 50% to the rapid transport regimes. This finding is consistent with the later finding that the physicochemical properties of Hg emissions together with the form of precipitation and transport history strongly influence the amount of Hg deposited.

Spatial Scale Hg depositions: individual event comparisons.

Comparison of large scale continental and Great Lakes regional interpolated maps revealed in Chapter I that the current national network regionally representative background Hg deposition collection underestimated regional and near-field enhanced deposition (hot-spots). These interpolations were aggregated long-term Hg deposition observations. To explore the importance of local hot-spots in the vicinity of known point sources, summertime precipitation events were concurrently collected in a near-field scale network surrounding the primary Steubenville, OH site. One of the most important findings of the work presented in Chapter III was the realization that the Hg concentration varied on spatial scales so small during individual events that spatial interpolation was not feasible. Individual case study analysis revealed that four local meteorological parameters drove the degree to which Hg was enhanced in near-field samples: wind speed during maximum rain rate, wind speed 24-hours prior to precipitation, mixing height and observed ceiling. These four variables describe the local boundary layer mixing ability, and when applied to the remainder of summertime precipitation events through multiple linear regression, it was found that 42% of the Hg concentration collected at near-field sites could be attributed to the adjacent coal-fired utility, which corresponds to an approximate 3 fold enhancement over regionally representative precipitation, collected less than 40 km away. In the longer term event

exploration, it was found that a particular synoptic situation, stagnant conditions with southwest flow, accounted for 24% of all wet deposited Hg to the receptor site. The majority of these events were summertime events, and five of the nine case studies explored in Chapter III fell into this flow regime, indicating that the cases studied were representative of wet deposition flux to the Ohio River Valley.

Scavenging coefficients and solubility.

Event Hg concentrations were compared to precipitation depth, Chapter V, as part of a long-term climatological analysis. It was noted that the long term scavenging coefficient (-0.14 slope of ln[Hg] versus depth) was much lower than for regionally representative values (-0.24 for Underhill, VT) and was similar to coefficients revealed in regions of local source influence (-0.16 for Chicago, IL). This indicated that for similar elements, inclusion behavior varied depending on the local airshed. Lower scavenging rates were hypothesized to represent the availability of Hg into the latter stages of the storm, and therefore allow for high volume samples that were also high in Hg concentration. This hypothesis was tested in Chapter V through sequential sub-event sampling and filtration of summertime precipitating events. In order to understand the implications and significance of the solubility and the trends in Hg concentration over the course of a precipitating event, Hg was compared to several other trace elements. Real-time filtration of event total precipitation revealed that 69% (±37%) of Hg in wet deposition was in a soluble form, while S, a co-pollutant, was >90% soluble. Hg concentrations for precipitation collected at STW, the 'upwind' site, revealed greater washout behavior with scavenging coefficients equal to -0.39 and -0.52 for STB and STW, respectively. By examining the same trace elements in differing regions of source influence for the same events, and with the assumption that the underlying chemistry remains intact, it can be concluded that the gaseous, soluble forms of Hg are fed into precipitation on local scales. Overall, the physicochemical properties of Hg emissions result in elevated deposition rates near point sources. This conclusion may not have been unexpected but showing this behavior in the field with actual measurements had previously not been accomplished.

Implications.

Through this work it has become evident that near-field impact of coal fired utility boilers on Hg deposition is significant and underestimated by the models that have been utilized in previous policy decision making. This underestimation is due (i) lack of Hg emission speciation, (ii) national network measurements that preclude measurements in point source impacted areas and (iii) the relatively elementary knowledge and consequent model construction of atmospheric Hg chemistry. Any policy promulgated thus far has been based on the success of the EPA's Acid Rain program. It is vital to understand for policy makers, however, is that Hg does not behave in the same fashion as sulfur and nitrogen compounds, the precursors of acid rain. SO_2 is transformed relatively slowly into sulfuric acid, causing emissions from the industrialized Ohio River Valley to be transported, and diluted through mixing and transport distance, as far as, and adversely effect through acid rain, the Adirondack Mountains. Here, we have shown that a significant portion of the Hg deposited in the immediate vicinity of coal fired utilities can be directly attributed to that local point source. This implies, therefore, that policy that allows purchasing of Hg credits could cause certain industrialized regions to maintain the current level, or even increase Hg emissions, leading to deposition hotspots and a consequent negative impact on local populations. Other researcher have shown that methylmercury concentrations in fish are proportional to the overall wet deposition to an area, so it is likely that the impact of coal fired utility boilers on biogeochemical cycling of Hg is also underestimated in the vicinity of these sources. Current published research on piscivorous species has been primarily conducted on bird and mammalian populations in relatively remote regions and adverse neurological, behavior and reproductive effects have been found at even low blood Hg levels. The implications, therefore, of Hg deposition hotspots to certain industrial or urban regions is drastically detrimental to wildlife. It is therefore imperative that the governing agencies develop timely and stringent policies that implement Maximum Available Control Technology, as well as encourage advanced control technology research.

Future Work.

Every precipitation sample was event-specific, and if nothing else, I learned that the atmosphere is one gigantic ill-posed problem: the solutions are infinite, and the more parameters that can be objectively defined, the better we are able to describe the causes of Hg concentration variability. I think that a study such as that presented here would greatly benefit from the use of an on-site sounder. Mixing height was difficult to accurately determine, but was found significantly correlated to Hg concentration variablity for nine event case studies, and I believe it would have been found significant for the entire study period if it was a local and reliable portion of the station specific meteorological variables, rather than 40 km grid modeled output. Real-time meteorological evaluation would also be advantageous, and make working with a long term data set more manageable.

The summertime spatially distributed network of precipitation collection allowed us to discern a Hg deposition gradient about coal fired utility boilers (CFUB). While CFUBs are the main contributors to Hg deposition in the Ohio River Valley, other point source types may dominate in other regions, and it would be advantageous to conduct a similar study in the vicinity of such sources. This would encourage understanding of the importance of Hg emission speciation on atmospheric transport.

Sequential sampling was shown to have the ability to tell us much about the behavior of Hg in the vicinity of sources over the course of the study, and meant nothing without the comparison to other trace elements and another upwind measurement site. More sub-events in remote sites as well as year-round collection at an industrial site would be recommended if this experiment were to be repeated, as this would likely lead to a more robust conclusion. Likewise, while the results from the near-field network sampling showed significant differences on an event basis, a full year of this type of evaluation may lead to better impact estimates.

APPENDICES

APPENDIX A

United States EPA 2002 National Emissions Inventory of Mercury Point Sources

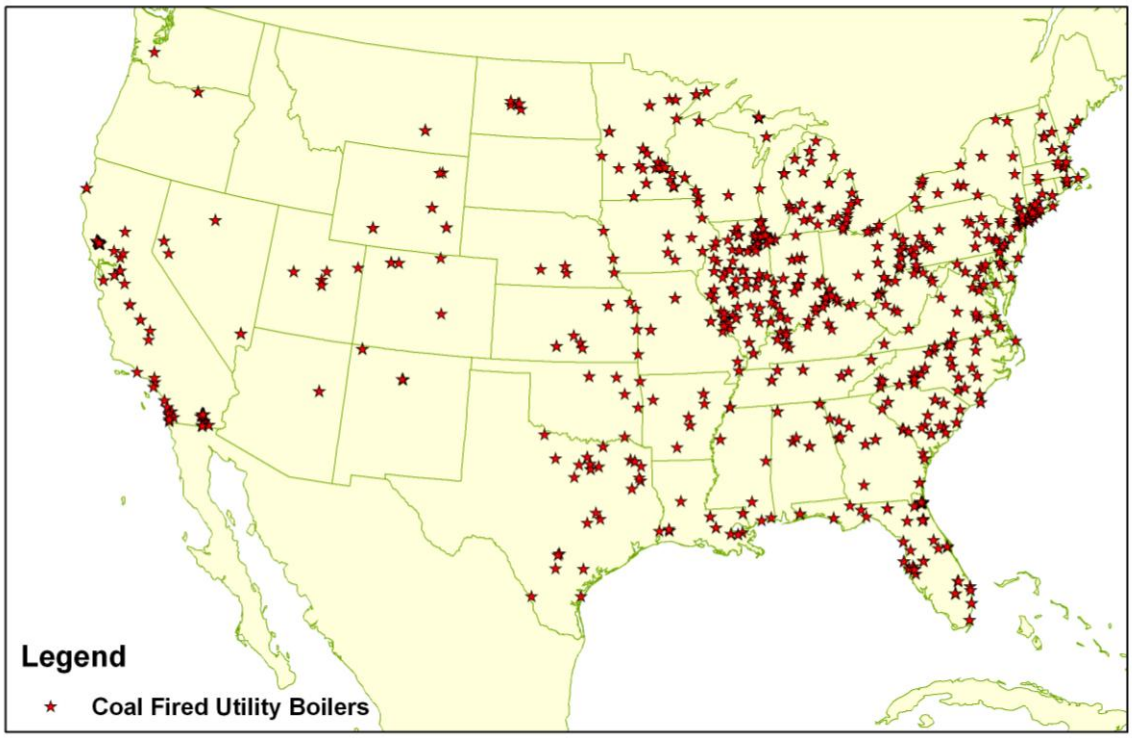

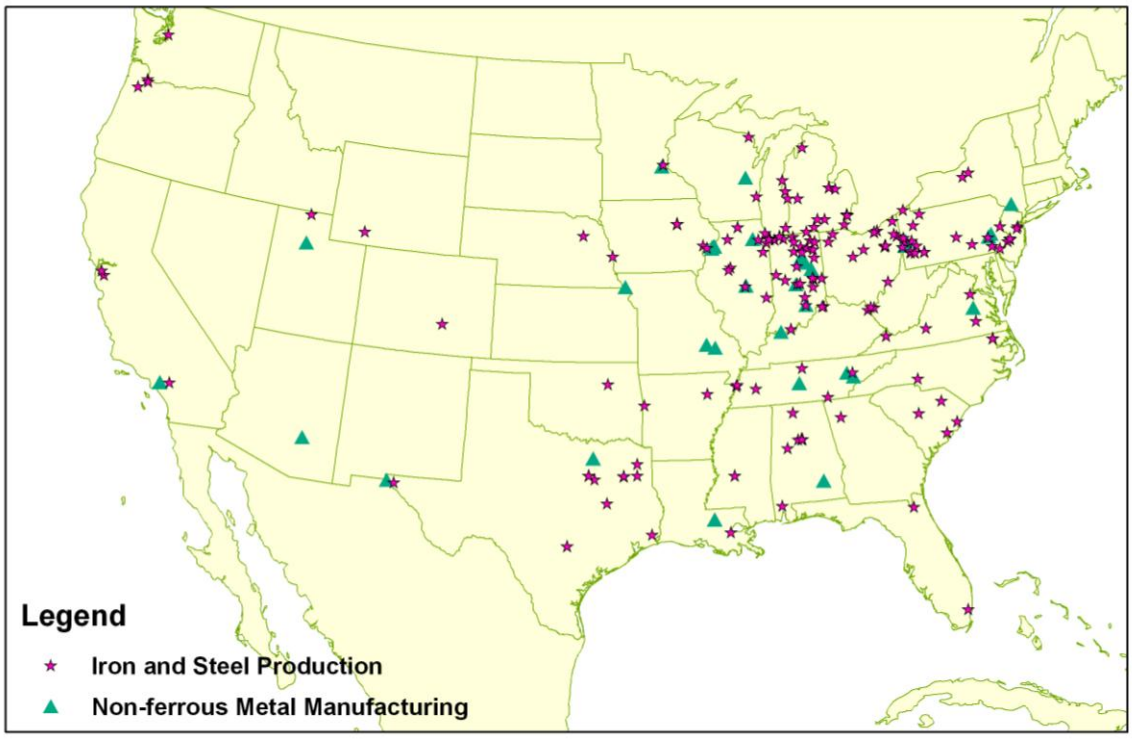

Figures A.1 and A.2: United States National Emissions Inventory location mercury point sources: Coal Fired Utility Boilers and Metals Manufacturing.

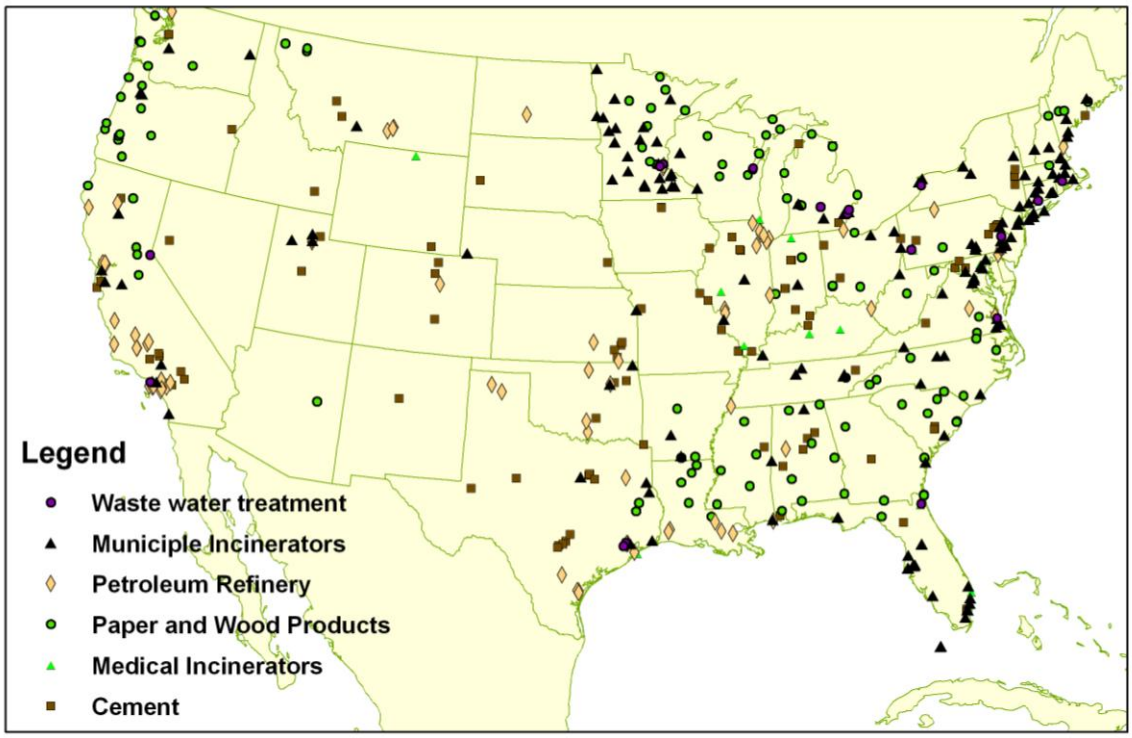

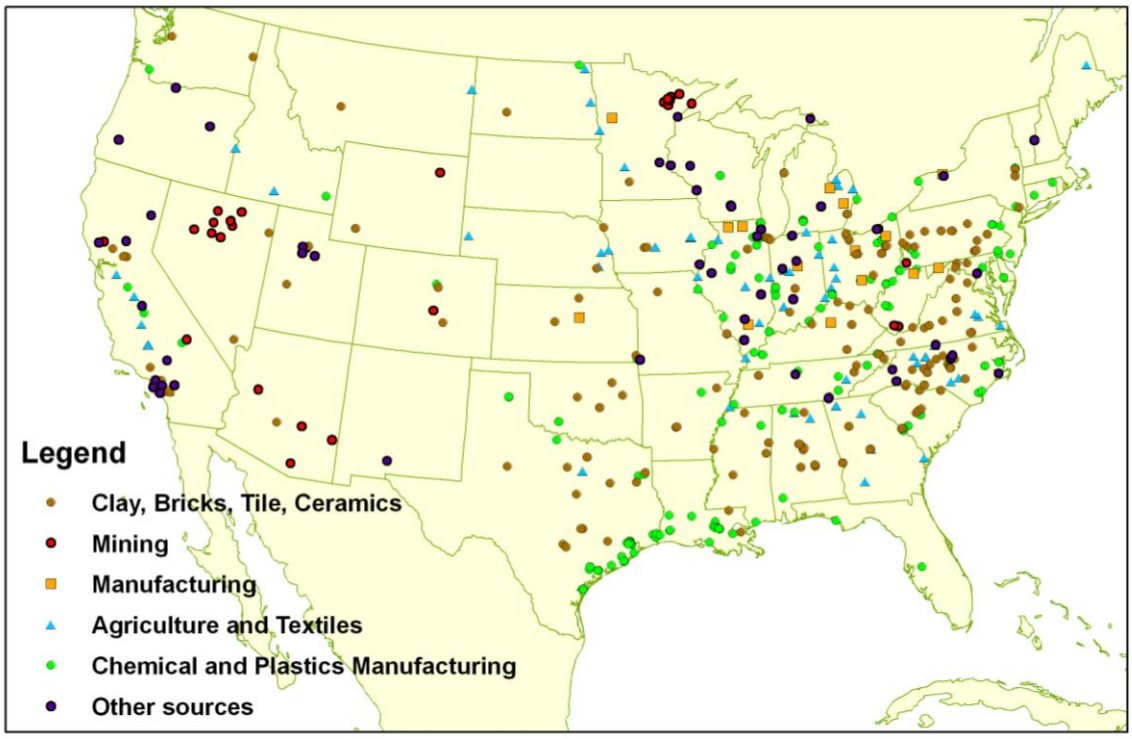

Figures A.3 and A.4: United States National Emissions Inventory location of mercury point sources: Incineration, Refineries, Paper and Cement Manufacturing, Minerals, Mining, Agriculture and Chemicals and Plastics.

APPENDIX B

Pearson Correlation Coefficients for Hg concentrations by Cluster

	ALL Rain	R1	R2	R3	R4	R5	R6	R7	R8	R9
Depth	-0.3751	-0.3464	-0.3910	-0.4130	-0.1272	-0.4446	-0.5820	-0.2349	-0.3925	-0.1239
	<.0001	0.0067	0.0396	0.0323	0.5931	0.0229	0.0089	0.3189	0.0785	0.9209
S	0.5214	0.4962	0.6394	0.7271	0.5639	0.6596	0.4830	0.5020	0.4071	0.9832
	<.0001	<.0001	0.0002	<.0001	0.0096	0.0002	0.0362	0.0241	0.067	0.117
Fe	0.5038	0.4021	0.6925	0.5127	0.2208	0.6536	0.3668	0.6787	0.6327	0.9779
	<.0001	0.0015	<.0001	0.0063	0.3495	0.0003	0.1224	0.001	0.0021	0.134
Cl	0.2859	0.3690	0.8309	0.4770	0.4029	0.5728	0.3128	0.0874	0.6997	0.9991
	<.0001	0.0037	<.0001	0.0119	0.0782	0.0022	0.1923	0.7142	0.0004	0.0276
La	0.3845	0.3449	0.3108	0.4099	0.0248	0.3473	0.6578	0.7548	0.6886	0.9465
	<.0001	0.007	0.1075	0.0337	0.9175	0.0822	0.0022	0.0001	0.0006	0.2092
Pb	0.4774	0.5250	0.6527	0.6776	0.4452	0.3986	0.1818	0.5293	0.0864	0.3426
	<.0001	<.0001	0.0002	0.0001	0.0492	0.0437	0.4563	0.0164	0.7095	0.7774
P	0.3180	-0.0495	0.8588	0.3139	-0.0346	0.1758	0.4558	0.4952	0.4165	0.9405
	<.0001	0.7074	<.0001	0.1109	0.8849	0.3902	0.0498	0.0264	0.0603	0.2208
Se	0.3323	0.4893	0.3085	0.4195	0.2613	0.5567	0.1992	0.3667	0.2427	-0.0680
	<.0001	<.0001	0.1102	0.0294	0.2658	0.0031	0.4136	0.1117	0.2892	0.9567
D1	-0.1318	-0.1736	-0.1691	0.1785	-0.1005	0.0295	-0.0739	0.0085	-0.0496	0.7666
	0.0488	0.1846	0.3898	0.3731	0.6732	0.8863	0.7637	0.9717	0.8308	0.4439
D2	-0.1368	-0.1661	-0.1914	0.2163	-0.1399	0.0067	-0.0288	-0.0148	-0.0835	0.8407
	0.0408	0.2046	0.3292	0.2786	0.5562	0.9741	0.9067	0.9505	0.7191	0.3643
D3	-0.1459	-0.1609	-0.2082	0.2230	-0.1696	-0.0277	0.0192	-0.0365	-0.1373	0.8901
	0.029	0.2193	0.2878	0.2636	0.4747	0.893	0.9379	0.8787	0.5528	0.3013
D6	-0.1753	-0.1437	-0.2242	0.1484	-0.2380	-0.1276	0.1096	-0.0467	-0.3633	0.9327
	0.0086	0.2735	0.2515	0.46	0.3124	0.5346	0.6551	0.8449	0.1055	0.2349
D12	-0.1734	-0.1699	-0.2016	-0.2530	-0.1610	-0.1277	0.0664	-0.0101	-0.3850	0.9208
	0.0093	0.1943	0.3036	0.203	0.4978	0.5342	0.7871	0.9663	0.0848	0.255

Table B.1: Pearson correlation coefficients for Hg concentration versus trace metals and 3 hour wind speeds upwind of the Steubenville receptor site for all rain clusters.

	ALL Rain	R1	R2	R3	R4	R5	R6	R7	R8	R9
D24	-0.1178	-0.2179	-0.0259	-0.2779	-0.0516	-0.1047	0.0041	-0.1286	-0.2247	-0.3291
	0.0786	0.0944	0.8958	0.1604	0.829	0.6108	0.9867	0.5889	0.3274	0.7865
D48	-0.0672	-0.2827	-0.0619	-0.2582	-0.0174	0.1218	-0.0161	-0.2029	-0.2055	-0.6485
	0.3166	**0.0286**	0.7543	0.1935	0.942	0.5535	0.9478	0.3908	0.3716	0.5508
D3_6	-0.1944	-0.0716	-0.2381	-0.0351	-0.2709	-0.2815	0.1457	-0.0478	-0.4847	0.9582
	0.0035	0.5867	0.2225	0.8619	0.248	0.1637	0.5518	0.8414	**0.026**	0.1848
D6_9	-0.1835	-0.1687	-0.1698	-0.2765	-0.1445	-0.1280	-0.1821	-0.0238	-0.2152	0.1983
	0.0059	0.1975	0.3876	0.1627	0.5432	0.5331	0.4556	0.9208	0.3488	0.8729
D9_12	-0.1102	-0.1993	-0.0974	-0.2373	0.1310	0.0126	-0.2720	0.0794	0.0401	-0.5188
	0.1001	0.1269	0.6219	0.2333	0.582	0.9512	0.2599	0.7392	0.8629	0.6527
D12_15	-0.0615	-0.0939	0.0129	-0.1593	0.0419	-0.0265	-0.1814	0.0324	0.0405	-0.7011
	0.3593	0.4755	0.948	0.4274	0.8609	0.8978	0.4573	0.8922	0.8617	0.5054
D15_18	-0.0362	-0.0726	0.1082	-0.2446	0.0437	-0.0102	-0.0802	-0.1036	0.1745	-0.8297
	0.5901	0.5816	0.5837	0.2188	0.8549	0.9604	0.7442	0.664	0.4495	0.377
D18_21	-0.0510	-0.2081	-0.0124	-0.2309	0.0257	0.0000	-0.0742	-0.2095	0.2061	-0.9900
	0.4478	0.1106	0.9499	0.2466	0.9142	1	0.7629	0.3753	0.3701	0.0901
D21_24	-0.0569	-0.2165	-0.1638	-0.2109	0.0449	-0.0808	0.0992	-0.1996	0.2251	-0.2450
	0.3967	0.0966	0.4048	0.2909	0.851	0.6946	0.6863	0.3987	0.3265	0.8424
D24_27	-0.0879	-0.2302	-0.2379	-0.2121	0.0361	-0.1658	0.0624	-0.2118	0.1009	-0.2688
	0.19	0.0769	0.2229	0.2881	0.88	0.4182	0.7996	0.37	0.6633	0.8267
D27_30	-0.1062	-0.2357	-0.3467	-0.2113	0.0562	-0.1815	0.0386	-0.2520	-0.0163	-0.6497
	0.1131	0.0699	0.0707	0.2901	0.8138	0.3748	0.8753	0.2838	0.9442	0.5498
D30_33	-0.1099	-0.2209	-0.3042	-0.2069	0.0448	-0.0513	-0.1346	-0.1987	-0.1445	-0.7889
	0.1009	0.0898	0.1155	0.3004	0.8512	0.8035	0.5826	0.401	0.5321	0.4213
D33_36	-0.0998	-0.2419	-0.2238	-0.2101	-0.1729	0.0870	-0.1869	-0.0897	-0.1891	-0.9174
	0.1366	0.0626	0.2523	0.2928	0.4661	0.6727	0.4437	0.7068	0.4116	0.2606
D36_39	-0.0921	-0.2908	-0.1709	-0.2391	-0.1460	0.0773	-0.1605	-0.0086	-0.1655	-0.9999
	0.1696	**0.0242**	0.3845	0.2296	0.5392	0.7076	0.5115	0.9713	0.4734	**0.0089**
D39_42	-0.0698	-0.2187	-0.2161	-0.1463	0.2330	0.0797	-0.0968	-0.0130	-0.2340	-0.9735
	0.2985	0.0932	0.2694	0.4666	0.3228	0.6987	0.6935	0.9567	0.3073	0.1468
D42_45	-0.0657	-0.2208	-0.2522	-0.0430	0.4292	0.1126	-0.0991	0.0189	-0.3347	-0.9270
	0.3274	0.0901	0.1954	0.8315	0.059	0.584	0.6864	0.937	0.138	0.2447

	ALL Rain	R1	R2	R3	R4	R5	R6	R7	R8	R9
D45_48	-0.0931	-0.1382	-0.3130	0.0266	0.5185	0.0163	-0.1579	-0.1140	-0.3371	-0.9999
	0.1651	0.2923	0.1048	0.8952	**0.0192**	0.9369	0.5185	0.6324	0.1351	**0.0101**
D48_51	-0.0996	-0.0683	-0.2526	0.0555	0.4145	-0.0678	-0.2346	-0.1856	-0.3671	-0.9993
	0.1372	0.6039	0.1947	0.7832	0.0692	0.742	0.3337	0.4333	0.1017	**0.0244**
D51_54	-0.0723	-0.0384	-0.2021	0.1482	0.2764	-0.0579	-0.2356	-0.1452	-0.3428	-0.9046
	0.2815	0.7709	0.3024	0.4608	0.2382	0.7789	0.3316	0.5415	0.1282	0.2803
D54_57	-0.0412	-0.0445	-0.2050	0.1625	0.1461	0.0054	-0.1614	-0.0271	-0.2270	-0.4703
	0.5396	0.7358	0.2954	0.4181	0.5389	0.9793	0.5092	0.9099	0.3224	0.6883
D57_60	-0.0597	-0.0884	-0.2907	0.2077	-0.0316	-0.0366	-0.1064	-0.0336	-0.1115	-0.2884
	0.3737	0.502	0.1335	0.2987	0.8948	0.859	0.6646	0.888	0.6303	0.8137
D60_63	-0.0229	-0.0908	-0.1913	0.2648	-0.0645	-0.0132	-0.0759	-0.0616	0.0864	-0.0890
	0.734	0.4902	0.3391	0.1819	0.7871	0.949	0.7574	0.7964	0.7097	0.9433
D63_66	0.0206	-0.0559	0.2120	-0.0578	-0.2179	-0.1207	-0.0170	-0.0406	0.1910	-0.1975
	0.7605	0.6713	0.2884	0.7791	0.3561	0.5571	0.9451	0.8649	0.407	0.8735
D66_69	0.0217	-0.0133	0.1539	-0.0750	-0.1509	-0.1039	-0.0567	0.0319	0.1810	-0.0534
	0.7481	0.9198	0.4529	0.716	0.5255	0.6135	0.8178	0.8938	0.4323	0.966
D69_72	0.0013	0.1475	0.1368	-0.0978	-0.1134	-0.1000	-0.1642	-0.0535	0.1977	0.3341
	0.9847	0.2608	0.5053	0.6347	0.6341	0.627	0.5018	0.8228	0.3904	0.7831

Table B.2: Pearson correlation coefficients for Hg concentration versus trace metals and 3 hour wind speeds upwind of the Steubenville receptor site for all snow and mixed precipitation clusters.

	ALL	S/M 1	S/M 2	S/M 3	S/M 4	S/M 5
Depth	-0.3272	-0.5241	-0.3314	-0.3231	-0.3828	-0.3082
	0.0101	0.0803	0.2687	0.2223	0.1967	0.5013
S	0.5800	0.7381	0.5952	0.3473	0.7264	-0.1029
	<.0001	**0.0061**	**0.0319**	0.1875	**0.0049**	0.8262
Fe	0.4563	0.2876	0.7467	0.5374	0.6439	0.3664
	0.0002	0.3647	**0.0034**	**0.0318**	**0.0176**	0.4189
Cl	0.3417	0.2366	0.5228	0.3000	0.3460	-0.4766
	0.007	0.459	0.0668	0.2589	0.2469	0.2795
La	0.1852	0.2412	0.5631	0.4400	0.1744	0.5819
	0.153	0.4501	**0.0451**	0.0881	0.5688	0.1705
Pb	0.4840	0.6259	0.4354	0.5966	0.5538	0.8822
	<.0001	**0.0295**	0.137	**0.0147**	**0.0496**	**0.0086**
P	0.1038	0.6437	0.5437	0.2780	0.4186	-0.0374
	0.4262	**0.0239**	0.0548	0.2971	0.1546	0.9366
Se	0.2963	0.4636	0.0128	0.7491	0.5857	-0.3793
	0.0204	0.129	0.9668	**0.0008**	**0.0354**	0.4013
D1	-0.1740	0.1621	-0.3864	-0.4575	-0.0732	-0.5770
	0.1798	0.6148	0.1922	0.0748	0.8121	0.175
D2	-0.1846	0.0945	-0.4191	-0.4782	-0.0946	-0.5837
	0.1544	0.7703	0.154	0.061	0.7586	0.1689
D3	-0.2001	-0.0300	-0.4428	-0.4592	-0.1211	-0.5863
	0.122	0.9263	0.1297	0.0735	0.6935	0.1665
D6	-0.2571	-0.3394	-0.4794	-0.3329	-0.2098	-0.6020
	0.0455	0.2805	0.0974	0.2077	0.4915	0.1527
D12	-0.1833	-0.5700	-0.4032	-0.2078	-0.2275	-0.5102
	0.1573	0.053	0.1719	0.44	0.4548	0.2421
D24	-0.0850	-0.6426	-0.2962	-0.2718	-0.3249	-0.0758
	0.5147	**0.0242**	0.3257	0.3085	0.2787	0.8717
D48	0.0873	-0.0891	0.4048	0.1355	-0.5246	0.0052
	0.5037	0.7831	0.17	0.6168	0.0657	0.9912
D3_6	-0.2850	-0.5277	-0.3645	-0.2394	-0.2619	-0.6159
	0.026	0.0779	0.2207	0.3718	0.3874	0.1409
D6_9	-0.1233	-0.6031	-0.0728	0.1915	-0.3171	-0.4309
	0.3437	**0.0379**	0.8132	0.4773	0.2912	0.3345
D9_12	0.0044	-0.4044	-0.1925	0.0439	0.0196	0.2825
	0.973	0.1923	0.5287	0.8719	0.9494	0.5393
D12_15	0.0520	-0.4287	-0.0108	0.2025	0.0525	0.5139
	0.6907	0.1644	0.9721	0.4519	0.8647	0.238
D15_18	0.0241	-0.5098	-0.1068	-0.0800	-0.0919	0.6587
	0.8538	0.0904	0.7283	0.7683	0.7653	0.1076
D18_21	0.0025	-0.3959	-0.0069	-0.0694	-0.4782	0.5945
	0.9848	0.2026	0.9822	0.7983	0.0984	0.1592
D21_24	-0.0228	-0.3828	0.0643	0.0185	-0.5395	0.2935
	0.8616	0.2194	0.8346	0.9459	0.0571	0.5229

D27_30	0.0946	-0.0044	0.2688	0.2571	-0.5535	0.4095
	0.4682	0.9892	0.3746	0.3363	**0.0497**	0.3617
D30_33	0.1176	0.1374	0.3915	0.2291	-0.4551	0.1673
	0.3667	0.6703	0.1859	0.3935	0.1181	0.72
D33_36	0.1385	0.0936	0.4975	0.2606	-0.4158	0.1439
	0.2872	0.7723	0.0836	0.3297	0.1576	0.7583
D36_39	0.1656	0.0009	0.5529	0.3727	-0.4514	0.2831
	0.2021	0.9977	0.05	0.1551	0.1216	0.5384
D39_42	0.1512	0.1508	0.5302	0.3663	-0.4520	0.5467
	0.2487	0.6399	0.0624	0.1629	0.121	0.2616
D42_45	0.1869	0.1835	0.5802	0.3809	-0.4272	0.6781
	0.1528	0.5681	**0.0376**	0.1455	0.1454	0.1387
D45_48	0.2319	0.0141	0.6099	0.3579	-0.3939	0.7597
	0.0746	0.9654	**0.0269**	0.1735	0.1829	0.0797
D48_51	0.0813	-0.1643	0.2503	0.3536	-0.3003	0.6746
	0.5403	0.6098	0.4327	0.1791	0.3188	0.1416
D51_54	0.0368	-0.1223	0.0456	0.2985	-0.2929	0.5638
	0.7822	0.705	0.888	0.2615	0.3314	0.2439
D54_57	-0.0280	0.0334	-0.1264	0.1807	-0.3190	0.6348
	0.8332	0.9179	0.6954	0.5031	0.288	0.1757
D57_60	-0.0687	0.0791	-0.1880	0.1096	-0.3637	0.4247
	0.6084	0.8171	0.5586	0.6863	0.2218	0.4012
D60_63	-0.0771	-0.0328	-0.1855	0.0963	-0.4036	0.6598
	0.5723	0.9284	0.5639	0.7229	0.1714	0.2257
D63_66	-0.1853	-0.2514	-0.3618	0.0522	-0.5597	0.7569
	0.1715	0.4835	0.2479	0.8477	**0.0467**	0.1385
D66_69	-0.2733	-0.4314	-0.5714	0.1049	-0.6204	0.6863
	0.0415	0.2131	0.0523	0.6989	**0.0237**	0.2007
D69_72	-0.2482	-0.4157	-0.5724	0.1119	-0.5400	0.5383
	0.0651	0.2322	0.0518	0.68	0.0568	0.3493